UNIVERSIDAD AUTÓNOMA DE SAN LUÍS POTOSÍ

Doctorado Institucional en Ingeniería y Ciencia de Materiales

Separation of fluoride from wet-process phosphoric acid and associated wastewater

PARA OBTENER EL GRADO DE

DOCTOR EN INGENIERÍA Y CIENCIA DE MATERIALES

QUE PRESENTA

Yingxin Chen

DIRECTOR y CO-DIRECTORA

Dr. Shaoxian Song y Dra. Jessica Viridiana García Meza

PATROCINADO POR SECIHTI Beca número 1327530

San Luis Potosí, SLP, noviembre de 2026

UNIVERSIDAD AUTÓNOMA DE SAN LUÍS POTOSÍ

Doctorado Institucional en Ingeniería y Ciencia de Materiales

Separation of fluoride from wet-process phosphoric acid and associated wastewater

QUE PARA OBTENER EL GRADO DE

DOCTOR EN INGENIERÍA Y CIENCIA DE MATERIALES

QUE PRESENTA

Yingxin Chen

DIRECTOR y CO-DIRECTORA

Dr. Shaoxian Song y Dra. Jessica Viridiana García Meza

Sinodales

Dr. Shaoxian Song _____

Dra. Jessica Viridiana García Meza _____

Dr. Damiano Sarocchi _____

Dr. Armando Encinas Oropesa _____

Dr. Edgar Daniel Páez Pérez _____

Dra. Ma. Selene Berber Mendoza _____

San Luis Potosí, SLP, noviembre de 2026



Separation of fluoride from wet-process phosphoric acid and associated wastewater by Yingxin Chen is licensed under Attribution-NonCommercial-NoDerivatives 4.0 International

Acknowledgement

This thesis begins with the acknowledgement section, in which I would like to express my sincere respect and gratitude to my advisors, family, friends, and fellow students for their selfless guidance, encouragement, and support throughout my doctoral study.

Advisors are the pillars of my academic journey. I feel truly fortunate to have joined the Group Song family and to spend unforgettable years with them. First, I am deeply grateful to my advisors, Professor Shaoxian Song and Professor J. Viridiana García Meza. During my doctoral studies, they provided many invaluable suggestions for my research, enabling me to face every challenge and setback with confidence while continually improving my work. Their patience, encouragement, and unwavering support carried me through my doctoral studies. Moreover, during my stay in Mexico, Professor J. Viridiana García Meza took excellent care of me in every aspect of my daily life. She introduced me to the beautiful scenery, rich culture, and delicious food of Mexico, which deepened my appreciation for the country. Her kindness and care made me never feel lonely in a foreign land. Also, I would like to express my sincere gratitude to Professor Hongqiang Li. From my master's studies to my doctoral training, he devoted tremendous time and effort to my research. He taught me not only how to conduct scientific research, but also how to improve my efficiency and, more importantly, how to become an excellent researcher. These three advisors' rigorous academic attitudes, profound expertise, and dedication to scientific research have influenced me and will continue to inspire me throughout my future career. In addition, I also want to show my sincere thanks to the members of my doctoral committee, Professor Damiano Sarocchi, Professor Lorenzo Borselli, Professor Edgar Daniel Páez Pérez, Professor Ma. Selene Berber Mendoza, and Professor Armando Encinas. Their invaluable suggestions during each of my presentations were indispensable to the successful completion of this thesis. Furthermore, I would also like to express my heartfelt appreciation to all the staff of the DICIM office. Their patience, kindness, and willingness to answer every question, no matter how small, greatly facilitated my daily life at the university. Finally, I am also sincerely grateful to Xiaoqing Weng, Qian Chen and the other teachers of the Group Song for their selfless support and assistance throughout my doctoral studies and daily life.

Family is the strongest support throughout my academic journey. From primary

school to my doctoral studies, they have always supported me unconditionally and provided me with the best possible opportunities, allowing me to pursue my education without worries and successfully complete every stage of my studies. Their love, sacrifice, and unwavering support have been the foundation of everything I have achieved. I will continue to work hard to live up to their expectations in the future.

Friends and fellow students are companions throughout my academic journey. I feel incredibly fortunate to meet so many like-minded friends and fellow students during my studies, with whom I shared countless wonderful memories. I would like to express my sincere gratitude to everyone in Laboratory 219 at Wuhan Institute of Technology, the members of Group Song, and my fellow students at UASLP. We supported one another in both our studies and daily lives, growing together like a family. I believe that these friendships will last a lifetime, and I hope that we will always remain connected in the years to come.

My doctoral studies were generously supported by the scholarship (CVU 1327530) provided by the Secretariat of Science, Humanities, Technology and Innovation (SECIHTI) of Mexico. I would like to express my sincere gratitude to them.

Yingxin Chen

Mexico

Abstract

Owing to the indispensable role of fluorine products in the new energy sector and other emerging fields, ensuring a sustainable supply of strategic fluorine resources has become important. With the gradual depletion of fluorite, the efficient recovery of fluorine associated with phosphoric chemical production is becoming a preferred approach. Wet-process phosphoric acid (WPA), as the major intermediate product of phosphate rock processing, is an important medium for fluorine recovery due to the migration and enrichment of fluorine in this process. Meanwhile, large volumes of acidic fluoride-rich phosphate chemical wastewater are generated during this process. Therefore, efficient fluorine recovery from WPA and deep fluoride removal from the associated wastewater are of great significance for sustainable fluorine utilization and environmental protection. Nevertheless, two key challenges remain: 1) the lack of highly efficient fluorine-spillover reagents during WPA evaporation concentration limits fluorine recovery, resulting in the waste of valuable fluorine resources; and 2) the existing treatment methods for the associated wastewater, particularly chemical precipitation, have limitations in achieving deep fluoride removal and may generate large amounts of fluoride-containing precipitates, posing potential environmental pollution risks and hindering the subsequent reuse of the wastewater.

To address these challenges, this study first developed silicon powder (SP) as a highly efficient fluorine-spillover reagent. The results showed that the introduction of SP significantly improved fluorine recovery from WPA during the concentration process, thereby reducing the loss of fluorine resources. Subsequently, three natural silicate mineral-based composites were prepared through loading engineering and crosslinking engineering strategies for the treatment of acidic phosphate chemical wastewater. These composites exhibited excellent acid resistance, high fluoride adsorption capacity, remarkable selectivity, and outstanding stability under acidic conditions, enabling the deep removal of fluoride. Overall, this thesis provides valuable insights and technical support for the efficient separation of fluoride from WPA produced in the phosphoric chemical industry and its associated acidic phosphate chemical wastewater.

Keywords: Wet-process phosphoric acid; Acidic chemical wastewater; Fluoride separation; Silicon powder; Natural silicate mineral-based composites.

Resumen

Debido al papel indispensable que desempeñan los productos fluorados en el sector de las nuevas energías y otros campos emergentes, garantizar un suministro sostenible de recursos estratégicos de flúor ha adquirido una importancia creciente. Ante el agotamiento gradual de los recursos de fluorita, la recuperación eficiente del flúor asociado a la producción de la industria química del fósforo se está convirtiendo en una estrategia preferente. El ácido fosfórico obtenido por vía húmeda (wet-process phosphoric acid, WPA), como principal producto intermedio del procesamiento de la roca fosfórica, constituye un medio importante para la recuperación de flúor debido a la migración y el enriquecimiento de este elemento durante dicho proceso. Al mismo tiempo, durante este proceso se generan grandes volúmenes de aguas residuales ácidas de la industria química del fósforo con altas concentraciones de fluoruro. Por lo tanto, la recuperación eficiente de flúor del WPA y la eliminación profunda de fluoruro de las aguas residuales asociadas son de gran importancia para el aprovechamiento sostenible de los recursos de flúor y la protección ambiental. No obstante, aún persisten dos desafíos clave: 1) la falta de reactivos altamente eficientes que favorezcan la transferencia del flúor durante la concentración por evaporación del WPA limita la recuperación de flúor, lo que provoca la pérdida de valiosos recursos de flúor; y 2) los métodos existentes para el tratamiento de las aguas residuales asociadas, en particular la precipitación química, presentan limitaciones para lograr una eliminación profunda del fluoruro y pueden generar grandes cantidades de precipitados que contienen fluoruro, lo que plantea riesgos potenciales de contaminación ambiental y dificulta su posterior reutilización.

Para abordar estos desafíos, en este estudio se desarrolló, en primer lugar, polvo de silicio (SP) como un reactivo altamente eficiente para favorecer la transferencia del flúor. Los resultados demostraron que la incorporación de SP mejoró significativamente la recuperación de flúor del WPA durante el proceso de concentración, reduciendo así la pérdida de recursos de flúor. Posteriormente, se prepararon tres materiales compuestos basados en minerales de silicato natural mediante estrategias de ingeniería de carga e ingeniería de entrecruzamiento para el tratamiento de aguas residuales ácidas de la industria química del fósforo. Estos materiales compuestos presentaron una excelente resistencia a medios ácidos, una elevada capacidad de adsorción de fluoruro, una notable selectividad y una sobresaliente estabilidad en condiciones ácidas,

permitiendo así la eliminación profunda del fluoruro. En conjunto, esta tesis proporciona conocimientos valiosos y apoyo técnico para la separación eficiente de fluoruro del WPA producido en la industria química del fósforo y de las aguas residuales ácidas asociadas de dicha industria.

Palabras clave: Ácido fosfórico por vía húmeda; Aguas residuales químicas ácidas; Separación de fluoruro; Polvo de silicio; Materiales compuestos basados en minerales de silicato naturales.

Extended Abstract

The rapid development of the new energy sector and other emerging fields has increased the demand for fluorine resources. With the continuous decline in fluorite reserves, the recovery and utilization of fluorine associated with phosphate rock have become increasingly important. Wet-process phosphoric acid (WPA) is the major intermediate product of phosphate rock processing. Therefore, achieving efficient fluorine recovery during the evaporation concentration process of WPA is a key focus for the phosphoric chemical industry. Nevertheless, the lack of highly efficient fluorine-spillover reagents severely limits this process. Moreover, in addition to efficient fluorine recovery, the large volumes of acidic fluoride-containing chemical wastewater generated during this production should also receive attention, as they may adversely affect human health, ecosystems, and subsequent production unless effectively treated before discharge or reuse.

Herein, to enhance fluorine recovery during the evaporation concentration process of WPA, silicon powder (SP) was first used as an efficient fluorine-spillover reagent, and its regulatory behaviors and underlying mechanism regarding fluorine migration and transformation were systematically investigated. The results demonstrated that SP altered the transformation pathways and phase distribution of fluorine in WPA by promoting the formation and volatilization of SiF_4 gas while inhibiting the formation of sodium fluorosilicate (Na_2SiF_6) and potassium fluorosilicate (K_2SiF_6) precipitates, thereby effectively facilitating the transfer of fluorine from the liquid and solid phases to the gas phase. Under optimal conditions, the fluorine recovery reached 81.13%, representing an increase of 31.08% compared with the blank concentration experiment and exceeding that achieved with conventional reagents, such as diatomite, white carbon black (WCB), and zeolite powder (ZP).

To achieve deep fluoride removal from associated acidic phosphate chemical wastewater, a $La(OH)_3$-modified diatomite (La/D) composite was synthesized via the loading engineering strategy based on the inherent acid resistance of both diatomite and $La(OH)_3$, and the relationship between its structural characteristics and fluoride adsorption behavior was systematically investigated. The loading of $La(OH)_3$ changed the surface properties of diatomite by increasing the available adsorption sites and regulating the surface charge while maintaining structural stability under acidic conditions. Through the synergistic effects of electrostatic interactions, ligand exchange,

and coordination complexation, the La/D composite achieved a maximum adsorption capacity of 135.93 mg/g at pH 3. In addition, the composite reduced the fluoride concentration in real acidic phosphate chemical wastewater from 70.49 mg/L to 3.83 mg/L with a removal efficiency of 94.56%, meeting the Chinese industrial wastewater discharge standard (GB 39371-2020, <10 mg/L).

To improve the sedimentation and separation performance of the composite, a lanthanum (La)-aluminum (Al) bimetallic hydroxides-loaded montmorillonite (LAM) composite was designed based on the strong fluoride affinity of La and Al, the remarkable acid resistance of $La(OH)_3$, and the coagulation-flocculation properties of polyaluminum chloride (PAC). The introduction of bimetallic hydroxides enabled functional complementarity: $La(OH)_3$ not only enhanced the acid resistance of the composite but also served as the primary active component for fluoride adsorption, whereas $Al(OH)_3$ improved the sedimentation performance and provided auxiliary adsorption sites. Governed by ligand exchange, electrostatic attraction, hydrogen bonding, and coordination complexation, the optimized LAM-3 composite (La:Al mass ratio = 3:1) exhibited outstanding fluoride removal performance, achieving a maximum adsorption capacity of 130.87 mg/g and complete sedimentation within 2 h. Notably, the LAM-3 composite reduced the fluoride concentration in real acidic phosphate chemical wastewater from 100.62 mg/L to 4.96 mg/L, achieving deep fluoride removal.

Keywords: Wet-process phosphoric acid; Acidic chemical wastewater; Fluoride separation; Silicon powder; Natural silicate mineral-based composites.

Contents

Acknowledgement I
Abstract III
Resumen IV
Extended Abstract VI
Index of Figures XI
Index of Tables XIV
Chapter 1 . Introduction 1
1.1. Justification 1
1.2. Objectives 2
1.2.1. General objective 2
1.2.2. Goals 3
1.3. References 3
Chapter 2 . Literature Review 6
2.1. Introduction 6
2.2 Recovery technologies of fluorine from WPA 8
2.2.1 Chemical precipitation 8
2.2.2 Solvent extraction 10
2.2.3 Evaporation concentration 11
2.2.4 Air stripping 12
2.2.5 Other technologies 13
2.3 Fluoride removal from acidic phosphoric chemical wastewater 14
2.3.1 Metal-based composites 15
2.3.2 Carbon-based composites 16
2.3.3 Natural silicate mineral-based composites 17
2.4 Research gap 18
2.5 References 19
Chapter 3 . Efficient fluorine recovery from wet-process phosphoric acid using silicon powder as a fluorine-spillover reagent 28
3.1. Introduction 28
3.2. Experimental 30
3.2.1. Materials and reagents 30
3.2.2. Fluorine recovery test 31

3.2.3. Spillover kinetics test 32
3.2.4. Determination of fluorine contents 33
3.2.5 Characterizations 33
3.3. Results and discussion 34
3.3.1. Different reagent comparative test 34
3.3.2. Gasification behavior of fluorine using SP 35
3.3.3. Gasification mechanism of fluorine using SP 38
3.4. Conclusions 46
3.5. References 46
Chapter 4 . Lanthanum-functionalized diatomite enabling highly efficient fluoride removal from acidic phosphate chemical wastewater 51
4.1. Introduction 51
4.2. Experimental 53
4.2.1. Material and reagents 53
4.2.2. Preparation of La/D composite 54
4.2.3. Adsorption experiments 54
4.2.4. Characterizations 55
4.3. Results and discussion 56
4.3.1. Characterization of La/D composite 56
4.3.2. Adsorption experiments 59
4.3.3. Removal mechanism of La/D composite 68
4.3.4. Fluoride removal from real acidic phosphate chemical wastewater . 71
4.4. Conclusions 72
4.5. References 73
Chapter 5 . Synergistic and efficient fluoride removal from acidic phosphate chemical wastewater enabled by bimetallic hydroxides-loaded montmorillonite 80
5.1. Introduction 80
5.2. Experiments 83
5.2.1. Materials and reagents 83
5.2.2 Syntheses of LAM composite 83
5.2.3. Adsorption experiments 84
5.2.4. Characterizations 85
5.3. Results and discussion 86
5.3.1. Effect of La/Al mass ratio on fluoride adsorption 86

5.3.2. Characterization of the LAM-3 composite 87
5.3.3. Fluoride adsorption on the LAM-3 composite..... 90
5.3.4. Removal mechanism 95
5.3.5 Reusability and practical application performance 99
5.4. Conclusions 101
5.5. References 101
Chapter 6 . Conclusions.....110
Appendix I. Articles published during the Ph. D study.....112
Appendix II. Experimental data 114

Index of Figures

Fig. 2.1 Overview of common technologies for fluorine recovery from WPA. 8
Fig. 2.2 Schematic illustration of fluorine recovery from WPA via chemical precipitation process. 9
Fig. 2.3 Schematic illustration of fluorine recovery from WPA via solvent extraction process. 10
Fig. 2.4 Schematic illustration of the evaporation concentration process for fluorine recovery from WPA. 12
Fig. 2.5 Schematic illustration of the air stripping process for fluorine recovery from WPA. 13
Fig. 2.6 Classification of common technologies and adsorbents for fluoride removal from acidic phosphate chemical wastewater. 15
Fig. 3.1 XRD patterns of (a) SP, (b) Diatomite, (c) WCB and (d) ZP. 31
Fig. 3.2 The diagram of the fluorine recovery test device. 32
Fig. 3.3 The standard line for fluorine contents. 33
Fig. 3.4 Effect of different reagents on (a) the fluorine contents of AS, WPA, and DS, and (b) fluorine recovery (dosage: 0.5 g, stirring speed: 1800 r/min, concentration temperature: 150°C, and absorptive water initial mass: 200 g). 34
Fig. 3.5 Effect of SP dosage on (a) the fluorine contents of AS, WPA, and DS, and (b) fluorine recovery (stirring speed: 1800 r/min, concentration temperature: 150°C, and absorptive water initial mass: 200 g). 35
Fig. 3.6 Effect of stirring speed on (a) the fluorine contents of AS, WPA, and DS, and (b) fluorine recovery (SP dosage: 0.5 g, concentration temperature: 150°C, and absorptive water initial mass: 200 g). 36
Fig. 3.7 Effect of concentration temperature on (a) the fluorine contents of AS, WPA, and DS, and (b) fluorine recovery (SP dosage: 0.5 g, stirring speed: 1800 r/min, and absorptive water initial mass: 200 g). 37
Fig. 3.8 Effect of initial mass of absorptive water on (a) the fluorine contents of AS, WPA, and DS, and (b) fluorine recovery (SP dosage: 0.5 g, stirring speed: 1800 r/min, and concentration temperature: 150°C). 38
Fig. 3.9 (a) The concentration time curve of fluorine content in AS and (b) fitting curve of apparent kinetic equation. 39
Fig. 3.10 SEM images of DS before (a, c) and after (b, d) SP treatment. 41
Fig. 3.11 The F and Na elemental mappings of DS in the absence (a, c) and presence (b, d) of SP. 42
Fig. 3.12 XRD patterns of DS before (a) and after (b) SP treatment. 43
Fig. 3.13 The gasification mechanism diagram of fluorine with SP treatment. 46
Fig. 4.1 The synthesis process of the La/D composite. 54
Fig. 4.2 Standard line of fluoride. 56
Fig. 4.3 XRD patterns of diatomite and the La/D composite. 57

Fig. 4.4 (a) The N_2 adsorption-desorption isotherms and (b) related pore size distributions of diatomite and the La/D composite. 58
Fig. 4.5 (a) FTIR spectra of diatomite and the La/D composite and (b) XPS survey scan of the La/D composite. 59
Fig. 4.6 (a-b) SEM images and (c-f) EDS mapping images of the La/D composite. 59
Fig. 4.7 Effect of initial pH on fluoride adsorption performance of the La/D composite (fluoride concentration: 100 mg/L, the La/D composite dosage: 0.5 g/L, T: 25℃, and t: 12 h). 60
Fig. 4.8 (a) Adsorption kinetics, (b) intra-particle diffusion model of fluoride on the La/D composite (initial pH: 3, the La/D composite dosage: 0.5 g/L, and T: 25℃). 62
Fig. 4.9 (a-b) Adsorption isotherms and (c) the R_L values of fluoride on the La/D composite (initial pH: 3, the La/D composite dosage: 0.5 g/L, and T: 25℃) 64
Fig. 4.10 Adsorption thermodynamic of fluoride on the La/D composite (initial pH: 3, the La/D composite dosage: 0.5 g/L, and T: 25℃) 65
Fig. 4.11 Effect of co-exist anion types and concentration on the fluoride adsorption on the La/D composite (fluoride concentration: 100 mg/L, the La/D composite dosage: 0.5 g/L, T: 25℃, and t: 12 h). 67
Fig. 4.12 (a) Regeneration performance of the La/D composite; (b) La leaching concentration and leaching percentage in fluoride solution during regeneration process (initial pH: 3, fluoride concentration: 100 mg/L, the La/D composite dosage: 0.5 g/L, T: 25℃, and t: 12 h). 67
Fig. 4.13 SEM images (a-c) and EDS mapping images (d-h) of La/D composite after fluoride adsorption. 68
Fig. 4.14 FTIR spectra of the La/D composite before and after fluoride adsorption. 69
Fig. 4.15 (a) The wide scan XPS, (b) F 1s, (c) O 1s, and (d) La 3d spectra of the La/D composite before and after fluoride adsorption. 70
Fig. 4.16 Schematic diagram of fluoride adsorption on the La/D composite. 71
Fig. 4.17 Effect of the La/D composite dosage on fluoride q_e and R in real acidic phosphogypsum wastewater (T: 25 ℃ and t: 12 h) 72
Fig. 5.1 The standard line of fluoride. 85
Fig. 5.2 (a) Effect of La/Al mass ratio on fluoride adsorption capacities, and (b) the pictures of different adsorbents after sedimentation of different time (fluoride concentration: 100 mg/L, the LAM composite dosage: 0.5 g/L, T: 25℃, and t: 12 h). 87
Fig. 5.3 XRD patterns of MMT and the LAM-3 composite. 88
Fig. 5.4 FTIR spectra of MMT and the LAM-3 composite. 88
Fig. 5.5 (a) The N_2 adsorption-desorption isotherms and (b) related pore size distributions of MMT and the LAM-3 composite. 89
Fig. 5.6 (a) SEM and (b-f) EDS images of the LAM-3 composite. 90
Fig. 5.7 Effect of (a) initial pH and (b) coexisting ions on the adsorption performance of the LAM-3 composite (fluoride concentration: 100 mg/L, the LAM-3 composite dosage: 0.5 g/L, T: 25℃, and t: 12 h). 92
Fig. 5.8 (a) Adsorption kinetics and (b) intra-particle diffusion of fluoride on the LAM-3

composite (initial pH: 3 and the LAM-3 composite dosage: 0.5 g/L). 93
Fig. 5.9 Adsorption isotherms of fluoride on the LAM-3 composite (initial pH: 3 and the LAM-3 composite dosage: 0.5 g/L). 94
Fig. 5.10 (a1-a2) SEM and (b1-b6) EDS mapping images of the LAM-3 composite after fluoride adsorption. 96
Fig. 5.11 FTIR spectra of the LAM-3 composite before and after fluoride adsorption. 97
Fig. 5.12 (a) wide scan XPS spectra, (b) O 1s, (c) La 3d, (d) Al 2p, and (e) F 1s narrow spectra of the LAM-3 composite before and after fluoride adsorption. 98
Fig. 5.13 Schematic diagram of fluoride removal mechanism by the LAM-3 composite. 99
Fig. 5.14 (a) Regeneration performance and (b) La and Al leaching percentages during the adsorption–desorption cycles (initial pH: 3, fluoride concentration: 100 mg/L, the LAM-3 composite dosage: 0.5 g/L, T: 25 ℃, and t: 12 h). 100
Fig. 5.15 Actual acidic wastewater treatment performance of the LAM-3 composite. 100

Index of Tables

Table 3.1 The anions and cations contents of WPA (wt%). 30
Table 3.2 The compositions of different reagents used in the experiments (wt%). 31
Table 3.3 The repeated experiments on WPA concentration under the optimal conditions of SP. 38
Table 3.4 The contents of anions and cations in concentrated WPA before and after SP treatment (wt%). 41
Table 3.5 The elements contents of DS in the absence and presence of SP (wt%). 42
Table 4.1 The compositions of diatomite used in the experiments (wt%). 54
Table 4.2 Information about the pore distribution of diatomite and the La/D composite. 58
Table 4.3 Zeta potential of diatomite, the La/D composite and after adsorption at pH of 3. 61
Table 4.4 The detail information of adsorption kinetics, isotherm and thermodynamic equations. 62
Table 4.5 Adsorption kinetics model parameters of fluoride on the La/D composite. 63
Table 4.6 Adsorption isotherms models parameters of fluoride on the La/D composite. 64
Table 4.7 Adsorption thermodynamics parameters of fluoride on the La/D composite. 65
Table 4.8 Comparison of the adsorption capacities and corresponding parameters of various adsorbents. 65
Table 4.9 Elements contents of the La/D composite before and after adsorption of fluoride (wt%). 68
Table 4.10 Atomic concentrations of the La/D composite before and after adsorption of fluoride (%). 70
Table 4.11 The concentration of anions and cation in real phosphogypsum wastewater (mg/L). 71
Table 5.1 The used materials and reagents of the experiments in this work. 83
Table 5.2 The specific conditions and parameters of adsorption kinetics and isotherms. 85
Table 5.3 The relevant details of characterizations for prepared adsorbents. 85
Table 5.4 Information about the pore distribution of natural MMT and the LAM-3 composite. 89
Table 5.5 Zeta potential of natural MMT, the LAM-3 composite and after adsorption at pH of 3. 91
Table 5.6 Adsorption kinetics parameters of fluoride on the LAM-3 composite. 93
Table 5.7 Adsorption isotherm parameters of fluoride on the LAM-3 composite. 94
Table 5.8 Adsorption thermodynamic parameters of fluoride on the LAM-3 composite. 94
Table 5.9 Fluoride removal efficiency of the LAM-3 composite compared with other adsorbents reported in previous literature. 95
Table 5.10 Elements contents of the LAM-3 composite before and after fluoride adsorption (wt%). 96
Table 5.11 The characteristic information of pH, anions and cation concentration in the real

wastewater (mg/L). 100

Chapter 1. Introduction

1.1. Justification

Fluorine is an indispensable strategic resource that has been widely applied in critical fields such as new energy, semiconductor manufacturing, aerospace, and pharmaceuticals [1–3]. In nature, fluorine resources are mainly found in fluorite and phosphate rock [4,5]. With the gradual depletion of fluorite resources, the efficient recovery of fluorine from phosphate rock (approximately 90% of the total fluorine resources) has become an important approach for ensuring the sustainable supply of fluorine resources [6]. Phosphate rock is the primary raw material for the production of phosphoric acid, and the wet process, which involves the decomposition of phosphate rock with sulfuric acid (H_2SO_4), is the predominant method [7]. In this process, most of the fluorine present in phosphate rock is transferred into wet-process phosphoric acid (WPA), which causes a series of adverse effects on the environment and downstream products. For instance, excess fluorine in WPA reduces production efficiency and fertilizer quality while increasing the risk of fluoride accumulation in soil and groundwater [8,9]. In light of the above considerations, for the sustainable development of the fluorochemical and phosphoric chemical industries, there is an urgent need to prioritize the recovery of fluorine from WPA.

For fluorine recovery from WPA, several methods have been employed. Among these methods, evaporation concentration, which enables fluorine recovery through the conversion of liquid fluorosilicic acid (H_2SiF_6) into gaseous silicon tetrafluoride (SiF_4), is considered to be promising due to its simple operation and low operational cost [10,11]. Furthermore, it is observed that increasing the production of SiF_4 gas is the key to enhancing fluorine recovery. For this purpose, active silicon-containing reagents, such as diatomite and white carbon black, have been widely used for recovering fluorine from WPA due to their unique lattice structures and affinities for fluorine [12]. Nevertheless, these traditional reagents still exhibit unsatisfactory performance, which is attributed to the adverse effects of inherent impurities on their reactions with fluorine, as well as their undesirable adsorption of fluorine [13,14]. Therefore, it is necessary to develop novel and efficient fluorine-spillover reagents to overcome the limitations of conventional reagents and enhance fluorine recovery.

Nevertheless, the efficient recovery of fluorine from WPA alone is insufficient to

address the fluorine-related challenges. It cannot be ignored that large volumes of associated fluoride-rich acidic phosphate chemical wastewater, including phosphogypsum wastewater and WPA washing wastewater, are inevitably generated during WPA production and fluorine recovery. These wastewaters are characterized by strong acidity (pH of 1-4), high fluoride concentrations (50 mg/L-200 mg/L), and complex chemical compositions (Cl^-, SO_4^{2-}, PO_4^{3-}, and so on). Without effective treatment, they will pose serious threats to the environment and hinder subsequent reuse [15,16]. Recently, adsorption has emerged as one of the most promising technologies for addressing the fluoride hazards in these wastewaters owing to its high removal efficiency, deep purification capability, simple operation, and environmental friendliness [17,18]. To this end, various adsorbents, including carbon-based composites [19], metal-organic frameworks (MOFs) [20], mineral-based composites [21], and metal-based composites [22], have been developed. Nevertheless, most adsorbents still exhibit limited fluoride removal performance because of the structural collapse and the dissolution of active sites under acidic conditions. Such pH sensitivity remains a major barrier to their practical application. For this reason, the targeted design of adsorbents with excellent acid resistance, high fluoride removal efficiency, good structural stability, high selectivity, and good reusability is of great importance for adapting to the complex environment of acidic phosphate chemical wastewater and enabling the deep removal of fluoride.

1.2. Objectives

1.2.1. General objective

Based on the occurrence characteristics of fluorine in WPA and the complex chemical environment of the associated acidic phosphate chemical wastewater, this study aims to first develop a novel and highly efficient fluorine-spillover reagent to enhance fluorine recovery from WPA. Subsequently, a series of natural silicate mineral-based composites are designed to overcome the limitations of insufficient acid resistance and poor adsorption performance under complex acidic wastewater conditions, thereby enabling deep fluoride removal. This study is expected to provide a theoretical basis, technical support, and practical guidance for the comprehensive recovery of fluorine resources from WPA and the remediation of fluoride-contaminated acidic wastewater in the phosphoric chemical industry.

1.2.2. Goals

(1) To develop silicon powder (SP) as a novel fluorine-spillover reagent, systematically investigate its effects on the volatilization behavior of fluorine in WPA, and reveal the migration pathway and recovery mechanism of fluorine, thereby achieving efficient fluorine recovery.

(2) To fabricate a series of natural silicate mineral-based adsorbents (the La/D composite, the LAM composite, and [redacted]) via loading engineering and [redacted] for deep fluoride removal from associated acidic phosphate chemical wastewater. The adsorption performance, adsorption behavior, functional properties, and practical application potential are systematically evaluated, and the underlying removal mechanisms are further elucidated, thereby establishing the structure-performance relationships of the natural silicate mineral-based composites for fluoride removal.

1.3. References

[1] S.J. Ouedraogo, Y. Vinh, P. (Lek) Noophan, V. Naddeo, C.-W. Li, Dissolution of aluminum hydroxide to provide Al and to neutralize acidity for the removal and recovery of fluoride through cryolite crystallization, Journal of Cleaner Production 404 (2023) 136987. https://doi.org/10.1016/j.jclepro.2023.136987.

[2] F. Cheng, S. Lianjun, W. Shihan, L. Dongming, L. Tianxiang, S. Yanfeng, Z. Jing, A fundamental investigation into the separation of phosphorus and fluorine from wet-process phosphoric acid wastewater: Determination of phase equilibria in the CaF_2–$CaSO_4$–H_3PO_4(–H_2SO_4)–H_2O system, Journal of the Indian Chemical Society 103 (2026) 102805. https://doi.org/10.1016/j.jics.2026.102805.

[3] C. Yu, S. Huang, H. Xu, J. Yan, K. Rong, M. Sun, Optimal charging of lithium-ion batteries based on lithium precipitation suppression, Journal of Energy Storage 82 (2024) 110580. https://doi.org/10.1016/j.est.2024.110580.

[4] L. Lv, H. Duan, W. Liu, T. Yue, Flotation separation of fluorite from calcite using bis hydroxamic acid collector, Minerals Engineering 187 (2022) 107803. https://doi.org/10.1016/j.mineng.2022.107803.

[5] Z. Shou, D. Xu, W. Yang, C. Hu, X. Wang, Z. Yan, A novel process for preparing calcium magnesium polyphosphate and recovering fluorine by utilizing the fluorine-containing phosphoric acid residue and phosphate tailings, Chemical Engineering Journal 519 (2025) 165160. https://doi.org/10.1016/j.cej.2025.165160.

[6] B. Peng, X. Li, Z. Ma, Y. Qi, Release of fluorine and chlorine during increase of phosphate rock grade by calcination and digestion, Environmental Pollution 270 (2021) 116321. https://doi.org/10.1016/j.envpol.2020.116321.

[7] F. Wu, D. Chen, Q. Niu, X. Xiao, Current status of phosphoric acid preparation technology and future application directions of microbial methods, Sustainable Chemistry and Pharmacy 43 (2025) 101882. https://doi.org/10.1016/j.scp.2024.101882.

[8] L. Wang, C. Wang, Y. Yu, X. Huang, Z. Long, Y. Hou, D. Cui, Recovery of fluorine from bastnasite as synthetic cryolite by-product, Journal of Hazardous Materials 209–210 (2012) 77–83. https://doi.org/10.1016/j.jhazmat.2011.12.069.

[9] J. Lv, Y. Zheng, X. Tong, X. Li, Clean utilization of waste rocks as a novel adsorbent to treat the beneficiation wastewater containing arsenic and fluorine, Journal of Cleaner Production 293 (2021) 126160. https://doi.org/10.1016/j.jclepro.2021.126160.

[10] B. Peng, Z. Ma, Y. Zhu, L. Tang, Release and recovery of fluorine and iodine in the production and concentration of wet-process phosphoric acid from phosphate rock, Minerals Engineering 188 (2022) 107843. https://doi.org/10.1016/j.mineng.2022.107843.

[11] B. Long, S. Chen, Z. Li, Y. Ding, Solubility of ammonium fluoride in aqueous sodium fluoride solutions of various concentrations from dilute to saturated at 298.15 K for fluorine recovery from wet-process phosphoric acid, Journal of Molecular Liquids 299 (2020) 112247. https://doi.org/10.1016/j.molliq.2019.112247.

[12] R.Y. Ning, Reactive silica in natural waters — A review, Desalination and Water Treatment 21 (2010) 79–86. https://doi.org/10.5004/dwt.2010.1229.

[13] K. Rangsriwatananon, A. Chaisena, C. Thongkasam, Thermal and acid treatment on natural raw diatomite influencing in synthesis of sodium zeolites, J Porous Mater 15 (2008) 499–505. https://doi.org/10.1007/s10934-007-9098-2.

[14] L. Xu, X. Gao, Z. Li, C. Gao, Removal of fluoride by nature diatomite from high-fluorine water: An appropriate pretreatment for nanofiltration process, Desalination 369 (2015) 97–104. https://doi.org/10.1016/j.desal.2015.04.033.

[15] S. Muthu Prabhu, M. Yusuf, Y. Ahn, H.B. Park, J. Choi, M.A. Amin, K.K. Yadav, B.-H. Jeon, Fluoride occurrence in environment, regulations, and remediation methods for soil: A comprehensive review, Chemosphere 324 (2023) 138334. https://doi.org/10.1016/j.chemosphere.2023.138334.

[16] F. Chen, Y. Liang, M. Hu, S. Zeng, Z. Zhou, M. Cao, B. Chen, P. Wang, J. Shi, Y. Liang, In situ solidification of fluoride in industrial wastewater using Ca-modified hydrophilic sludge ceramsite, Journal of Water Process Engineering 82 (2026) 109393. https://doi.org/10.1016/j.jwpe.2025.109393.

[17] B. Luo, Y. Liu, Y. Yan, H. He, J. Yu, Q. Chen, Research on the removal of fluoride from low-concentration fluorine-containing industrial wastewater using adsorption methods, Biochemical Engineering Journal 216 (2025) 109668. https://doi.org/10.1016/j.bej.2025.109668.

[18] F. Li, X. Li, J. Yu, S. Li, L. Guo, C. Xiao, J. Li, Y. Zhang, R. Chi, Enhanced removal of phosphate and fluoride from phosphogypsum leachate by cerium/iron-

based zeolite: Adsorption behaviors and competition mechanisms, Separation and Purification Technology 376 (2025) 134185. https://doi.org/10.1016/j.seppur.2025.134185.

[19] X. Zhang, J. He, X. Ding, Z. Mao, R. Hong, D. Xu, C. Peng, J. Wang, S. Sun, Z. Lv, S. Chen, A waste-treats-waste strategy: Upcycling dual solid wastes into a La-modified biochar for sustainable deep fluoride removal, Journal of Water Process Engineering 92 (2026) 110671. https://doi.org/10.1016/j.jwpe.2026.110671.

[20] R. Foroutan, A. Tutunchi, M. Foroughi, B. Ramavandi, Efficient fluoride removal from water and industrial wastewater using magnetic chitosan/β-cyclodextrin aerogel enhanced with biochar and MOF composites, Separation and Purification Technology 363 (2025) 132128. https://doi.org/10.1016/j.seppur.2025.132128.

[21] Y. Jiang, L. He, Y. Tang, W. Chen, L. Shao, X. Wang, K. Wang, High-efficiency removal of fluoride ions in real fluorine-containing wastewater using red mud-metakaolin based geopolymer microspheres, Applied Clay Science 285 (2026) 108145. https://doi.org/10.1016/j.clay.2026.108145.

[22] C. Liu, L. Li, R. Jiao, H. He, Z. Zhang, F. Yu, J. Zhang, W. Zhang, Sulfate-regulated crystallization mechanism of LaF_3 for efficient defluorination in high-sulfate fluoride wastewater, Water Research 302 (2026) 126058. https://doi.org/10.1016/j.watres.2026.126058.

Chapter 2. Literature Review

2.1. Introduction

Fluorine, a halogen element with an average abundance of approximately 585 mg/kg in the Earth's crust, is an important strategic resource [1]. In recent years, the rapid development of the new energy, electronics, metallurgical, and pharmaceutical industries has continuously increased the demand for fluorine-containing products, making fluorine an indispensable raw material for modern industry [2,3]. It has been reported that fluorine resources are mainly associated with fluorite (CaF_2) and phosphate rock, with fluorine mainly present in the form of fluorapatite ($Ca_5F(PO_4)_3$) [4,5]. As a non-renewable mineral resource, the continuous exploitation of fluorite has resulted in a significant decline in its reserves, leading to an increasingly constrained supply [6,7]. In contrast, phosphate rock contains abundant associated fluorine and has become an important alternative source of fluorine. It is estimated that approximately 90% of the world's fluorine resources are associated with phosphate rock [8]. Therefore, to alleviate the growing shortage of fluorite resources, the efficient recovery and utilization of fluorine from phosphate rock have emerged as an important approach for the future development of the fluorochemical industry.

In the phosphoric chemical industry, phosphate rock is the primary raw material for the production of phosphoric acid. The conventional phosphoric acid production technologies include the thermal process and the wet process [9,10]. Among these, the wet process is the dominant technology utilized in the industry because of its operational simplicity and stability, broad applicability, and low production cost [11,12]. The production of wet-process phosphoric acid (WPA) involves the leaching of phosphate rock with sulfuric acid (H_2SO_4), producing crude WPA and insoluble calcium sulfate crystals (phosphogypsum). The crude WPA is subsequently purified to obtain the desired WPA product. The overall reaction is shown in Eq. (2.1) [13,14].

$$Ca_5F(PO_4)_3+5H_2SO_4+10H_2O=3H_3PO_4+5CaSO_4\bullet 2H_2O+HF\uparrow \quad (2.1)$$

Most phosphate rock in China is of medium- to low-grade and contains approximately 2%-4% associated fluorine. During WPA production, about 65%-70% of the fluorine in phosphate rock is transferred into WPA, 15%-30% is retained in phosphogypsum, and only 5%-10% is released into the gas phase for recovery [15,16].

Consequently, a large proportion of the associated fluorine is transferred into WPA, where its efficient recovery remains challenging. Of greater concern, the residual fluorine causes a series of adverse effects on WPA production and downstream products. Specifically, the presence of fluorine decreases the silicon-to-fluorine molar ratio in WPA, resulting in increased slurry viscosity, poor phosphogypsum crystallization, and reduced filtration performance, thereby compromising the stable operation of WPA production [17]. Furthermore, residual fluorine in WPA adversely affects the quality of downstream phosphate fertilizers and feed products. For example, excessive fluorine may cause phosphate fertilizers to fail to meet relevant quality standards, while fluorine-rich feed can lead to fluorosis and severe skeletal disorders in animals [18].

It should be noted that efficient fluorine recovery from WPA alone is insufficient to address related fluorine pollution challenges in the phosphoric chemical industry. In addition to the fluorine retained in WPA, the production and purification of WPA inevitably generate large volumes of acidic phosphate chemical wastewater. Such wastewater usually contains high concentrations of fluoride, together with phosphate, sulfate, and various dissolved ions. Accordingly, the Chinese national discharge standard of fluoride concentration allowed in industrial wastewater is 10 mg/L (GB 39371-2020) [19]. Nevertheless, the wastewater generated by the phosphoric chemical industry is usually at high fluoride levels (50 - 200 mg/L) with strong acidity, which is higher than the emission standard and needs effective treatment before discharging or reusing [20]. If discharged without proper treatment, acidic fluoride-containing wastewater may contaminate surface water and groundwater, threatening human health and ecological systems. Drinking-water fluoride pollution has become a serious public health concern in several countries, including India, Mexico, and China [21]. Moreover, the direct reuse of such wastewater in the production process may result in the accumulation of fluoride and other impurities within the system, thereby compromising process stability and the quality of downstream products [22].

In summary, the associated fluorine not only compromises the stable operation of WPA production and the quality of downstream products but also leads to the generation of large volumes of acidic fluoride-containing chemical wastewater. The discharge of such wastewater without effective treatment poses serious risks. Nevertheless, it cannot be ignored that fluorine is also an important strategic resource for the fluorochemical industry. Therefore, the efficient recovery of fluorine from WPA and the deep removal of fluoride from associated acidic phosphate chemical wastewater

are important research focus in the phosphoric chemical industry.

2.2 Recovery technologies of fluorine from WPA

The recovery of fluorine from WPA has attracted considerable attention from researchers worldwide. Over the years, various technologies, as summarized in Fig. 2.1, have been developed and investigated for fluorine recovery from WPA, and each technology has its own advantages and limitations.

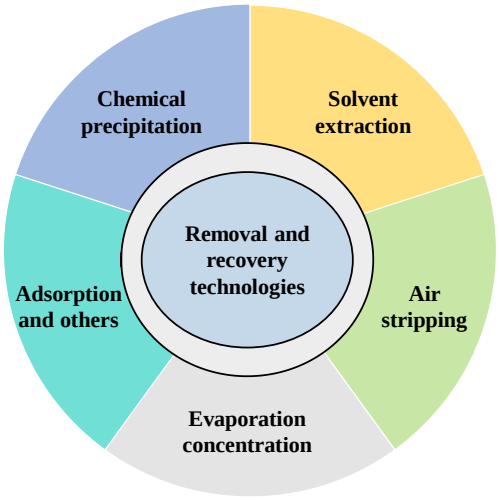


Fig. 2.1 Overview of common technologies for fluorine recovery from WPA.

2.2.1 Chemical precipitation

Chemical precipitation is one of the most mature and widely used technologies for fluorine recovery from WPA. During the treatment process, alkali metal salts, such as sodium and potassium salts, are generally used as precipitants. These salts react with fluorine species in WPA (mainly SiF_6^{2-}) to form sodium fluorosilicate (Na_2SiF_6) or potassium fluorosilicate (K_2SiF_6) precipitates, which are subsequently separated by filtration. In this way, fluorine can be effectively recovery from WPA [23]. To further promote the formation of SiF_6^{2-} and improve fluorine recovery efficiency, diatomite and white carbon black are often introduced as defluorination aids, as illustrated in Fig. 2.2. The main reactions involved in this process are shown below.

$$6HF+SiO_2=H_2SiF_6+2H_2O \quad (2.2)$$

$$2Na^+ +SiF_6^{2-}=Na_2SiF_6\downarrow \quad (2.3)$$

$$2K^+ +SiF_6^{2-}=K_2SiF_6\downarrow \quad (2.4)$$

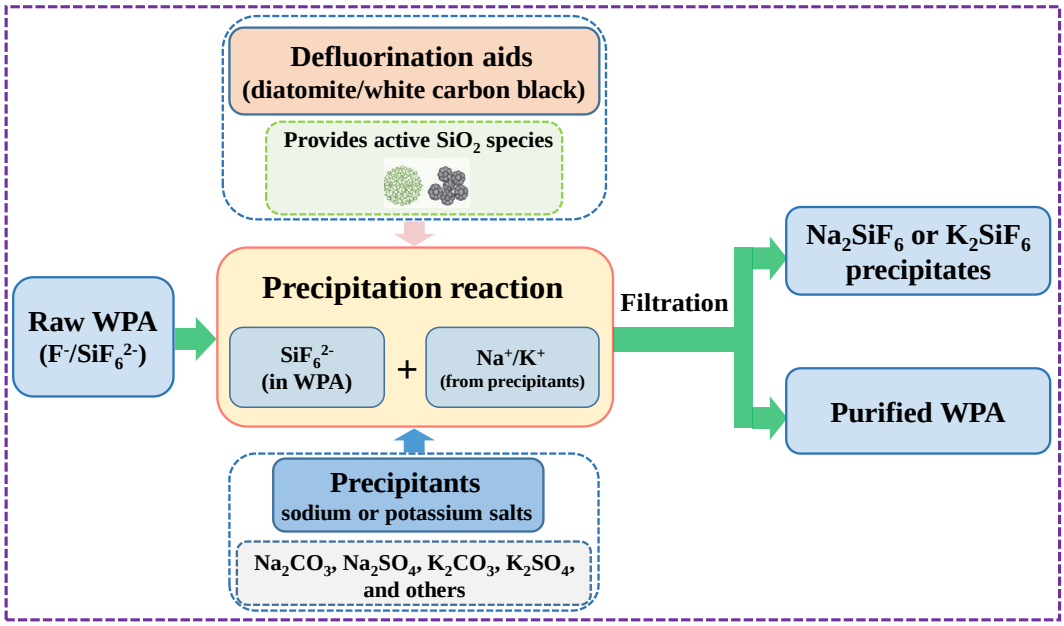


Fig. 2.2 Schematic illustration of fluorine recovery from WPA via chemical precipitation process.

EI-Asmy et al. investigated fluorine recovery from WPA using sodium carbonate (Na_2CO_3) as the precipitant and silicon dioxide (SiO_2) as a defluorination aid. Under the optimal conditions, in which 1.5772 g of Na_2CO_3 and 0.8885 g of SiO_2 were added to 150 mL of WPA at 70°C, the fluorine removal efficiency reached 93.89% [24]. He et al. proposed a two-step chemical precipitation strategy for fluorine recovery from WPA using anhydrous sodium sulfate (Na_2SO_4) and activated silica as precipitation reagents. The results showed that the fluorine content in WPA decreased from 1.21 wt% to 0.15 wt% after the two-step precipitation process, while the fluorine recovery and purity of the resulting Na_2SiF_6 product were 87.60% and >98.50 wt%, respectively. Further analysis revealed that H_2SiF_6 was removed during the first step, whereas HF and some fluorine-containing metal complexes were removed during the second step [25]. In addition, He's group proposed another economical strategy for the simultaneous removal of Al^{3+} and Mg^{2+} via the formation of aluminofluoride complexes ($NaMgAlF_6 \cdot H_2O$) using Na_2SO_4 and HF as precipitation reagents. The optimal operating conditions included a reaction temperature of 40°C, a reaction time of 12 min, and the addition of 4.00 g of Na_2SO_4 solution (40 wt%) and 4.50 g of HF solution (40 wt%) per 100 g of WPA (24.53 wt%). Due to the low solubility of the resulting complex in WPA, the removal efficiencies of Al^{3+} and Mg^{2+} reached 99.5% and 64.8%, respectively [26].

Chemical precipitation remains attractive because of its low equipment

requirements, low cost, and simple operation [27]. Although numerous precipitants and improved precipitation processes have been developed, this method still suffers from several shortcomings, including low fluorine recovery efficiency, a high residual fluorine content in WPA, and substantial P_2O_5 loss caused by the adsorption and inclusion of phosphoric acid by the precipitates [28]. Furthermore, the obtained fluorine-containing precipitates are generally of low purity, which hinders their direct utilization in subsequent processes. Currently, these shortcomings remain the major obstacles to the further industrial application of chemical precipitation.

2.2.2 Solvent extraction

Solvent extraction is another technology for fluorine recovery from WPA. As shown in Fig. 2.3, this process is based on the different distribution behaviors of fluorine species and phosphoric acid between the aqueous and organic phases. Specifically, WPA and the organic extractant are brought into countercurrent contact in an extraction unit, where H_3PO_4 is transferred into the organic phase, while most fluorine species remain in the aqueous phase. Subsequently, H_3PO_4 is back-extracted from the organic phase with water to obtain purified WPA [29].

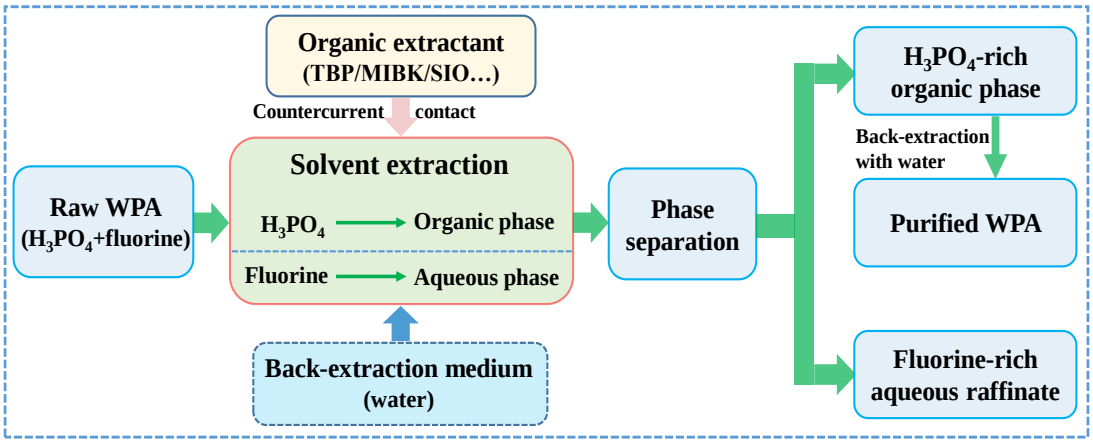


Fig. 2.3 Schematic illustration of fluorine recovery from WPA via solvent extraction process.

Ahmed et al. employed a binary solvent mixture of methyl isobutyl ketone (MIBK) and tributyl phosphate (TBP) for WPA purification. Based on a three-step extraction process, the optimal solvent composition for obtaining high WPA purity and maximum P_2O_5 recovery contained 55% MIBK. Meanwhile, a lower residual fluorine content was obtained when the percentages of MIBK and TBP in the binary solvent mixture were comparable [30]. Zuo et al. developed a liquid-liquid extraction method based on a bubble membrane for fluorine removal from WPA, with TBP and silicon oil (SIO)

chosen as the organic phase. The optimal conditions were a temperature of 90℃, a pH of 0.46, a volume ratio (TBP/SIO, v/v) of 7:3, a phase ratio (O/A) of 1:5, a stirring speed of 200 rpm, and an extraction time of 50 min. Under these conditions, the fluorine extraction efficiency reached 98.40% in a single extraction stage [31]. Amin et al. compared the fluorine removal performance of three extraction solvents, namely n-octanol, n-ethanol and n-butanol. They found that n-octanol exhibited the highest fluorine removal efficiency under identical extraction conditions. After treatment with n-octanol, the fluorine content in WPA decreased from an initial 0.70 wt% to 0.001 wt% [32].

Solvent extraction is a popular method for fluorine recovery from WPA. It offers the advantages of deep fluorine removal, no introduction of additional impurity ions, high product purity, and low environmental impact [1]. Nevertheless, this method also has several defects, including high extractant consumption, substantial equipment investment, extractant loss, and difficulties in the subsequent treatment or utilization of the large volumes of residual aqueous phase, thereby limiting its further industrial application [33].

2.2.3 Evaporation concentration

As one of the most popular technologies at present, evaporation concentration is commonly used for fluorine recovery from WPA. As illustrated in Fig. 2.4, the principle of this method is to first convert fluorine species in WPA into H_2SiF_6 by adding silicon-rich reagents, such as diatomite and white carbon black. WPA is then concentrated by heating, which increases both the solution temperature and the P_2O_5 content. Under these conditions, H_2SiF_6 decomposes into gaseous SiF_4 and HF, which volatilize from the WPA solution. Meanwhile, the residual HF further reacts with the added silicon-rich reagents to form H_2SiF_6, which decomposes again to form SiF_4 gas that escapes from the WPA solution. This cyclic reaction continues throughout the concentration process until efficient fluorine removal is achieved [34,35]. In addition to fluorine, other impurities containing iron, aluminum, calcium, and magnesium can be precipitated predominantly as metaphosphates or pyrophosphates during the concentration process and can therefore be readily removed by filtration. The relevant reactions are described as Eqs. (2.5) and (2.6).

$$H_2SiF_6 = SiF_4\uparrow + 2HF\uparrow \quad (2.5)$$

$$SiO_2 + 4HF = SiF_4\uparrow + 2H_2O \quad (2.6)$$

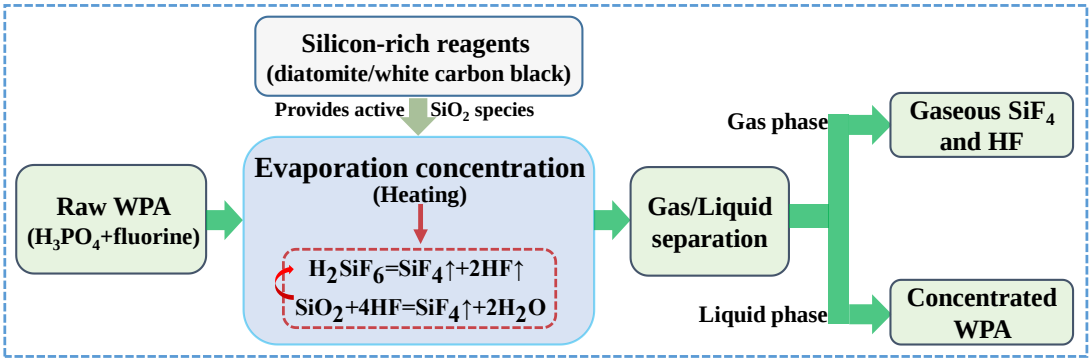


Fig. 2.4 Schematic illustration of the evaporation concentration process for fluorine recovery from WPA.

He and the co-authors proposed a microwave intensification flash evaporation (MFE) system to concentrate on highly corrosive WPA for the simultaneous preparation of polyphosphoric acid (PPA) and recovery of fluorine resources. The results showed that PPA with a P_2O_5 content of 75.36 wt% was successfully obtained, while the fluorine recovery reached 92.85%. Moreover, the operating cost of the MFE system was only 89.98% of that of the traditional system, highlighting its potential as an efficient and economical evaporation technology [36]. Peng et al. investigated the release and recovery behaviors of fluorine and iodine during the concentration process of WPA under vacuum evaporation conditions. Under the optimal concentration conditions of 15-17 kPa and 130℃, the P_2O_5 content of WPA increased to 52.34 wt%, while the recovery of fluorine and iodine reached 93.26% and 85.63%, respectively. In addition, the recovered fluorine- and iodine-containing products exhibited high purities of 97.24% and 99.47%, respectively, demonstrating that vacuum evaporation is effective for fluorine recovery [37].

Evaporation concentration provides an effective approach for reducing the fluorine content of WPA to a relatively low level while enabling fluorine recovery. Nevertheless, its performance is still limited by the lack of highly efficient fluorine-spillover reagents, resulting in unsatisfactory fluorine recovery efficiency [38].

2.2.4 Air stripping

Air stripping has emerged in recent years as a promising technology for fluorine recovery from WPA. It is well known that fluorine mainly exists in the forms of H_2SiF_6 and HF in WPA [39]. During the air stripping process, the WPA solution is heated while compressed air is introduced into the reactor. Under these conditions, the volatile fluorine-containing species are transferred from the liquid phase to the gas phase and carried away by the flowing air. To further enhance the stripping efficiency, diatomite,

white carbon black, and other reagents are often added to convert HF into the more volatile SiF_4, thereby increasing the fluorine volatilization efficiency from WPA, as schematically illustrated in Fig. 2.5. The chemical reactions involved in this process are the same as those occurring during evaporation concentration.

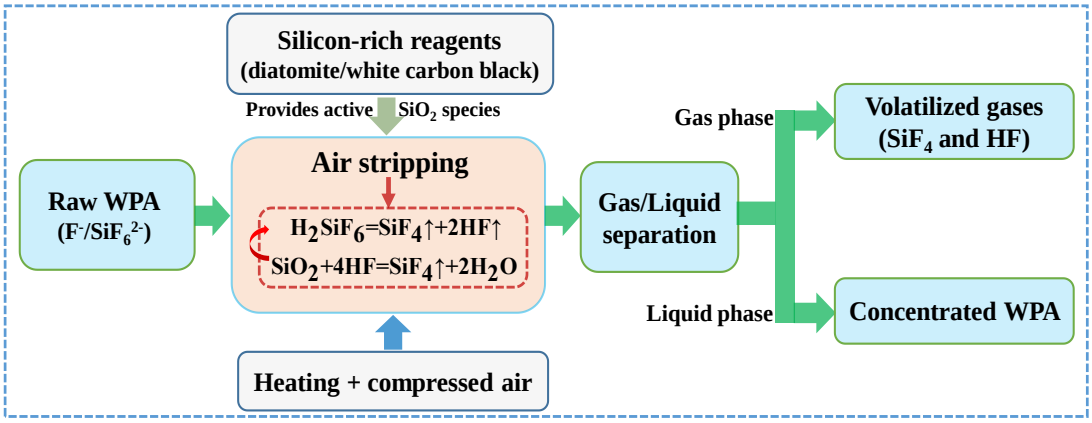


Fig. 2.5 Schematic illustration of the air stripping process for fluorine recovery from WPA.

Although air stripping has been applied in industrial practice for fluorine removal and recovery from WPA, systematic studies on this process remain relatively limited. Among the available studies, the fluorine recovery from WPA by air stripping was investigated by He et al. The authors found that H_2SiF_6 was stripped more readily than HF, while Al^{3+} inhibited fluorine recovery through the formation of Al-F complexes. Moreover, the addition of an active silicon reagent promoted fluorine recovery by facilitating the conversion of HF into H_2SiF_6 [40].

Air stripping has attracted considerable attention because of its high fluorine recovery efficiency and the production of high-purity WPA. Nevertheless, this method is limited by high equipment investment and operating costs, unstable performance, and high energy consumption, which restrict its large-scale industrial application.

2.2.5 Other technologies

Besides the above-mentioned technologies, several other technologies, including adsorption, membrane separation, and ion exchange [41,42], have also been investigated for fluorine recovery from WPA. Adsorption mainly relies on the interactions between fluorine and active sites on the adsorbent surface, thereby enabling the transfer of fluorine from the liquid phase to the solid phase. Membrane separation is based on the selective transport or retention of different species through membranes to achieve fluorine recovery from WPA, whereas ion exchange enables fluorine recovery through the exchange between fluorine-containing species and exchangeable

ions or functional groups on ion-exchange materials. These technologies provide alternative approaches for fluorine recovery from WPA and have shown potential under laboratory conditions. Nevertheless, due to the strong acidity and complex chemical environment of WPA, these technologies have limitations in terms of stability, separation efficiency, regeneration performance, and process adaptability. Therefore, their application remains largely at the laboratory scale, and large-scale industrial implementation is still limited.

2.3 Fluoride removal from acidic phosphoric chemical wastewater

For fluoride removal from acidic phosphate chemical wastewater, various technologies, including precipitation [43], ion exchange [44], electrochemical treatment [45], nanofiltration [46], and adsorption [47], have been developed and applied (as shown in Fig. 2.6). Among these technologies, adsorption is one of the most preferred approaches for fluoride removal because of its simple operation, high removal efficiency, low cost, and regenerability of adsorbents [48,49]. The performance of the adsorption process is largely determined by the properties of the adsorbent. In particular, the strong acidity and complex chemical composition of acidic phosphate chemical wastewater impose stringent requirements on the adsorption performance and structural stability of adsorbents. Under such harsh conditions, the adsorption performance and stability of adsorbents may be adversely affected, thereby limiting their long-term application in practical wastewater treatment. Whether an adsorbent is suitable for practical applications depends on several key factors, including adsorption capacity, selectivity toward fluoride, reusability, and cost. In this context, the development of adsorbents with high fluoride affinity, excellent acid resistance, structural stability, and reusability is crucial for the effective treatment of acidic phosphate chemical wastewater. Accordingly, various adsorbents have been investigated for fluoride removal from acidic phosphate chemical wastewater. Based on their composition, these adsorbents can generally be classified into metal-based composites, carbon-based composites, natural silicate mineral-based composites, as well as other functional composites.

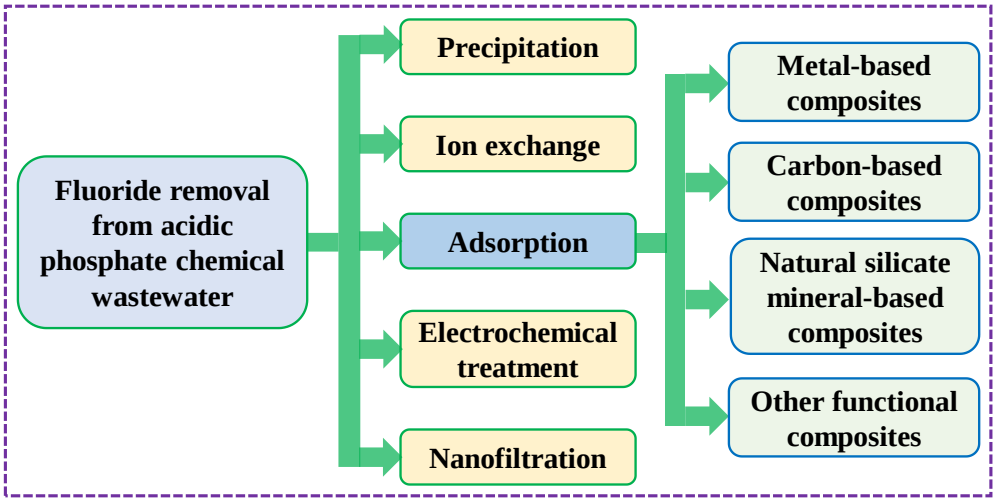


Fig. 2.6 Classification of common technologies and adsorbents for fluoride removal from acidic phosphate chemical wastewater.

2.3.1 Metal-based composites

In recent years, metal-based composites have been widely recognized highly effective adsorbents for fluoride removal from chemical wastewater or drinking water. Consequently, many metal-based composites have been developed and successfully applied by researchers, exhibiting good adsorption performance [50]. For metal-based composites, the selection of suitable metal components is of great importance and generally follows two key principles: 1) the metals should have a strong affinity for fluoride and possess excellent adsorption capacity, which is usually reflected by the formation of metal-fluoride species with sufficiently low solubility; 2) the metal resources should be abundant in nature and economically viable to facilitate large-scale practical applications. Based on these considerations and guided by the hard and soft acids and bases (HSAB) theory, researchers have identified metals such as La, Al, Fe, Ca, Ce, and Zr as suitable components for the preparation of fluoride adsorbents. In general, metal-based composites can be classified into monometallic, bimetallic, and trimetallic systems according to the number of metal components incorporated [51–53].

Shen et al. synthesized a zirconia (ZrO_2)-based composite (E-ELP-Zr) for fluoride removal. The obtained composite exhibited rapid adsorption kinetics and excellent selectivity toward fluoride. Its superior performance was mainly attributed to the strong electrostatic attraction and the specific affinity of Zr for fluoride [54]. Song et al. and Liu et al. further demonstrated that introducing two metal components is an effective strategy for enhancing fluoride adsorption. The bimetallic Ce/Zr-based metal–organic framework (Ce/Zr-MOFs) and La/Zr bimetallic-modified alumina (La/Zr-TAA) both

exhibited excellent fluoride removal performance, and the synergistic effect between the two metals enhanced fluoride adsorption [55,56]. Furthermore, Kabir et al. developed a trimetallic Mg-Al-Fe nanocomposite for fluoride removal. They systematically investigated the effects of the divalent-to-trivalent metal molar ratio and calcination temperature on fluoride adsorption, and the results showed that the optimized composite had the highest fluoride adsorption capacity of 90.68 mg/g under the conditions of a divalent-to-trivalent metal molar ratio of 5 and a calcination temperature of 400°C [57].

In summary, bimetallic and trimetallic composites generally exhibit physicochemical properties that are different from those of their monometallic counterparts. Compared with monometallic composites, bimetallic and trimetallic composites not only combine the advantages of their individual components but also show significantly improved adsorption capacities. Their superior fluoride removal efficiency is typically attributed to the synergistic effects of ligand exchange, surface protonation, and electrostatic interactions [58,59]. Nevertheless, some metal-based composites suffer from poor acid resistance, as strongly acidic conditions may cause the leaching of active metal components and structural collapse, which remains a major limitation to their application in the treatment of acidic phosphate chemical wastewater.

2.3.2 Carbon-based composites

Carbon materials have the characteristics of large specific surface areas, well-developed pore structures, abundant surface functional groups, and good physicochemical stability [60]. More importantly, carbon materials can serve as versatile support for loading metal oxides or other active components, thereby increasing the number of accessible adsorption sites and enhancing fluoride adsorption performance. Based on the above advantages, carbon materials have attracted considerable attention in the field of fluoride removal, and various carbon-based composites, including metal-loaded biochar [61], activated carbon composites [62], graphene oxide (GO)-based composites [63], and carbon nanotube composites [64], have been developed for deep fluoride removal from wastewater.

Li et al. investigated the potential of aluminum- and yttrium-modified sewage sludge biochar (Al/Y-CSBC) for efficient fluoride removal from wastewater. The results showed that Al/Y-CSBC exhibited excellent fluoride removal performance over a wide pH range. The adsorption process involved ion exchange, surface complexation, and electrostatic attraction, with a maximum adsorption capacity of 62.44 mg/g [65].

Moreover, the polyaluminum chloride (PAC) and GO co-modified zeolite (PAC@Zeolite@GO) composite was synthesized by Wang et al. for efficient fluoride removal. Under the optimal conditions, the composite showed an exceptionally high adsorption capacity of approximately 1264 mg/g and still reached 978.3 mg/g after three cycles, achieving efficient fluoride removal from acidic chemical wastewater [66]. Additionally, amorphous Al_2O_3 supported on carbon nanotubes (Al_2O_3/CNTs) and activated carbon supported Ce-Al oxides (Ce-Al-O/AC), reported by Li et al. and Guo et al., respectively, both exhibited good fluoride removal performance [67,68].

Overall, carbon-based composites are promising adsorbents for fluoride removal. Nevertheless, the affinity of carbon materials themselves for fluoride is generally lower than that of metal-based composites, and functionalization or surface modification is often required to introduce additional adsorption sites and enhance their performance. Therefore, rational modification strategies are essential for further improving the fluoride removal performance of carbon-based composites and promoting their potential application in acidic phosphate chemical wastewater treatment.

2.3.3 Natural silicate mineral-based composites

Natural silicate minerals are an important class of mineral materials, primarily composed of silicon-oxygen tetrahedra and various metal cations arranged in diverse framework, layered, or amorphous structures [69,70]. Most natural silicate minerals possess negatively charged surfaces, large specific surface areas, abundant surface hydroxyl groups, and excellent physical adsorption properties and surface chemical activity [71,72]. Owing to their abundant reserves, easy availability, low cost, high chemical stability, and ease of surface modification, natural silicate minerals, including diatomite, montmorillonite (MMT), attapulgite, and bentonite, have emerged in recent years as highly promising support materials for the preparation of adsorbents for fluoride removal from wastewater [73,74]. Nevertheless, pristine natural silicate minerals usually exhibit limited fluoride removal performance because of electrostatic repulsion, making them insufficient to meet practical application requirements. Accordingly, various modification strategies, such as metal loading [75,76], acid/base activation [77], or polymer modification [78], have been developed to improve the fluoride removal performance and engineering application potential of natural silicate minerals.

Zhang modified MMT with $CoFe_2O_4$ magnetic particles and Al-Fe fumarate metal-organic framework (Al-Fe Fum) to fabricate a magnetic composite for fluoride

removal. He found that the obtained MMT/$CoFe_2O_4$/Al–Fe Fum composite showed a maximum fluoride adsorption capacity of 27.20 mg/g, which was 1.89 times that of raw MMT (14.38 mg/g), demonstrating the effectiveness of the modification strategy [79]. La-, Mg-, and Mn-incorporated bentonite were investigated by Kamble et al. for fluoride removal from drinking water. The results showed that 10% La-bentonite exhibited superior fluoride removal performance to Mg-bentonite, Mn-bentonite and bare bentonite [80]. Furthermore, Zhang et al. studied the selective capture performance of polyethyleneimine (PEI)-modified diatomite for trace fluoride from aqueous solutions. The analyses revealed that amino functional groups were the dominant active sites responsible for fluoride removal. The modified composite exhibited an optimized microporous structure, resulting in 2.1 times increase in fluoride adsorption capacity compared with raw diatomite [81].

In addition to the aforementioned composites, many other natural silicate mineral-based composites have been developed by researchers, and they have shown great potential for fluoride removal from wastewater. These studies have demonstrated that natural silicate minerals are promising supports for constructing efficient fluoride removal composites through appropriate modification strategies.

2.4 Research gap

Over the past several decades, significant progress has been made in the field of fluorine recovery from WPA. Among the various technologies, evaporation concentration is the preferred method for fluorine recovery. Nevertheless, conventional reagents still suffer from limited reaction efficiency and low fluorine recovery, which not only result in the waste of valuable fluorine resources but also cause environmental pollution. Meanwhile, the regulation of fluorine migration, transformation, and interphase distribution in WPA by fluorine-spillover reagents and the underlying mechanisms remain insufficiently understood. Therefore, based on the reaction characteristics between fluorine species and fluorine-spillover reagents in WPA, elucidating the regulatory mechanisms of fluorine migration and transformation and developing novel reagents for efficient fluorine recovery from WPA are still among the most urgent issues to be addressed.

In addition, the associated acidic phosphate chemical wastewater is characterized by strong acidity and high fluoride concentrations, which may cause negative effects on the environment and subsequent production processes if left untreated. Nevertheless,

some currently developed adsorbents exhibit poor fluoride removal performance, mainly because of their insufficient acid resistance. Under high concentrations of hydrogen ions, these adsorbents may undergo structural collapse and the leaching of active components. More importantly, the relationships between the structural properties of composites and their fluoride adsorption behavior under strongly acidic conditions, as well as the mechanisms by which composite composition and structural regulation affect their adsorption performance and stability, still need to be further explored. Moreover, existing research has not focused sufficiently on the practical application of adsorbents in acidic phosphate chemical wastewater. Hence, elucidating the intrinsic relationships among composite structure, composition, and fluoride removal behavior, and developing targeted fluoride-removal composites with excellent acid resistance, high removal efficiency, and stable structures to adapt to the complex acidic phosphate chemical wastewater remain important issues that urgently need to be addressed.

2.5 References

[1] L. Yao, G. Shan, A. Laiba, Y. Zhao, Y. Zhang, R. Chi, B. Long, W. Li, J. Zhang, Fluoride species conversion-enhanced selective extraction: A green and safe strategy for fluorine recovery in wet-process phosphoric acid production, Journal of Environmental Chemical Engineering 13 (2025) 119345. https://doi.org/10.1016/j.jece.2025.119345.

[2] S. Luo, Y. Wang, Q. Liu, P. Li, Z. Wang, S. Yan, F. Teng, Recent progress and perspective of cathode recycling technology for spent $LiFePO_4$ batteries, Journal of Industrial and Engineering Chemistry 133 (2024) 65–73. https://doi.org/10.1016/j.jiec.2023.12.013.

[3] H. Hyrondelle, A. Terry, J. Lhoste, S. Tencé, K. Lemoine, J. Olchowka, D. Dambournet, C. Tassel, J. Gamon, A. Demourgues, Fluorine as a Key Element in Solid-State Chemistry of Mixed Anions 3d Transition Metal-Based Materials for Electronic Properties and Energy, Chem. Rev. 125 (2025) 4287–4358. https://doi.org/10.1021/acs.chemrev.4c00868.

[4] X. Xie, W. Li, L. Guo, X. Zhang, Q. Le, W. Hu, C. Hu, W. Chen, Hydrothermal synthesis of Na_2SiF_6 crystals from low-temperature activated fluorite ore: The effect of acid additives and characterization, Journal of Solid State Chemistry 362 (2026) 126200. https://doi.org/10.1016/j.jssc.2026.126200.

[5] W. Yang, J. Yang, S. Xiang, X. Zhou, X. Wang, Z. Yan, T. Luo, S. Xu, D. Xu, Separating fluorine from phosphate wastes residual via reactive roasting: Fluorine emission pattern and phosphorus polymerization mechanism, Separation and

Purification Technology 394 (2026) 137371. https://doi.org/10.1016/j.seppur.2026.137371.

[6] P. Gao, X. Wang, S. Yuan, Y. Tao, J. He, P. Tian, Mineral processing technology of fluorite: A review, JOM 77 (2025) 5151–5181. https://doi.org/10.1007/s11837-025-07399-8.

[7] H. Moradi, N. Farzi, The investigation of deep eutectic electrolyte based on Choline Chloride: Ethylene glycol in 1:3 M ratio and lithium hexafluorophosphate salt for application in Lithium-Ion batteries, Journal of Molecular Liquids 360 (2022) 119476. https://doi.org/10.1016/j.molliq.2022.119476.

[8] H. Li, C. Liu, Z. Peng, Q. Chen, R.M. Kasomo, Y. Jin, X. Weng, N.M. Ondiaka, Y. Chen, S. Song, Utilization of methyltrichlorosilane as a novel and efficient reagent to enhance fluorine recovery from wet-process phosphoric acid, Journal of Cleaner Production 444 (2024) 141295. https://doi.org/10.1016/j.jclepro.2024.141295.

[9] H. Ma, X. Feng, B. Zeng, Self-anticorrosion for the combustion tower of heat recovered thermal process phosphoric acid production, Process Safety and Environmental Protection 118 (2018) 330–347. https://doi.org/10.1016/j.psep.2018.07.008.

[10] H. Li, W. Ge, J. Zhang, R.M. Kasomo, J. Leng, X. Weng, Q. Chen, Q. Gao, S. Song, L. Xiao, C. Tian, Control foaming performance of phosphate rocks used for wet-process of phosphoric acid production by phosphoric acid, Hydrometallurgy 195 (2020) 105364. https://doi.org/10.1016/j.hydromet.2020.105364.

[11] U. Ryszko, P. Rusek, D. Kołodyńska, Quality of Phosphate Rocks from Various Deposits Used in Wet Phosphoric Acid and P-Fertilizer Production, Materials 16 (2023) 793. https://doi.org/10.3390/ma16020793.

[12] M. Forouzesh, E. Fatehifar, R. Khoshbouy, M. Daryani, Experimental investigation of iron removal from wet phosphoric acid through chemical precipitation process, Chemical Engineering Research and Design 189 (2023) 308–318. https://doi.org/10.1016/j.cherd.2022.11.041.

[13] Y. Mao, W. Zhang, H. Li, Q. Chen, R.M. Kasomo, H. Luo, S. Song, Utilization of Fenton oxidation approach in wet phosphoric acid process for mitigating foam generation, Colloids and Surfaces A: Physicochemical and Engineering Aspects 648 (2022) 129297. https://doi.org/10.1016/j.colsurfa.2022.129297.

[14] Y. Zhao, X. Li, J. Yu, C. Li, Y. Ruan, M.A. Abbas, R. Chi, Migration and transformation behaviors of phosphorus and associated elements in wet-process phosphoric acid: Acidolysis process and mechanism study, Journal of Environmental Chemical Engineering 13 (2025) 116327. https://doi.org/10.1016/j.jece.2025.116327.

[15] B. Long, Z. Wang, Q. Zhang, W. Ke, Y. Ding, Improved process to prepare high-purity anhydrous potassium fluoride from wet process phosphoric acid, Chemical Engineering Communications 205 (2018) 1342–1350. https://doi.org/10.1080/00986445.2018.1450246.

[16] Z. Shou, D. Xu, W. Yang, C. Hu, X. Wang, Z. Yan, A novel process for preparing calcium magnesium polyphosphate and recovering fluorine by utilizing the fluorine-containing phosphoric acid residue and phosphate tailings, Chemical Engineering Journal 519 (2025) 165160. https://doi.org/10.1016/j.cej.2025.165160.

[17] N.S. Awwad, Y.A. El-Nadi, M.M. Hamed, Successive processes for purification and extraction of phosphoric acid produced by wet process, Chemical Engineering and Processing: Process Intensification 74 (2013) 69–74. https://doi.org/10.1016/j.cep.2012.11.009.

[18] N. Makete, M. Rizzu, G. Seddaiu, L. Gohole, A. Otinga, Fluoride toxicity in cropping systems: Mitigation, adaptation strategies and related mechanisms. A review, Science of The Total Environment 833 (2022) 155129. https://doi.org/10.1016/j.scitotenv.2022.155129.

[19] L. Tong, X. Liu, Y. Liu, K. Zhou, S. Zhang, Q. Jia, W. Lu, Y. Huang, G. Ni, Accumulation of high concentration fluoride in the Ulungur Lake water through weathering of fluoride containing rocks in Xinjiang, China, Environmental Pollution 323 (2023) 121300. https://doi.org/10.1016/j.envpol.2023.121300.

[20] K. Wan, L. Huang, J. Yan, B. Ma, X. Huang, Z. Luo, H. Zhang, T. Xiao, Removal of fluoride from industrial wastewater by using different adsorbents: A review, Science of The Total Environment 773 (2021) 145535. https://doi.org/10.1016/j.scitotenv.2021.145535.

[21] K. Ding, S. Wu, H.-Y. Xia, H. Hu, Q. He, Y.-Y. Ding, Efficient adsorption of fluoride and phosphate from simulated wastewater using La-Mg-modified bovine bone-based biochar, Chemical Engineering Science 332 (2026) 124129. https://doi.org/10.1016/j.ces.2026.124129.

[22] H. Lü, Z. Huang, X. Wang, F. Tian, X. Lu, X. Peng, X. Hu, Near closed-loop recycling of strongly acidic wastewater via selective fluoride and heavy metal removal, Journal of Water Process Engineering 81 (2026) 109375. https://doi.org/10.1016/j.jwpe.2025.109375.

[23] R. Kijkowska, D. Pawlowska-Kozinska, Z. Kowalski, M. Jodko, Z. Wzorek, Wet-process phosphoric acid obtained from Kola apatite. Purification from sulphates, fluorine, and metals, Separation and Purification Technology 28 (2002) 197–205. https://doi.org/10.1016/S1383-5866(02)00048-5.

[24] A.A. El-Asmy, H.M. Serag, M.A. Mahdy, M.I. Amin, Purification of phosphoric acid by minimizing iron, copper, cadmium and fluoride, Separation and Purification Technology 61 (2008) 287–292. https://doi.org/10.1016/j.seppur.2007.11.004.

[25] B. He, Y. Zhu, Y. Zu, Y. Nie, Y. Mei, Efficient and cost-effective fluorine recovery from liquid-phase wet-process phosphoric acid via two-step precipitation method, Separation and Purification Technology 325 (2023) 124687. https://doi.org/10.1016/j.seppur.2023.124687.

[26] B. He, Y. Zhu, D. Xie, Y. Nie, Y. Mei, Removal of Al^{3+} and Mg^{2+} ions in wet-process phosphoric acid via the formation of aluminofluoride complexes,

Environmental Technology 44 (2023) 936–947. https://doi.org/10.1080/09593330.2021.1989055.

[27] L. Tian, L. Chen, A. Gong, X. Wu, C. Cao, Z. Xu, Recovery of rare earths, lithium and fluorine from rare earth molten salt electrolytic slag via fluoride sulfate conversion and mineral phase reconstruction, Minerals Engineering 170 (2021) 106965. https://doi.org/10.1016/j.mineng.2021.106965.

[28] A.A. El-Bayaa, N.A. Badawy, A.M. Gamal, I.H. Zidan, A.R. Mowafy, Purification of wet process phosphoric acid by decreasing iron and uranium using white silica sand, Journal of Hazardous Materials 190 (2011) 324–329. https://doi.org/10.1016/j.jhazmat.2011.03.037.

[29] Z. Wu, Y. Peng, J. Li, L. She, J. Xue, J. Ma, Y. Zheng, T. Wang, C. Wang, R. Peng, The mass transfer and mechanism of H_3PO_4 from low concentration HCl-route wet-process phosphoric acid by the mixture of n-butanol and isopropyl ether, Separation and Purification Technology 281 (2022) 119851. https://doi.org/10.1016/j.seppur.2021.119851.

[30] A. Hannachi, D. Habaili, C. Chtara, A. Ratel, Purification of wet process phosphoric acid by solvent extraction with TBP and MIBK mixtures, Separation and Purification Technology 55 (2007) 212–216. https://doi.org/10.1016/j.seppur.2006.12.014.

[31] Y. Zuo, Q. Chen, C. Li, C. Kang, X. Lei, Removal of fluorine from wet-process phosphoric acid using a solvent extraction technique with tributyl phosphate and silicon oil, ACS Omega 4 (2019) 11593–11601. https://doi.org/10.1021/acsomega.9b01383.

[32] M.I. Amin, M.M. Ali, H.M. Kamal, A.M. Youssef, M.A. Akl, Recovery of high grade phosphoric acid from wet process acid by solvent extraction with aliphatic alcohols, Hydrometallurgy 105 (2010) 115–119. https://doi.org/10.1016/j.hydromet.2010.08.007.

[33] K. Li, J. Chen, D. Zou, Recovery of fluorine utilizing complex properties of cerium(IV) to obtain high purity CeF_3 by solvent extraction, Separation and Purification Technology 191 (2018) 153–160. https://doi.org/10.1016/j.seppur.2017.09.010.

[34] B.S. Vieira, D. Gullberg, V. Perrot, Recent experience with metallic heaters for phosphoric acid evaporation, Procedia Engineering 138 (2016) 437–444. https://doi.org/10.1016/j.proeng.2016.02.103.

[35] X. Zhou, S. Tian, Y. Guo, W. Jiang, C. Bao, S. Ju, Case study of preparation polyphosphoric acid from wet phosphoric acid via microwave heating strengthen flash evaporation process: Production path, product analysis and economic evaluation, Separation and Purification Technology 375 (2025) 133228. https://doi.org/10.1016/j.seppur.2025.133228.

[36] B. He, S. Tian, S. Ju, Y. Zu, Y. Mei, Preparation of polyphosphoric acid and recovery of valuable fluorine resources though a microwave intensification flash

evaporation process, Chemical Engineering and Processing - Process Intensification 189 (2023) 109397. https://doi.org/10.1016/j.cep.2023.109397.

[37] B. Peng, Z. Ma, Y. Zhu, L. Tang, Release and recovery of fluorine and iodine in the production and concentration of wet-process phosphoric acid from phosphate rock, Minerals Engineering 188 (2022) 107843. https://doi.org/10.1016/j.mineng.2022.107843.

[38] B. He, Y. Zhu, Y. Zu, Y. Nie, Y. Mei, Designing an efficient fluorine recovery strategy for Wet-Process phosphoric acid purification by disclosing competitive complexation behavior between fluorine species and metal cations, Separation and Purification Technology 320 (2023) 124219. https://doi.org/10.1016/j.seppur.2023.124219.

[39] L. Li, J. Zhou, R. Yu, X. Chen, Y. Chen, K. Wu, Z. Gao, G. Zhu, W. Jiang, Study on the forms and volatilization behavior of hydrogen fluoride in phosphoric acid with deep potential molecular dynamics (DPMD), Journal of Molecular Liquids 441 (2026) 129066. https://doi.org/10.1016/j.molliq.2025.129066.

[40] B. He, Y. Zu, Y. Nie, Y. Mei, Investigation on the fluorine recovery mechanism by air stripping for synthetic and industrial wet process phosphoric acid, Carbon Lett. 33 (2023) 2313–2325. https://doi.org/10.1007/s42823-023-00573-5.

[41] J. Zhang, C. Tian, Y. Xu, J. Chen, L. Xiao, G. Wu, F. Jin, Effective removal of fluorine ions in phosphoric acid by silicate molecular sieve synthesized by hexafluorosilicic acid, Separation and Purification Technology 305 (2023) 122395. https://doi.org/10.1016/j.seppur.2022.122395.

[42] K. Khaless, H. Chanouri, S. Amal, A. Ouaattou, E.M. Mounir, H. Haddar, R. Benhida, Wet process phosphoric acid purification using functionalized organic nanofiltration membrane, Separations 9 (2022) 100. https://doi.org/10.3390/separations9040100.

[43] X. Lu, X. Hu, L. Kong, B. Men, J. Li, X. Peng, Removal of fluoride from strongly acidic wastewater using sodium methylsilicate: Efficiency and mechanism, Journal of Environmental Chemical Engineering 14 (2026) 122509. https://doi.org/10.1016/j.jece.2026.122509.

[44] Z. Chen, J. Qin, Q. Ren, X. Wang, J. Wang, X. Song, W. Yan, Z. Wang, Reversible and selective fluoride removal leveraging electrochemically switchable ion exchange of cis-polyaniline, Journal of Environmental Chemical Engineering 14 (2026) 123102. https://doi.org/10.1016/j.jece.2026.123102.

[45] P. Thamarai, V.C. Deivayanai, S. Karishma, P.R. Yaashikaa, A. Saravanan, Effective removal of fluoride ions from contaminated water using electrochemical techniques: A critical review on recent developments and environmental perspective, Journal of Hazardous Materials Advances 16 (2024) 100483. https://doi.org/10.1016/j.hazadv.2024.100483.

[46] S.V. Jadhav, Kumudini.V. Marathe, V.K. Rathod, A pilot scale concurrent removal of fluoride, arsenic, sulfate and nitrate by using nanofiltration: Competing ion

interaction and modelling approach, Journal of Water Process Engineering 13 (2016) 153–167. https://doi.org/10.1016/j.jwpe.2016.04.008.

[47] G. Zhang, H. He, S. Liu, Z. Du, L. Lv, L. Sun, J. Zhang, J. Liang, La-Al modified Fe3O4 adsorbent for adsorption performance and mechanism of low P concentration in water, Journal of Water Process Engineering 68 (2024) 106344. https://doi.org/10.1016/j.jwpe.2024.106344.

[48] S. Zheng, Y. Shu, C. Zhu, B. Chen, Y. Xu, W. Chen, M. Wang, S. Cao, Z. Liu, F. Wang, Y. Han, Z. Wang, Synergistic regulation of oxygen vacancies and surface hydroxyl groups in Fe-doped CeO_2 for enhanced fluoride adsorption, Chemical Engineering Journal 529 (2026) 172566. https://doi.org/10.1016/j.cej.2026.172566.

[49] Q. Zhou, H. Xiang, Y. Dai, J. Xiong, F. Jiang, Z. Lin, S. Wang, X. Yang, Rational design of MOF-COF composites for synergistic low-concentration fluoride adsorption: Mechanistic insights and DFT validation, Separation and Purification Technology 384 (2026) 136374. https://doi.org/10.1016/j.seppur.2025.136374.

[50] U.O. Aigbe, O.A. Osibote, Fluoride ions sorption using functionalized magnetic metal oxides nanocomposites: a review, Environ Sci Pollut Res 29 (2022) 9640–9684. https://doi.org/10.1007/s11356-021-17571-7.

[51] H. Ma, Y. Huang, J. Tang, W. Wang, B. Liu, H. Sun, S. Yang, G. Han, Enhanced fluoride removal via adsorption flotation based on La-MOF carrier morphology modulation strategy, Separation and Purification Technology 365 (2025) 132652. https://doi.org/10.1016/j.seppur.2025.132652.

[52] G. Sun, J. Zhen, Z. Shao, Z. Xu, J. Ming, X. Liu, S.-Q. Ni, Synthesis of La/Ce bimetallic MOF@Zeolite composites for efficient fluoride removal: Performance and mechanisms, Desalination 631 (2026) 120231. https://doi.org/10.1016/j.desal.2026.120231.

[53] X. Wang, H. Pfeiffer, J. Wei, J. Dan, J. Wang, J. Zhang, 3D porous Ca-modified Mg-Zr mixed metal oxide for fluoride adsorption, Chemical Engineering Journal 428 (2022) 131371. https://doi.org/10.1016/j.cej.2021.131371.

[54] D. Shen, Y. Song, X. Chen, Y. Zhou, H. Li, J. Pan, Fabricating ultrafine zirconium oxide based composite sorbents in “soft confined space” for efficiently removing fluoride from environmental water, Chemical Engineering Journal 444 (2022) 136199. https://doi.org/10.1016/j.cej.2022.136199.

[55] J. Song, L. Ji, L. Rao, Z. Zhang, X. Chen, Y. Wang, J. Hu, X.-G. Li, J. Ma, Enhanced fluoride adsorption onto bimetallic Ce/Zr-MOFs with a high selectivity: Characterization and mechanism, Journal of Colloid and Interface Science 704 (2026) 139370. https://doi.org/10.1016/j.jcis.2025.139370.

[56] Y. Liu, T. Liao, H. Xiang, M. Chen, S. Wang, Z. Wang, H. Li, H. Huang, Synergistic La–Zr modification of alumina enhanced charge number and active sites for superior fluoride adsorption, Colloids and Surfaces A: Physicochemical and Engineering Aspects 742 (2026) 140274. https://doi.org/10.1016/j.colsurfa.2026.140274.

[57] H. Kabir, A.K. Gupta, D. Debnath, Synthesis, optimization and characterization of mesoporous Mg-Al-Fe tri-metal nanocomposite targeting defluoridation: Synergistic interaction of molar ratio and thermal activation, Journal of Molecular Liquids 268 (2018) 376–385. https://doi.org/10.1016/j.molliq.2018.07.073.

[58] K. Yadav, O.P. Gautam, B.S. Rathore, M. Kour, N.P.S. Chauhan, Recent advances in bimetallic metal-organic frameworks (MOFs): Synthesis, properties, and their water remediation applications, Inorganic Chemistry Communications 186 (2026) 116316. https://doi.org/10.1016/j.inoche.2026.116316.

[59] Z. Zeng, Q. Li, J. Yan, L. Huang, S.R.B. Arulmani, H. Zhang, S. Xie, W. Sio, The model and mechanism of adsorptive technologies for wastewater containing fluoride: A review, Chemosphere 340 (2023) 139808. https://doi.org/10.1016/j.chemosphere.2023.139808.

[60] Y. Li, Y. Xiao, T. Lu, G. He, Z. Ding, D. Wang, P. Zhang, Y. Hu, MgO modified sucrose-derived porous carbon composite for fluoride adsorption, Desalination and Water Treatment 319 (2024) 100529. https://doi.org/10.1016/j.dwt.2024.100529.

[61] L. Huang, Z. Luo, X. Huang, Y. Wang, J. Yan, W. Liu, Y. Guo, S.R. Babu Arulmani, M. Shao, H. Zhang, Applications of biomass-based materials to remove fluoride from wastewater: A review, Chemosphere 301 (2022) 134679. https://doi.org/10.1016/j.chemosphere.2022.134679.

[62] F. Zheng, S. Guo, J. Xu, J. Jiang, C. Wu, Q. Sun, Y. Zheng, Y. Lin, Polyvinylpyrrolidone-modified Ce Al bimetallic oxide loaded on recyclable activated carbon for selective fluoride ion removal from aqueous solutions, Journal of Water Process Engineering 75 (2025) 107984. https://doi.org/10.1016/j.jwpe.2025.107984.

[63] L. Lalhmunsiama, N. Ngainunsiami, D.-J. Kim, D. Tiwari, Graphene based advanced materials in the remediation of aquatic environment contaminated with fluoride: Newer insights and applicability, Chemical Engineering and Processing - Process Intensification 165 (2021) 108428. https://doi.org/10.1016/j.cep.2021.108428.

[64] I. Rostami, A.H. Mahvi, M.H. Dehghani, A.N. Baghani, R. Marandi, Application of nano aluminum oxide and multi-walled carbon nanotube in fluoride removal, Desalination and Water Treatment 72 (2017) 368–373. https://doi.org/10.5004/dwt.2017.20699.

[65] S. Li, M. Song, L. Tong, C. Ye, Y. Yang, Q. Zhou, Enhancing fluoride removal from wastewater using Al/Y amended sludge biochar, Environ Sci Pollut Res 30 (2023) 125832–125845. https://doi.org/10.1007/s11356-023-31147-7.

[66] T. Wang, J. Liu, T. Li, J. Mao, Z. Shao, X. Li, S. Ren, Construction of PAC@Zeolite@GO composite with high adsorption capacity and environmentally friendly for defluoridation by synergistic effects, Microporous and Mesoporous Materials 387 (2025) 113521. https://doi.org/10.1016/j.micromeso.2025.113521.

[67] Y.-H. Li, S. Wang, A. Cao, D. Zhao, X. Zhang, C. Xu, Z. Luan, D. Ruan, J. Liang, D. Wu, B. Wei, Adsorption of fluoride from water by amorphous alumina

supported on carbon nanotubes, Chemical Physics Letters 350 (2001) 412–416. https://doi.org/10.1016/S0009-2614(01)01351-3.

[68] S. Guo, F. Zheng, J. Xu, J. Jiang, Z. Cui, C. Wu, Y. Lin, Q. Sun, Y. Zheng, B. Sa, Enhanced fluoride removal from drinking water by activated carbon supported Ce–Al oxides: performance and mechanism, RSC Adv. 15 (2025) 14363–14374. https://doi.org/10.1039/D5RA00397K.

[69] R. Srinivasan, Advances in application of natural clay and its composites in removal of biological, organic, and inorganic contaminants from drinking water, Advances in Materials Science and Engineering 2011 (2011) 1–17. https://doi.org/10.1155/2011/872531.

[70] X. Hang, Progress and perspectives on cost-effective and eco-friendly mineral functional materials for efficient capture of fluoride and phosphorus, Materials Today Sustainability 27 (2024) 100923. https://doi.org/10.1016/j.mtsust.2024.100923.

[71] S.I. Alhassan, H. Wang, Y. He, L. Yan, Y. Jiang, B. Wu, T. Wang, H. Gang, L. Huang, L. Jin, Y. Chen, Fluoride remediation from on-site wastewater using optimized bauxite nanocomposite (Bx-Ce-La@500): Synthesis maximization, and mechanism of F─ removal, Journal of Hazardous Materials 430 (2022) 128401. https://doi.org/10.1016/j.jhazmat.2022.128401.

[72] M. Mobarak, A.Q. Selim, E.A. Mohamed, M.K. Seliem, Modification of organic matter-rich clay by a solution of cationic surfactant/H_2O_2: A new product for fluoride adsorption from solutions, Journal of Cleaner Production 192 (2018) 712–721. https://doi.org/10.1016/j.jclepro.2018.05.044.

[73] G. Zhang, Z. He, W. Xu, A low-cost and high efficient zirconium-modified-Na-attapulgite adsorbent for fluoride removal from aqueous solutions, Chemical Engineering Journal 183 (2012) 315–324. https://doi.org/10.1016/j.cej.2011.12.085.

[74] A.W. Kalsido, A. Kumar, B. Tekola, B. Mogessie, E. Alemayehu, Evaluation of bentonite clay in modified and unmodified forms to remove fluoride from water, Water Science and Technology 84 (2021) 2661–2674. https://doi.org/10.2166/wst.2021.220.

[75] A. Vinati, B. Mahanty, S.K. Behera, Clay and clay minerals for fluoride removal from water: A state-of-the-art review, Applied Clay Science 114 (2015) 340–348. https://doi.org/10.1016/j.clay.2015.06.013.

[76] V. Kumari, R. Budania, V. Chavda, Design of iron-loaded montmorillonite clay–pectin polymer composite for efficient fluoride removal: Adsorption equilibrium, kinetics, and thermodynamic insights, Materials Chemistry and Physics 361 (2026) 132696. https://doi.org/10.1016/j.matchemphys.2026.132696.

[77] J. Wang, Y. Li, J. Liu, M. Zhai, M. Li, A. Xu, M. Jia, Resource utilization of acid-leaching clay wastewater to prepare layered double oxides for effective fluoride removal, Journal of Water Process Engineering 69 (2025) 106859. https://doi.org/10.1016/j.jwpe.2024.106859.

[78] Y. Zhang, H. Zhang, J. Zhao, X. Zhang, Z. Cao, B. Jiang, Efficient adsorption of fluoride ions by polyethyleneimine modified diatomite under different conditions in a fixed bed column, Desalination and Water Treatment 307 (2023) 153–161. https://doi.org/10.5004/dwt.2023.29906.

[79] M. Zhang, Enhanced fluoride removal using montmorillonite clay modified with $CoFe_2O_4$ and metal-organic frameworks, Environmental Research 258 (2024) 119389. https://doi.org/10.1016/j.envres.2024.119389.

[80] S.P. Kamble, P. Dixit, S.S. Rayalu, N.K. Labhsetwar, Defluoridation of drinking water using chemically modified bentonite clay, Desalination 249 (2009) 687–693. https://doi.org/10.1016/j.desal.2009.01.031.

[81] Y. Zhang, H. Zhang, J. Zhao, X. Zhang, Enhanced adsorption of fluoride ion by polyethylenimine modified diatomite in aqueous solution: adsorption optimization, models, and mechanism, Desalination and Water Treatment 283 (2023) 130–140. https://doi.org/10.5004/dwt.2023.29218.

Chapter 3. Efficient fluorine recovery from wet-process phosphoric acid using silicon powder as a fluorine-spillover reagent

3.1. Introduction

Fluorine is an important strategic resource that is widely used in metallurgy, electronics, agriculture, and others fields [1,2]. Most of the fluorine resources in nature were associated with fluorite and phosphate rock [3,4]. Fluorite, as a high-grade fluorine ore, has traditionally been the primary source of fluorine resources. However, the global reserve of fluorite was only 320 million tons in 2019 [5]. With the rapid development of fluorine-containing products, such as separator membranes for lithium-ion batteries and electrolytes, fluorite reserves were already in short supply [6]. In comparison, it has been reported that about 90% of fluorine resources in nature had existed in phosphate rock. The fluorine content in phosphate rock was usually 2 - 4 wt% [7]. In this case, it has become extremely urgent to utilize the fluorine resources from phosphate rock.

Phosphate rock is the main raw material for phosphoric acid production. According to available data, more than 90% of phosphate rock is currently used to produce wet-process phosphoric acid (WPA) in industry [8,9]. During the production process of WPA, fluorine affects the quality of WPA and downstream products. It has been reported that fluorine in phosphate rock could remain in WPA and enter downstream products. Fluorine-containing pollutants would then enter groundwater, air, and other environmental media, resulting in a significant hazard to human health and the environment [10]. In addition, fluorine could also cause trees and crops to turn yellow and even die; excessive fluorine intake could harm humans by causing skeletal fluorosis [11]. Given these adverse effects, it is necessary to remove fluorine from WPA. However, it should be noted that fluorine is also a valuable resource in a variety of applications and fields [12]. Therefore, separating and recovering fluorine from WPA are of great significance for protecting the environment and human health and providing low-cost raw materials for the fluorochemical industry.

Nowadays, for the separation and recovery of fluorine from WPA, evaporation concentration is considered to be a promising method due to its simple operation and

low operating cost. The principle of this method involves the conversion of liquid fluosilicic acid (H_2SiF_6) into gaseous silicon tetrafluoride (SiF_4) and hydrogen fluoride (HF) upon heating, along with the evaporation of HF originally present in WPA. By collecting and absorbing SiF_4 and HF gases into water, these two gases can be converted back into H_2SiF_6. In this way, fluorine resources could be recovered and utilized in an environmentally friendly manner [13]. The reaction was shown in Eq. (3.1). However, the traditional concentration method also suffers from low fluorine recovery, resulting in the waste of valuable fluorine resources [14]. For example, He et al. used an air stripping concentration method to treat WPA at 90℃ for 90 min, and the fluorine recovery was only about 38% [1]. Therefore, how to effectively improve the fluorine recovery from WPA is still of great significance, and the development of a novel strategy is urgently required.

$$SiF_4+2HF=H_2SiF_6 \quad (3.1)$$

It is well known that SiF_4 gas has higher vapor pressure than HF gas. As a result, researchers had observed that increasing the formation of SiF_4 gas was the key to enhancing fluorine recovery. For this purpose, the reagents containing active silicon had attracted considerable attention. These reagents had the characteristics of high active silicon content, irregular crystal structure and good reactivity. During the concentration process of WPA, they tend to react with H_2SiF_6 and HF to promote the formation of SiF_4 gas, thereby increasing the fluorine recovery [15,16]. Accordingly, diatomite and white carbon black (WCB) were the most commonly used reagents for fluorine recovery. However, these traditional silicon-rich reagents have limited efficiency in promoting SiF_4 formation and volatilization because their reactions with fluorine species are hindered by inherent impurities [17]. Furthermore, these reagents had some adsorption effects on fluorine, and a portion of fluorine would migrate into the solid phase during the concentration process [16,18]. Therefore, investigating new environmentally friendly and efficient reagents to enhance the fluorine recovery during the concentration process of WPA is of great practical significance.

Among the many reagents, active silicon powder (SP) caught the authors' attention. SP is a substance that contains activated monatomic silicon [19]. It has been reported that SP is characterized by a large specific surface area and an uneven crystal structure [20]. These characteristics make it highly reactive. In addition, the adsorption properties of SP toward fluorine have not been reported yet. Hence, the above advantages of SP make up for some defects of traditional reagents and have the potential to further

enhance fluorine recovery from WPA. However, the application of SP in promoting fluorine recovery from WPA and its gasification mechanism have not been studied yet.

As such, the objective of this work is to investigate the performance of SP as the fluorine-spillover reagent to enhance fluorine gasification during the concentration process of WPA. The superiority of SP was evaluated through comparative experiments. On this basis, the effects of operating parameters in the reaction system, including SP dosage, stirring speed, and concentration temperature, as well as those in the absorptive system, including initial mass of absorptive water, were systematically investigated. Finally, spillover kinetics, thermodynamic calculations, and a series of characterizations were used to preliminarily explore the gasification mechanism.

3.2. Experimental

3.2.1. Materials and reagents

The WPA sample used in this experiment was obtained from Hubei Sanning Chemical Co. Ltd. The detailed information on the anion and cation contents of WPA was presented in Table 3.1. As can be seen, the content of phosphate (PO_4^{3-}) was 36.11 wt%, which was suitable for further concentration experiments. The fluorine content in WPA reached 0.80 wt%, indicating the need for fluorine removal and recovery. Besides these, the contents of all other metallic impurities were less than 1 wt%.

Table 3.1 The anions and cations contents of WPA (wt%).

Composition	PO_4^{3-}	F	Cl^-	SO_4^{2-}	Ca^{2+}	Mg^{2+}	Al^{3+}	Fe^{3+}	Si^{4+}	Na^+	K^+
Mass fraction	36.11	0.80	0.16	2.89	0.06	0.94	0.42	0.13	0.24	0.14	0.32

SP was procured from Xintie Metal Co Ltd, China. Diatomite, WCB, and zeolite powder (ZP) were all obtained from Lingshou Minerals Co., Ltd, China. The compositions and physical phases of these reagents are shown in Table 3.2 and Fig. 3.1. The main component of SP is Si, with a content of 99.65 wt%. Correspondingly, the sharp diffraction peaks attributed to Si are observed in the XRD pattern of SP, while no obvious impurity peaks are observed, implying the high purity of this reagent (Fig. 3.1a). In contrast, the principal component of diatomite, WCB and ZP is SiO_2 with contents of 94.18, 91.77, and 85.26 wt%, respectively. Apart from SiO_2, some associated impurities, such as Na_2O, Al_2O_3, and Fe_2O_3, are also present. The XRD patterns of these three reagents also confirm the above results, with several impurity peaks observed in their patterns (Fig. 3.1b-d).

Table 3.2 The compositions of different reagents used in the experiments (wt%).

SP	Compositions	Si	CaO	Fe_2O_3	Others	
	Contents	99.65	0.02	0.04	0.29	
Diatomite	Compositions	SiO_2	Na_2O	Al_2O_3	Fe_2O_3	Others
	Contents	94.18	1.97	2.15	1.06	0.64
WCB	Compositions	SiO_2	Na_2O	Al_2O_3	Fe_2O_3	Others
	Contents	91.77	2.28	2.34	1.22	2.39
ZP	Compositions	SiO_2	Na_2O	Al_2O_3	Fe_2O_3	Others
	Contents	85.26	1.52	8.07	3.14	2.01

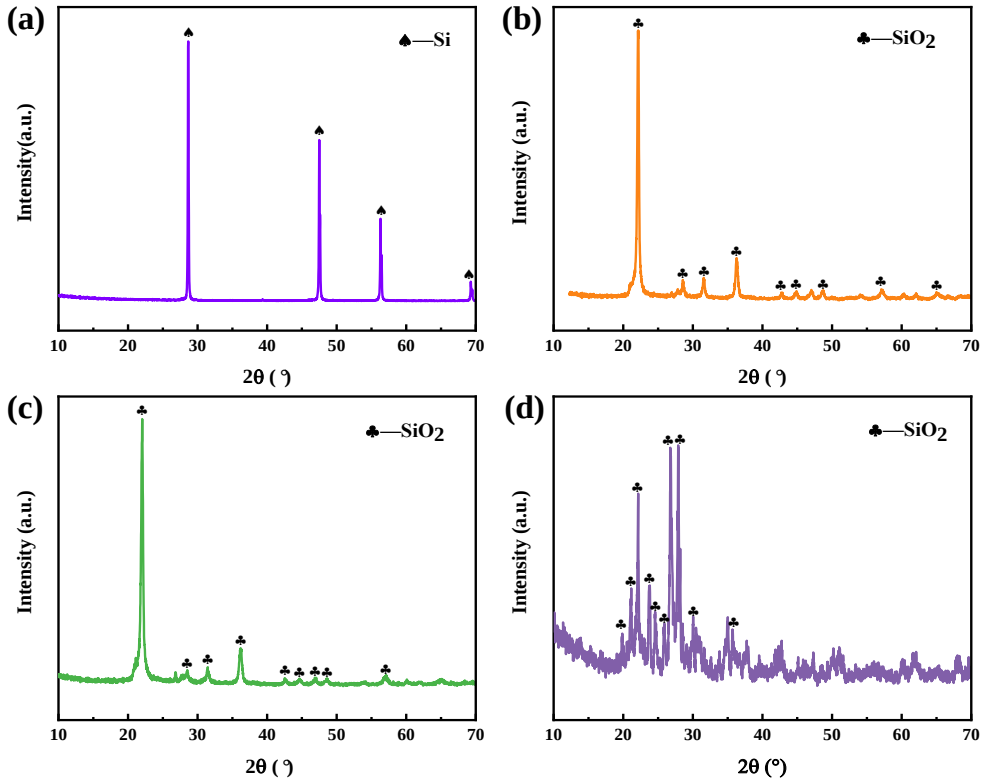


Fig. 3.1 XRD patterns of (a) SP, (b) Diatomite, (c) WCB and (d) ZP.

Hydrochloric acid (HCl), nitric acid (HNO_3), sodium hydroxide (NaOH), citric acid ($C_6H_5O_7 \cdot 2H_2O$), and trisodium citrate ($Na_3C_6H_5O_7 \cdot 2H_2O$) were purchased from Sinopharm Chemical Reagent Corporation Ltd., China, and used to determine the fluorine contents. All the purchased reagents were of analytical grade and used without additional purification. The deionized water (18.25 MΩ) was directly obtained from Milli-Q Direct 16 water purification system (Millipore Q, USA) and used throughout the experiments.

3.2.2. Fluorine recovery test

The fluorine recovery experiments were conducted using a homemade device. This device was designed based on the principle of the evaporation concentration

method and existing industrial WPA concentration systems. A thermostatic magnetic stirrer, a 250 mL three-neck flask, and a straight condenser were comprised in the device (Fig. 3.2). The fluorine recovery experiments were carried out as follows. First, 100.00 g of WPA with a blank (0.00 g) and four masses of SP (0.25, 0.50, 0.75, and 1.00 g) were added into the three-neck flask and sealed with rubber plug. The flask was placed in the oil bath and heated at different temperatures and agitated at different speeds to get a uniform slurry mixture. Meanwhile, the evolved gas was collected into deionized water through the straight condenser. When the WPA solution was concentrated to about half of its original mass, the heating was stopped, and the total mass of the absorptive solution (AS) was recorded. Afterwards, the concentrated WPA was cooled and filtered to obtain purified WPA and de-fluorinated slag (DS). DS was dried at 200℃ for 120 min and ground into a powder. The masses of purified WPA and dried DS were also recorded. Finally, the fluorine contents of WPA, AS and DS were measured to calculate the fluorine recovery. The calculation equation was shown in Eq. (3.2).

$$R=\frac{m_2\beta}{m_1\alpha+m_2\beta+m_3\gamma}\times 100 \tag{3.2}$$

where R represents the recovery of fluorine, %; m_1, m_2, and m_3 are the masses of WPA, AS and DS, respectively, g; α, β and γ are fluorine contents of WPA, AS and DS, respectively, wt%.

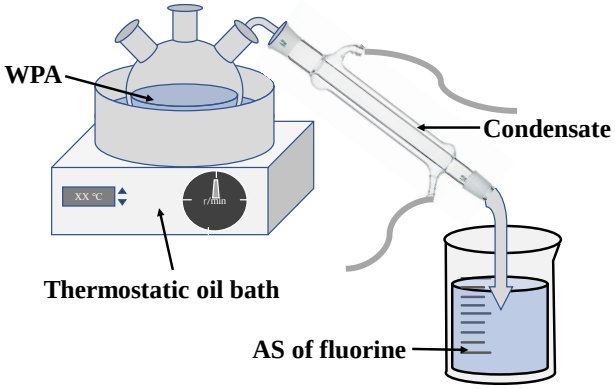


Fig. 3.2 The diagram of the fluorine recovery test device.

3.2.3. Spillover kinetics test

The spillover kinetics test was carried out under the optimal concentration conditions of SP. In this process, 3 mL AS samples were taken using a syringe at selected times (5, 10, 20, 30, 40, 60, 90, 120, 150, and 180 min). The collected solutions were immediately used for the measurement of the fluorine contents to obtain the kinetics data.

3.2.4. Determination of fluorine contents

In this work, Fluorine Ion Selective Electrode (PF-2-01) was used to measure the fluorine contents of WPA and AS. The details of this method had been described elsewhere [1,21]. Typically, it should be noted that the measurement conditions, such as stirring speed, must remain consistent during each measurement. The measured value would be recorded when it remained stable for 20 seconds.

The fluorine content of DS was also measured by Fluorine Ion Selective Electrode. This method was adapted from a Chinese graduation thesis, and the specific procedure was as follows. First, 4.00 g of NaOH was placed in a nickel crucible and melted at 320 °C for 5 min. After cooling to room temperature, 1.00 g of DS was placed in the nickel crucible and covered with 4.00 g of NaOH. The crucible was then heated at 650 °C for 10 min and allowed to cool to 50°C. Next, the crucible was placed in a 250 mL beaker, 50 mL of boiling water was added, and the crucible was immediately covered with a watch glass for 5 min. The watch glass was removed and rinsed with a small volume of water, and boiling water was used to rinse the crucible. Then, 10 mL of concentrated HCl was added, and the solution was heated with stirring until clear. After cooling to room temperature, the solution was diluted to 250 mL. Finally, the solution was filtered and used to measure the fluorine content of DS. The measurement process was consistent with the described measurement method of WPA.

The fluorine standard line was shown in Fig. 3.3. The correlation coefficient (R^2) was 0.998, which is satisfied for calculation of fluorine contents.

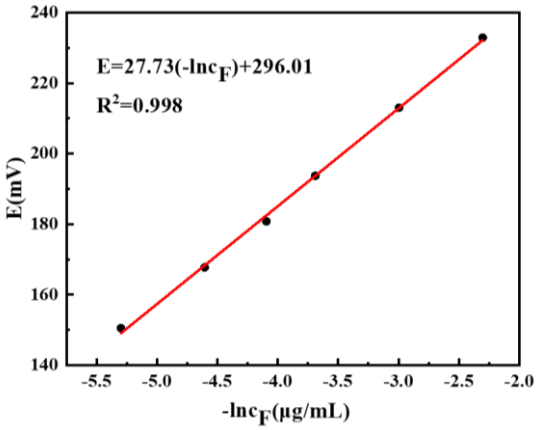


Fig. 3.3 The standard line for fluorine contents.

3.2.5 Characterizations

Ion Chromatograph (IC: Metrohm ICS-1100) and Inductively Coupled Plasma Optical Emission Spectrometer (ICP-OES: Thermo Fisher Scientific, ICAP 7400, USA) were adopted to gain the contents of anions and cations in concentrated WPA,

respectively. The morphological features and elemental distribution of DS were observed using a scanning electron microscope (SEM: JSM-IT800, JEOL, Japan) with an energy dispersive spectrometer (EDS). X-ray diffraction (XRD) patterns of DS were obtained by a Bruker D8 Advance X-ray diffractometer in the test range of 10 - 70°. The tube voltage and current were 40 kV and 150 mA, respectively. The scanning mode of the instrument was reflection mode. The scanning step and speed were 0.02° and 5°/min, respectively.

3.3. Results and discussion

3.3.1. Different reagent comparative test

In order to explore the fluorine recovery performance of SP, the traditional reagents, diatomite, WCB, and ZP, were chosen for comparative tests, and the results are shown in Fig. 3.4a and b. Diatomite, WCB and ZP could all reduce the fluorine content of WPA and facilitate fluorine recovery to some extent. The fluorine recovery was approximately 64.00% after the treatment with these three reagents. The reason may mainly be that diatomite, WCB, and ZP are silicon-rich reagents containing impurity components that adversely affect the reaction. Meanwhile, these reagents also exhibit fluorine adsorption properties [16]. During the concentration process of WPA, some fluorine was transferred from the solution to the solid phase, resulting in an increase in fluorine recovery of only about 14%. In contrast, compared to these traditional reagents, SP could reduce the fluorine contents of WPA and DS, yielding a significant increase in fluorine recovery to 81.13%, which was 17.13% higher than that achieved with the traditional reagents. These results demonstrated that SP had a better fluorine recovery performance during the concentration process of WPA.

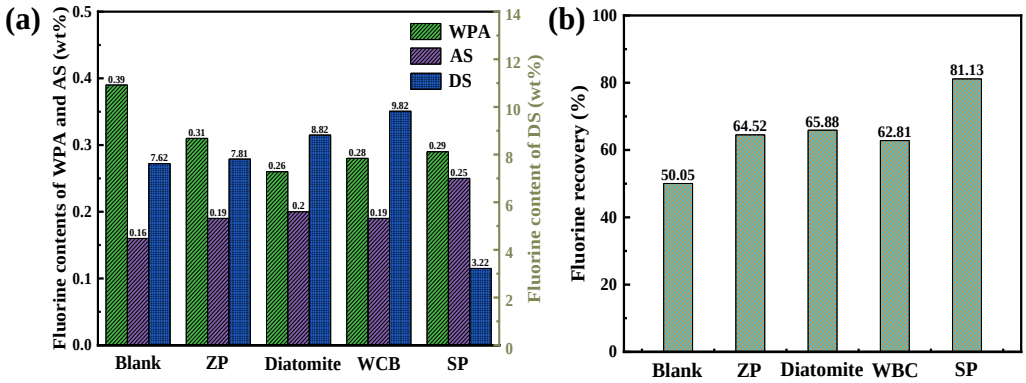


Fig. 3.4 Effect of different reagents on (a) the fluorine contents of AS, WPA, and DS, and (b) fluorine recovery (dosage: 0.5 g, stirring speed: 1800 r/min, concentration temperature: 150℃, and absorptive water initial mass: 200 g).

3.3.2. Gasification behavior of fluorine using SP

During the concentration process of WPA, the concentration device can be divided into two systems: the reaction system and the absorptive system. In order to evaluate the effect of SP on the improvement of fluorine recovery, various factors, including SP dosage, stirring speed, and concentration temperature in reaction system, and initial mass of absorptive water in absorptive system, were explored.

3.3.2.1 Gasification behavior in reaction system

Fig. 3.5a and b show the migration behaviors of fluorine among AS, WPA, and DS and fluorine recovery at different SP dosages. In the absence of SP, the fluorine content in AS was determined to be 0.15 wt%, yielding a corresponding recovery of 50.05%. Meanwhile, the fluorine content in WPA decreased from 0.80 to 0.39 wt%, with 7.62 wt% of fluorine migrating to DS. When SP was introduced and its dosage increased from 0.00 to 0.50 g per 100 g WPA, the fluorine content in AS increased from 0.15 to 0.25 wt%. Notably, the corresponding fluorine recovery experienced a 31.08% increase (from 50.05 to 81.13%), indicating that SP could react with fluorine in WPA, thereby promoting the formation of fluorine-containing gases and enhancing fluorine recovery. Both the fluorine contents in WPA and DS showed a decreasing trend with increasing SP dosage, confirming that the addition of SP accelerated the conversion of fluorine from the solution to the gas phase. However, further increasing the SP dosage had a negative impact on fluorine recovery, as the fluorine recovery decreased from 81.13 to 56.42%. These results demonstrated that an excessive SP dosage was not conducive to the gasification of fluorine in WPA. Hence, the optimal SP dosage for fluorine recovery was 0.50 g per 100 g WPA.

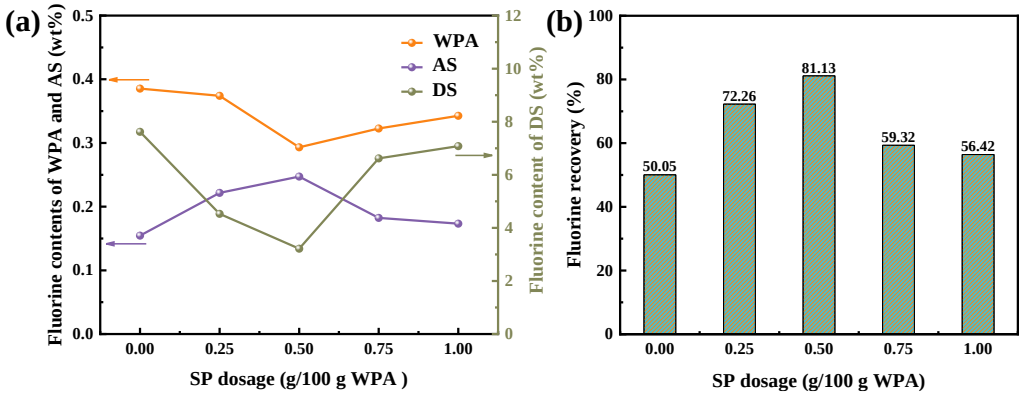


Fig. 3.5 Effect of SP dosage on (a) the fluorine contents of AS, WPA, and DS, and (b) fluorine recovery (stirring speed: 1800 r/min, concentration temperature: 150°C, and absorptive water initial mass: 200 g).

Increasing the stirring speed tends to enhance the reaction kinetics by improving the mixing of reaction materials and accelerating mass transfer [22]. The effect of stirring speed on the migration behaviors of fluorine among AS, WPA, and DS and the fluorine recovery is presented in Fig. 3.6a and b. As the stirring speed increased from 1200 to 1800 r/min, the fluorine contents of AS continuously increased, with the maximum AS fluorine content and fluorine recovery being 0.25 wt% and 81.13%, respectively. Simultaneously, the fluorine contents in WPA and DS were 0.29 and 3.21 wt%, respectively, both of which were relatively low. With a further increase in stirring speed, no obvious changes were observed in the fluorine contents of AS, WPA, and DS or in the fluorine recovery. This occurred because the reaction between WPA and SP was a solid-liquid reaction. SP could not be evenly dispersed in WPA or react fully with the fluorine species when the stirring speed was low. Increasing the stirring speed could improve the contact area between SP and the WPA solution, thereby accelerating the reaction kinetics [23]. In this case, the stirring speed of 1800 r/min was considered to be optimal.

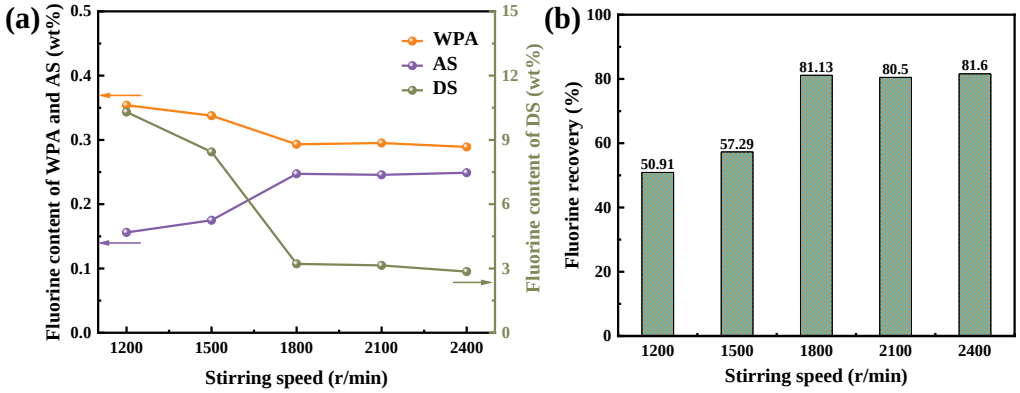


Fig. 3.6 Effect of stirring speed on (a) the fluorine contents of AS, WPA, and DS, and (b) fluorine recovery (SP dosage: 0.5 g, concentration temperature: 150°C, and absorptive water initial mass: 200 g).

Temperature is one of the important factors affecting the reaction process. In this case, Fig 3.7a and b show the effect of concentration temperature on the migration behaviors of fluorine among AS, WPA, and DS and the fluorine recovery. Increasing the temperature from 90 to 150 °C enhanced the fluorine content of AS from 0.19 to 0.25 wt%. The fluorine recovery also increased from 58.01 to 81.13%. Simultaneously, the fluorine contents of WPA and DS decreased from 0.38 and 7.30 wt% to 0.29 and 3.21 wt%, respectively. This was primarily because increasing the temperature increased the free energy of molecules in the system and promoted the movement of molecules. The probability of intermolecular collisions increased, resulting in an

intensive reaction between SP and fluorine [24]. To sum up, low concentration temperatures did not favor the reaction between SP and fluorine. The optimum concentration temperature was determined to be 150℃.

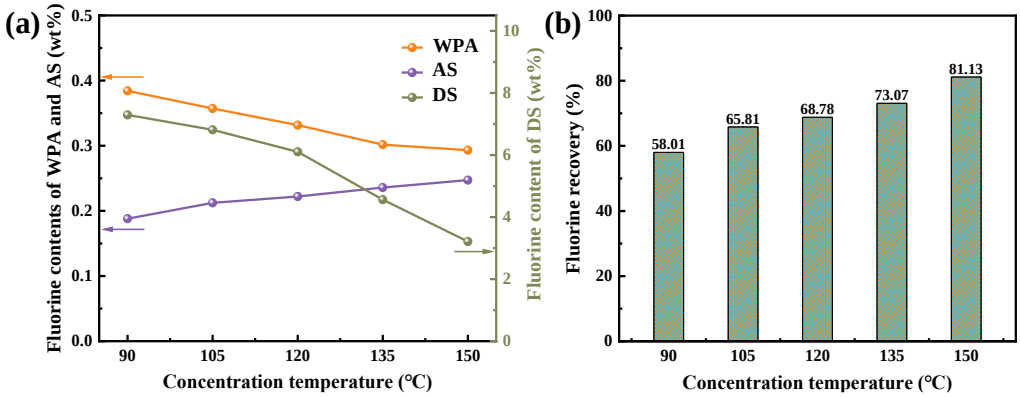


Fig. 3.7 Effect of concentration temperature on (a) the fluorine contents of AS, WPA, and DS, and (b) fluorine recovery (SP dosage: 0.5 g, stirring speed: 1800 r/min, and absorptive water initial mass: 200 g).

3.3.2.2 Gasification behavior in absorptive system

Fig. 3.8a and b present the effect of the initial mass of absorptive water on the migration behaviors of fluorine among AS, WPA, and DS and the fluorine recovery. Obviously, with an increase in the initial mass of absorptive water, the fluorine content of AS decreased from 0.48 to 0.18 wt%, whereas the fluorine recovery increased from 60.88 to 81.13% and then reached equilibrium. This was mainly because the AS gradually became saturated with fluorine and the fluorine-containing gas could not be absorbed any further when the initial mass of absorptive water was low [25]. At a high initial mass of absorptive water, although the fluorine content of AS was low, the total mass of fluorine in AS was high, yielding a higher fluorine recovery. Moreover, increasing the initial mass of absorptive water had a negligible effect on the fluorine contents of WPA and DS. The primary reason for this is that only the absorptive system was changed under this condition and the reaction between WPA and SP was not affected. Hence, 200 g was selected as the optimum initial mass of absorptive water.

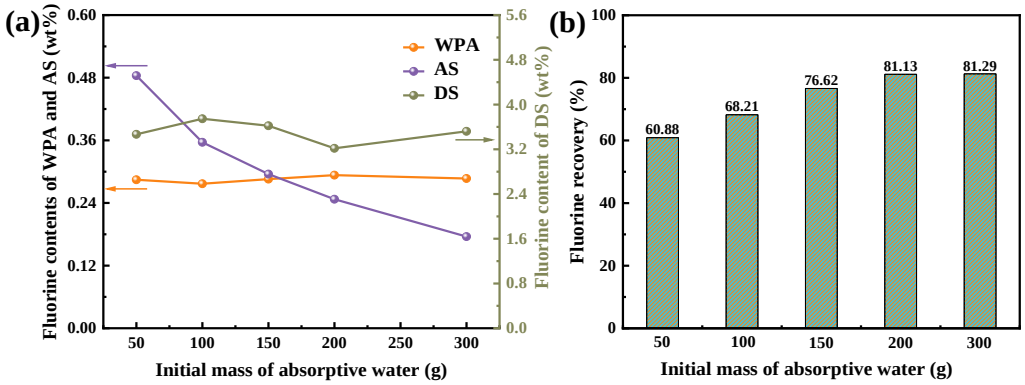


Fig. 3.8 Effect of initial mass of absorptive water on (a) the fluorine contents of AS, WPA, and DS, and (b) fluorine recovery (SP dosage: 0.5 g, stirring speed: 1800 r/min, and concentration temperature: 150℃).

Afterwards, in order to further verify the accuracy of the obtained results of fluorine contents and recovery, the repeated experiments under the above optimal conditions were carried out, and the results are presented in Table 3.3. It could be seen that the measured fluorine contents of AS, WPA and DS were all close, and fluorine recoveries were all approximately 81%. These results suggested that the above obtained results of fluorine contents and recovery in this work were accurate and reliable.

Table 3.3 The repeated experiments on WPA concentration under the optimal conditions of SP.

Experiments	Fluorine contents of WPA (wt%)	Fluorine contents of AS (wt%)	Fluorine contents of DS (wt%)	Fluorine recovery (%)	Fluorine recovery deviation (%)
First	0.293	0.247	3.216	81.13	
Second	0.295	0.243	3.596	80.69	-0.44
Third	0.287	0.252	2.882	82.37	+1.24

3.3.3. Gasification mechanism of fluorine using SP

In this section, spillover kinetics, thermodynamics calculation, and four analyses, namely IC, ICP, SEM-EDS and XRD, were determined to explore the gasification mechanism of fluorine using SP.

3.3.3.1 Spillover kinetics

The kinetics was an important factor for characterizing the reaction rate of each reaction substance in the process of a chemical reaction [26]. Spillover kinetics could help to understand the production regularity of fluorine-containing gases during the concentration process of WPA, so as to further explore the gasification mechanism of fluorine. The fluorine concentration in AS as a function of concentration time under the

optimal conditions was shown in Fig. 3.9a. The fluorine content of AS increased slowly in the first 40 min of concentration, only from 0.00 to 0.06 wt%. Between 40 min and 90 min, the fluorine content showed a sharp increase, from 0.06 to 0.30 wt%, and then gradually reached equilibrium. Simultaneously, from the experimental phenomenon, it was also found that a large number of bubbles were generated and ruptured in the WPA solution after 40 min of concentration.

The apparent reaction order (n) was a significant kinetic parameter for determining the reaction rate and effectively controlling the reaction [27]. In this work, the fluorine contents of AS (c_A) from 5 min to 60 min were used to characterize the spillover kinetics and calculate n. The relevant equation was as follows:

$$\frac{dc_A}{dt} = kc_A^n \tag{3.3}$$

Logarithmic form is:

$$ln\frac{dc_A}{dt} = lnk + nlnc_A \tag{3.4}$$

where c_A represents the fluorine concentration, mol/L; t is the concentration time, min; k represents the apparent rate constant; n is the apparent reaction order. The fitting line is drawn in Fig. 3.9b. The $ln(dc_A/dt)$ and lnc_A showed a good linear relationship, with an R^2 of 0.994, suggesting that the apparent reaction equation could describe the spillover kinetics well. Based on the fitting results, the calculated value of n was only 0.56. According to previous studies, the value of n represents the reaction rate in general chemical reactions. The reaction rate would be slower when the value of n was lower. In this process, the relatively low value of n indicated that the reaction rate between SP and fluorine was very slow [28]. This also explained why the fluorine contents of AS were very low during the first 40 min of concentration.

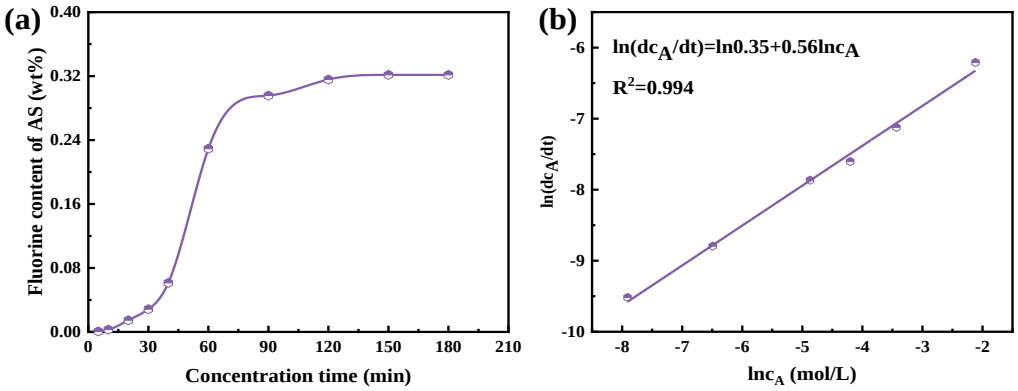


Fig. 3.9 (a) The concentration time curve of fluorine content in AS and (b) fitting curve of apparent kinetic equation.

3.3.3.2 IC and ICP analyses of WPA

Exploring the changes of anion and cation contents in WPA before and after SP treatment was important for mechanism analysis. In this case, the contents of anions and cations in concentrated WPA were evaluated by IC and ICP analyses. From Table 3.4, the fluorine content in concentrated WPA was still at a high level before SP treatment, reaching 0.39 wt%. This was because only a portion of H_2SiF_6 was thermally decomposed into SiF_4 gas during the blank concentration, while these gases combined with Na^+ to form Na_2SiF_6 precipitate. Most of the fluorine still remained in the WPA solution. After SP treatment, the content of fluorine in concentrated WPA was reduced from the original 0.80 to 0.24 wt%, suggesting that SP was an effective reagent for removing fluorine from the WPA solution. As for SO_4^{2-}, its content in concentrated WPA increased to 4.42 wt% in the absence of SP. This was attributed to the volatilization of water during the concentration process of WPA. In the presence of SP, the content decreased to 4.27 wt%. Although the content was high, the presence of SO_4^{2-} in WPA could be tolerated in many downstream chemical production processes [29]. Furthermore, it could be also found that the contents of PO_4^{3-} did not change significantly in concentrated WPA before and after SP treatment. These results clearly showed that SP could selectively gasify fluorine from WPA without affecting the quality of WPA.

The contents of cations in concentrated WPA before and after SP treatment are also shown in Table 3.4. It was obvious that there was no appreciable difference in the contents of Mg^{2+}, Al^{3+}, and Fe^{3+} between the absence and presence of SP, while their contents all increased compared with those in the original WPA. This was due to that the water was evaporated from WPA during the concentration process. As for Si^{4+}, Na^+, and K^+, the contents decreased from the initial 0.24 wt%, 0.14 wt%, and 0.32 wt% to 0.089 wt%, 0.018 wt%, and 0.08 wt% before SP treatment, respectively. This is mainly because Na^+ and K^+ could react with SiF_6^{2-} to form Na_2SiF_6 and K_2SiF_6 precipitates during the blank concentration process [30]. Interestingly, after SP treatment, the Si^{4+} content in concentrated WPA did not change. This suggested that the added SP reacted preferentially with fluorine, without appreciable dissolution of Si from SP into the solution. The contents of Na^+ and K^+ in the WPA solution increased after SP treatment, indicating that the addition of SP hindered the formation of Na_2SiF_6 and K_2SiF_6 precipitates during the concentration process.

Table 3.4 The contents of anions and cations in concentrated WPA before and after SP treatment (wt%).

WPA	PO_4^{3-}	F	Cl^-	SO_4^{2-}	Ca^{2+}	Mg^{2+}	Al^{3+}	Fe^{3+}	Si^{4+}	Na^+	K^+
Initial	36.11	0.80	0.16	2.89	0.06	0.94	0.42	0.13	0.24	0.14	0.32
Before SP treatment	61.58	0.39	0.04	4.42	0.02	3.11	1.08	0.38	0.089	0.018	0.08
After SP treatment	61.71	0.24	0.01	4.27	0.003	3.15	1.18	0.39	0.087	0.064	0.16

3.3.3.3 SEM-EDS analysis of DS

In order to investigate the morphology and elements changes of DS before and after SP treatment, SEM-EDS analysis was performed. Fig. 3.10 shows the SEM images of DS before and after SP treatment. It could be seen that DS exhibited dispersed spherical and rectangular shapes before SP treatment, which were consistent with the shapes of Na_2SiF_6 reported in previous studies (Fig. 3.10a and c) [31]. In contrast, DS treated with SP gathered together and showed an amorphous shape and agglomerative phenomenon (Fig. 3.10b and d). This phenomenon suggested that the addition of SP could alter the reaction pathway of DS during the concentration process of WPA. In other words, the addition of SP might reduce the formation of Na_2SiF_6 precipitates in DS.

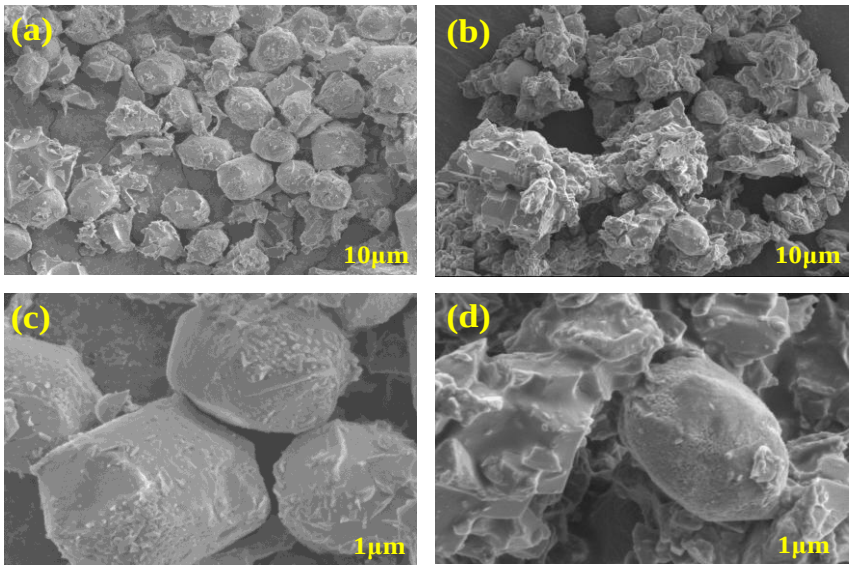


Fig. 3.10 SEM images of DS before (a, c) and after (b, d) SP treatment.

The elemental mappings of F and Na and the elemental contents of DS in the absence and presence of SP are shown in Fig. 3.11 and Table 3.5. In the absence of SP, the contents of F, Na, and Si were 10.84 wt%, 10.27 wt%, and 6.00 wt%, respectively. This was attributed to the formation Na_2SiF_6 precipitates [32]. However, it could be

noted that the contents of F and Na decreased to 1.95 and 1.93 wt%, respectively, in the presence of SP. This clearly demonstrated that the introduction of SP could reduce the formation of Na_2SiF_6 and other fluorine precipitates, resulting in a decrease in fluorine migration from the WPA solution to the solid phase. Also, the content of Si increased from 6.00 to 27.63 wt% in the presence of SP. This might be because some SP did not participate in the reaction during the concentration process, and the unreacted SP entered DS when the concentration was finished. In addition, the contents of Ca and S increased from 0.83 and 0.98 wt% to 4.70 and 2.34 wt%, respectively. The results suggested that the addition of SP promoted the crystallization of $CaSO_4$. The main reason for this was that the contents of Na^+ and K^+ in the WPA solution increased in the presence of SP, which was beneficial to the growth of $CaSO_4$ crystals [33].

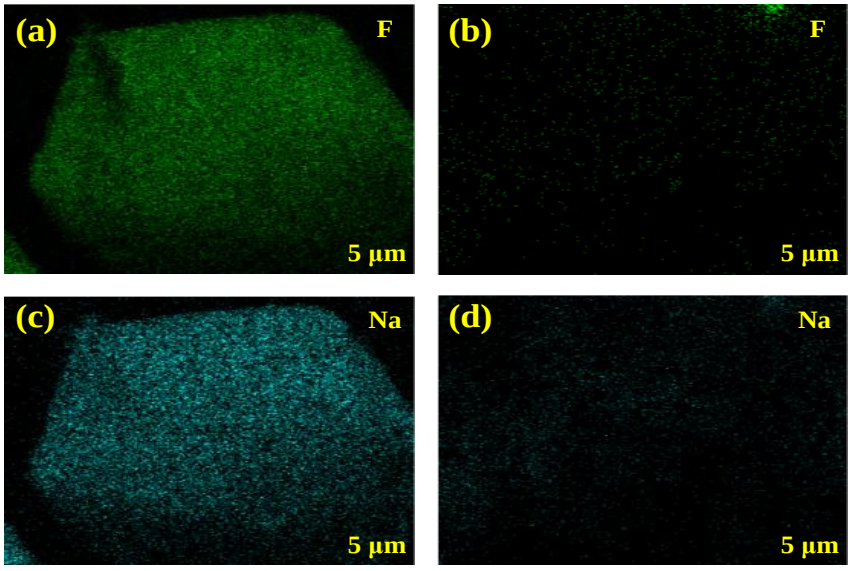


Fig. 3.11 The F and Na elemental mappings of DS in the absence (a, c) and presence (b, d) of SP.

Table 3.5 The elements contents of DS in the absence and presence of SP (wt%).

Element	O	F	Na	Al	Si	Ca	S	Others
In the absence of SP	17.19	10.84	10.27	0.32	6.00	0.83	0.98	53.57
In the presence of SP	38.18	1.95	1.93	0.33	27.63	4.70	2.34	22.94

3.3.3.4 XRD analysis of DS

To further illustrate the gasification mechanism of SP, the changes in the crystalline phases of DS before and after SP treatment were characterized by XRD. In Fig. 3.12a, DS before SP treatment showed peaks at 17.589°, 20.029°, 21.079°, 26.777°, 29.237°, 39.484°, 44.657°, 47.789°, 51.906°, 55.236°, 58.002°, 63.305°, and 67.069°, which could be assigned to the (0 0 1), (1 1 0), (1 0 1), (1 1 1), (2 0 1), (0 3 1), (2 2 1),

(1 2 2), (3 2 0), (3 2 1), (1 4 1), (5 0 1), and (1 4 2) planes. These values agreed well with the standard data from JCPDS card 72-1115, indicating that the main crystalline phase of DS before SP treatment was Na_2SiF_6. Meanwhile, the other two peaks at 25.446° and 36.300° were assigned to the (0 2 0) and (2 2 0) planes, which agreed well with the standard data from JCPDS card 86-2270, suggesting that $CaSO_4$ was another crystalline phase of DS. This was quite consistent with previous researches [34,35]. Differently, after SP treatment, DS showed peaks at 28.501°, 47.404°, 56.246°, and 69.290°, which could be assigned to the (1 1 1), (2 2 0), (3, 1 1), and (4 0 0) planes of Si (JCPDS card 77-2180). Meanwhile, the other four peaks at 25.502°, 31.422°, 38.740°, and 40.918° in Fig. 3.12b could be assigned to the (0 2 0), (2 1 0), (2 2 0), and (2 1 2) planes of $CaSO_4$ (JCPDS card 74-2421). The results suggested that some SP might not be involved in the reaction during the concentration process of WPA, which corresponded to SEM-EDS analysis. The formation of $CaSO_4$ was attributed to water evaporation and the increase of Na^+, and K^+ contents in WPA [36]. Furthermore, the apparent absence of detectable fluorine crystalline phase in DS may be caused by the low contents of fluorine compounds, resulting in inconspicuous phase detection. In general, the XRD analysis also proved that the introduction of SP reduced the formation of fluorine-containing precipitates. This was consistent with the above other analyses.

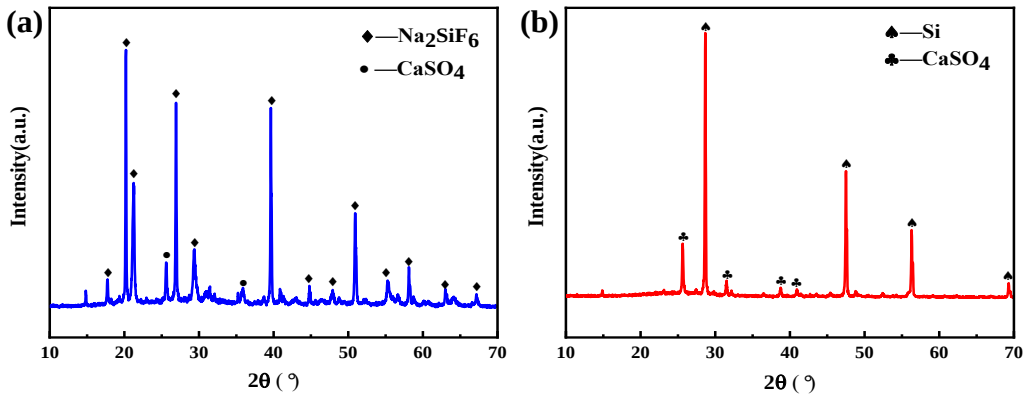


Fig. 3.12 XRD patterns of DS before (a) and after (b) SP treatment.

3.3.3.5 Gasification path analysis

Based on the above analyses, it was clear that the addition of SP reduced the fluorine content in WPA and the formation of fluorine-containing precipitates. From the previous literatures, fluorine was mainly present in the forms of HF, H_2SiF_6, and M-F complexes (M means a metal element, such as Al and Fe) in industrial dilute WPA [12]. Among these species, the existences states of M-F complexes are highly stable [14]. Hence, the above results suggested that SP might react with HF and H_2SiF_6 in WPA to enhance the gasification of fluorine. Furthermore, it was also reported that SiF_4 had a

higher vapor pressure than HF, and the addition of activated silicon could promote the formation of SiF_4 gas. [30,37]. Therefore, in this work, it could be reasonably inferred that, with the introduction of SP, a large proportion of fluorine was converted to SiF_4 gas with a higher vapor pressure, while a portion of H_2SiF_6 was thermally decomposed into HF and SiF_4 gases. Afterwards, the generated fluorine-containing gases would be collected and absorbed into water and converted back into H_2SiF_6. The corresponding gasification equations were stipulated as follows:

$$H_2SiF_6 \triangleq SiF_4\uparrow + 2HF\uparrow \quad (3.5)$$

$$Si + 4HF \triangleq SiF_4\uparrow + 2H_2 \quad (3.6)$$

$$Si + 2H_2SiF_6 \triangleq 3SiF_4\uparrow + 2H_2 \quad (3.7)$$

Besides HF, H_2SiF_6, and M-F complexes, there were also some cationic impurities (such as Na^+, K^+, Fe^{3+}, and Al^{3+}) in industrial dilute WPA. During the blank concentration process, H_2SiF_6 tended to react with Na^+ and K^+ to form Na_2SiF_6 and K_2SiF_6 precipitates, resulting in large amounts of fluorine entering DS. The main reactions were as follows:

$$2Na^+ + H_2SiF_6 \triangleq Na_2SiF_6\downarrow + 2H^+ \quad (3.8)$$

$$2K^+ + H_2SiF_6 \triangleq K_2SiF_6\downarrow + 2H^+ \quad (3.9)$$

In contrast, after SP treatment, the formation of Na_2SiF_6 and K_2SiF_6 was significantly reduced. This suggested that SP could preferentially and continuously react with H_2SiF_6 in WPA to produce SiF_4 gas when it was added into WPA, as shown in Eq. (3.7). As a result, H_2SiF_6 in WPA was constantly consumed, and its content always remained at a relatively low level, thereby limiting its reaction with Na^+ and K^+ to form Na_2SiF_6 and K_2SiF_6 precipitates. Hence, the reactions shown in Eq. (3.8) and Eq. (3.9) were inhibited.

3.3.3.6 Reaction thermodynamic calculation

In order to adequately elucidate the mechanism by which SP promotes fluorine gasification and further highlight the advantages of SP for fluorine recovery from the theoretical level, the thermodynamic data of reactions between SP, diatomite, WCB, ZP and fluorine was calculated at 150℃ using HSC Chemistry 6.0 software. From the above analyses, the reactions of SP with HF and H_2SiF_6 in WPA are shown as Eq. (3.6) and Eq. (3.7). The calculated ΔG values of these two reactions were -399.224 kJ and -413.200 kJ, respectively. As for diatomite, WCB and ZP, it was well known that the reactions of these reagents with HF and H_2SiF_6 were as follows:

$$SiO_2 + 4HF \triangleq SiF_4\uparrow + 2H_2O \quad (3.10)$$

$$SiO_2+2H_2SiF_6 \triangleq 3SiF_4\uparrow+2H_2O \quad (3.11)$$

By calculation, the ΔG values of these two equations were -11.243 kJ and -25.219 kJ, respectively. The negative ΔG values indicated that the reactions of SP, diatomite, WCB, and ZP with fluorine were thermodynamically favorable. This helped explain why these reagents could enhance fluorine recovery during the concentration process of WPA. However, the ΔG values of the reactions involving SP were much lower than those involving diatomite, WCB, and ZP, suggesting that the thermodynamic tendency to react with HF and H_2SiF_6 was greater for SP than for the traditional reagents. SP exhibited better performance in promoting fluorine gasification from WPA.

Meanwhile, the performances of SP, diatomite, WCB, and ZP to promote the conversion of fluorine-containing precipitates into the gas phase from WPA were also analyzed through thermodynamic calculations. By combining Eq. (3.7) with Eq. (3.8) and Eq. (3.9), respectively, the conversion reactions involving SP could be obtained as Eq. (3.12) and Eq. (3.13):

$$Si+2Na_2SiF_6+4H^+ \triangleq 3SiF_4\uparrow+2H_2+4Na^+ \quad (3.12)$$

$$Si+2K_2SiF_6+4H^+ \triangleq 3SiF_4\uparrow+2H_2+4K^+ \quad (3.13)$$

Through the calculation, the ΔG values of these two reactions were -369.767 kJ and -393.068 kJ, respectively. As for diatomite, WCB, and ZP, the conversion reactions were shown as follows:

$$SiO_2+2Na_2SiF_6+4H^+ \triangleq 3SiF_4\uparrow+2H_2O+4Na^+ \quad (3.14)$$

$$SiO_2+2K_2SiF_6+4H^+ \triangleq 3SiF_4\uparrow+2H_2O+4K^+ \quad (3.15)$$

The calculated ΔG values of the reactions in Eq. (3.14) and Eq. (3.15) were 18.214 kJ and -5.807 kJ, respectively. Similarly, the results showed that the corresponding conversion reactions involving SP had much lower ΔG values than those involving the traditional reagents, indicating that SP was thermodynamically more favorable for converting Na_2SiF_6 and K_2SiF_6 precipitates into SiF_4 gas in acidic solution. The addition of SP was beneficial for reducing the formation of fluorine-containing precipitates.

To sum up, the gasification mechanism of SP was analyzed and proposed in Fig. 3.13. The addition of SP altered the original transformation pathways of fluorine in WPA, intensified the gasification reaction of HF and H_2SiF_6 in WPA, and reduced the formation of fluorine-containing precipitates. Through these two pathways, the formation of SiF_4 gas and the corresponding fluorine recovery were greatly improved.

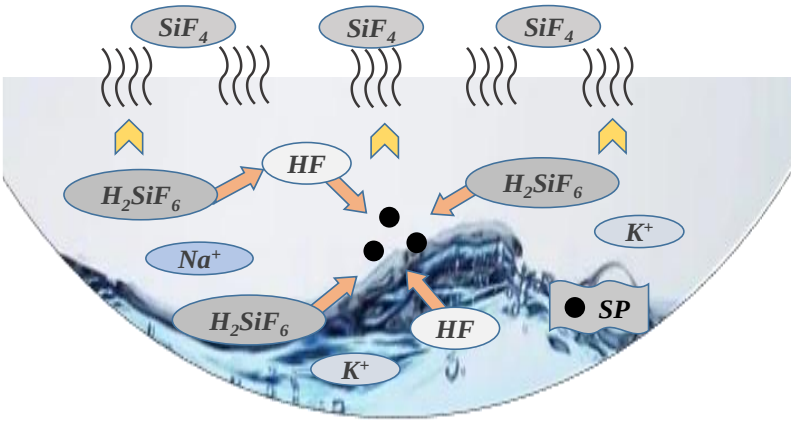


Fig. 3.13 The gasification mechanism diagram of fluorine with SP treatment.

3.4. Conclusions

In this work, SP was first utilized to enhance fluorine recovery during the concentration process of WPA. SP showed excellent fluorine recovery performance, which was superior to that of traditional reagents (diatomite, WCB, and ZP). The optimal concentration conditions were an SP dosage of 0.50 g per 100 g WPA, a stirring speed of 1800 r/min, a concentration temperature of 150 ℃ and an initial mass of absorptive water of 200 g. Under these conditions, the fluorine recovery reached 81.13%, which exhibited a significant increase of 31.08% compared with the blank concentration. Simultaneously, the fluorine contents of WPA and DS were 0.29 wt% and 3.21 wt%, respectively, both of which were at the lowest levels. In addition, the reaction rate between SP and fluorine was low, with the apparent reaction order of 0.56. During the concentration process of WPA, SP could selectively and efficiently enhance fluorine recovery without affecting the quality of WPA. The increased formation of SiF_4 gas and the reduced formation of Na_2SiF_6 and K_2SiF_6 precipitates played vital roles in improving fluorine recovery, and the proposed mechanism was supported by IC, ICP, SEM-EDS, XRD and thermodynamic calculations.

3.5. References

[1] B. He, Y. Zu, Y. Nie, Y. Mei, Investigation on the fluorine recovery mechanism by air stripping for synthetic and industrial wet process phosphoric acid, Carbon Lett. (2023). https://doi.org/10.1007/s42823-023-00573-5.

[2] S.J. Ouedraogo, Y. Vinh, P. (Lek) Noophan, V. Naddeo, C.-W. Li, Dissolution of aluminum hydroxide to provide Al and to neutralize acidity for the removal and recovery of fluoride through cryolite crystallization, Journal of Cleaner Production 404 (2023) 136987. https://doi.org/10.1016/j.jclepro.2023.136987.

[3] L. Lv, H. Duan, W. Liu, T. Yue, Flotation separation of fluorite from calcite using bis hydroxamic acid collector, Minerals Engineering 187 (2022) 107803. https://doi.org/10.1016/j.mineng.2022.107803.

[4] B. Peng, X. Li, Z. Ma, Y. Qi, Release of fluorine and chlorine during increase of phosphate rock grade by calcination and digestion, Environmental Pollution 270 (2021) 116321. https://doi.org/10.1016/j.envpol.2020.116321.

[5] B. He, Y. Zhu, Y. Zu, Y. Nie, Y. Mei, Efficient and cost-effective fluorine recovery from liquid-phase wet-process phosphoric acid via two-step precipitation method, Separation and Purification Technology 325 (2023) 124687. https://doi.org/10.1016/j.seppur.2023.124687.

[6] H. Moradi, N. Farzi, The investigation of deep eutectic electrolyte based on Choline Chloride: Ethylene glycol in 1:3 M ratio and lithium hexafluorophosphate salt for application in Lithium-Ion batteries, Journal of Molecular Liquids 360 (2022) 119476. https://doi.org/10.1016/j.molliq.2022.119476.

[7] B. Peng, Z. Ma, Y. Zhu, L. Tang, Release and recovery of fluorine and iodine in the production and concentration of wet-process phosphoric acid from phosphate rock, Minerals Engineering 188 (2022) 107843. https://doi.org/10.1016/j.mineng.2022.107843.

[8] S. Kounbach, M. Ben Embarek, L. Mahi, R. Boulif, R. Beniazza, R. Benhida, Simultaneous determination of H_2SiF_6, HF and total fluoride in fluorosilicic acid recovered from wet phosphoric acid production by potentiometric titration, Microchemical Journal 175 (2022) 107152. https://doi.org/10.1016/j.microc.2021.107152.

[9] H. Li, Y. Chen, H. Zheng, P. Huang, P. Yang, Q. Chen, X. Weng, D. He, S. Song, Effect of geological origin of apatite on reverse flotation separation of phosphate ores using phosphoric acid as depressant, Minerals Engineering 172 (2021) 107182. https://doi.org/10.1016/j.mineng.2021.107182.

[10] L. Wang, C. Wang, Y. Yu, X. Huang, Z. Long, Y. Hou, D. Cui, Recovery of fluorine from bastnasite as synthetic cryolite by-product, Journal of Hazardous Materials 209–210 (2012) 77–83. https://doi.org/10.1016/j.jhazmat.2011.12.069.

[11] J. Lv, Y. Zheng, X. Tong, X. Li, Clean utilization of waste rocks as a novel adsorbent to treat the beneficiation wastewater containing arsenic and fluorine, Journal of Cleaner Production 293 (2021) 126160. https://doi.org/10.1016/j.jclepro.2021.126160.

[12] D. Lisbona, K. Steel, Recovery of fluoride values from spent pot-lining: Precipitation of an aluminium hydroxyfluoride hydrate product, Separation and Purification Technology 61 (2008) 182–192. https://doi.org/10.1016/j.seppur.2007.10.012.

[13] B.S. Vieira, D. Gullberg, V. Perrot, Recent experience with metallic heaters for phosphoric acid evaporation, Procedia Engineering 138 (2016) 437–444. https://doi.org/10.1016/j.proeng.2016.02.103.

[14] B. He, Y. Zhu, Y. Zu, Y. Nie, Y. Mei, Designing an efficient fluorine recovery strategy for Wet-Process phosphoric acid purification by disclosing competitive complexation behavior between fluorine species and metal cations, Separation and Purification Technology 320 (2023) 124219. https://doi.org/10.1016/j.seppur.2023.124219.

[15] R. Kijkowska, D. Pawlowska-Kozinska, Z. Kowalski, M. Jodko, Z. Wzorek, Wet-process phosphoric acid obtained from Kola apatite. Purification from sulphates, fluorine, and metals, Separation and Purification Technology 28 (2002) 197–205. https://doi.org/10.1016/S1383-5866(02)00048-5.

[16] L. Xu, X. Gao, Z. Li, C. Gao, Removal of fluoride by nature diatomite from high-fluorine water: An appropriate pretreatment for nanofiltration process, Desalination 369 (2015) 97–104. https://doi.org/10.1016/j.desal.2015.04.033.

[17] K. Rangsriwatananon, A. Chaisena, C. Thongkasam, Thermal and acid treatment on natural raw diatomite influencing in synthesis of sodium zeolites, J Porous Mater 15 (2008) 499–505. https://doi.org/10.1007/s10934-007-9098-2.

[18] B. Xiang, J. Tang, X. Feng, Y. Zhu, Y. Li, T. Tan, Preparation of aluminium-hydroxide-modified diatomite and its fluoride adsorption mechanism, Sci Rep 13 (2023) 3871. https://doi.org/10.1038/s41598-023-30901-8.

[19] X. Li, G. Lv, W. Ma, T. Li, R. Zhang, J. Zhang, S. Li, Y. Lei, Review of resource and recycling of silicon powder from diamond-wire sawing silicon waste, Journal of Hazardous Materials 424 (2022) 127389. https://doi.org/10.1016/j.jhazmat.2021.127389.

[20] S. Yang, W. Ma, K. Wei, K. Xie, Z. Wang, Thermodynamic analysis and experimental verification for silicon recovery from the diamond wire saw silicon powder by vacuum carbothermal reduction, Separation and Purification Technology 228 (2019) 115754. https://doi.org/10.1016/j.seppur.2019.115754.

[21] M.I. Amin, M.M. Ali, H.M. Kamal, A.M. Youssef, M.A. Akl, Recovery of high grade phosphoric acid from wet process acid by solvent extraction with aliphatic alcohols, Hydrometallurgy 105 (2010) 115–119. https://doi.org/10.1016/j.hydromet.2010.08.007.

[22] B. Teoman, S. Shastry, S. Abdelhamid, P.M. Armenante, Imaging method for the determination of the minimum agitation speed, N, for solids suspension in stirred vessels and reactors, Chemical Engineering Science 231 (2021) 116263. https://doi.org/10.1016/j.ces.2020.116263.

[23] M. Tang, C. Zhou, J. Pan, N. Zhang, C. Liu, S. Cao, T. Hu, W. Ji, Study on extraction of rare earth elements from coal fly ash through alkali fusion – Acid leaching, Minerals Engineering 136 (2019) 36–42. https://doi.org/10.1016/j.mineng.2019.01.027.

[24] W. Zhong, C. Wang, H. Zhao, S. Peng, Z. Tian, R. Shu, Y. Chen, Synergistic effect of photo-thermal catalytic glycerol reforming hydrogen production over 2D Au/TiO_2 nanoflakes, Chemical Engineering Journal 446 (2022) 137063. https://doi.org/10.1016/j.cej.2022.137063.

[25] T. Dahlke, O. Ruffiner, R. Cant, Production of HF from H_2SiF_6, Procedia Engineering 138 (2016) 231–239. https://doi.org/10.1016/j.proeng.2016.02.080.

[26] L. Zhang, T. Zhang, Y. Zhao, G. Dong, S. Lv, S. Ma, S. Song, M. Quintana, Doping engineering of lithium-aluminum layered double hydroxides for high-efficiency lithium extraction from salt lake brines, Nano Res. (2023). https://doi.org/10.1007/s12274-023-5950-1.

[27] T.A. Al-Attas, R.A. Lucky, M.M. Hossain, Apparent kinetics of co-gasification of biomass and vacuum gas oil (VGO), Chemistry An Asian Journal 16 (2021) 507–520. https://doi.org/10.1002/asia.202001271.

[28] Y. Liu, E. Lotero, J.G. Goodwin, Effect of water on sulfuric acid catalyzed esterification, Journal of Molecular Catalysis A: Chemical 245 (2006) 132–140. https://doi.org/10.1016/j.molcata.2005.09.049.

[29] L. Yang, J. Cao, T. Luo, Effect of Mg^{2+}, Al^{3+}, and Fe^{3+} ions on crystallization of type α hemi-hydrated calcium sulfate under simulated conditions of hemi-hydrate process of phosphoric acid, Journal of Crystal Growth 486 (2018) 30–37. https://doi.org/10.1016/j.jcrysgro.2018.01.014.

[30] A.N. Joshi, A review of processes for separation and utilization of fluorine from phosphoric acid and phosphate fertilizers, Chem. Pap. 76 (2022) 6033–6045. https://doi.org/10.1007/s11696-022-02323-9.

[31] M. Kumar, M.N. Babu, T.R. Mankhand, B.D. Pandey, Precipitation of sodium silicofluoride (Na_2SiF_6) and cryolite (Na_3AlF_6) from HF/HCl leach liquors of alumino-silicates, Hydrometallurgy 104 (2010) 304–307. https://doi.org/10.1016/j.hydromet.2010.05.014.

[32] L. Tian, L. Chen, A. Gong, X. Wu, C. Cao, Z. Xu, Recovery of rare earths, lithium and fluorine from rare earth molten salt electrolytic slag via fluoride sulfate conversion and mineral phase reconstruction, Minerals Engineering 170 (2021) 106965. https://doi.org/10.1016/j.mineng.2021.106965.

[33] X. Mu, G. Zhu, X. Li, S. Li, X. Gong, H. Li, G. Sun, Effects of Impurities on $CaSO_4$ Crystallization in the $Ca(H_2PO_4)_2$–H_2SO_4–H_3PO_4–H_2O System, ACS Omega 4 (2019) 12702–12710. https://doi.org/10.1021/acsomega.9b01114.

[34] R.K. Will, The benefits of isolating & utilizing fluorine from phosphate operations, Procedia Engineering 138 (2016) 267–272. https://doi.org/10.1016/j.proeng.2016.02.084.

[35] J. Zhang, C. Tian, Y. Xu, J. Chen, L. Xiao, G. Wu, F. Jin, Effective removal of fluorine ions in phosphoric acid by silicate molecular sieve synthesized by hexafluorosilicic acid, Separation and Purification Technology 305 (2023) 122395. https://doi.org/10.1016/j.seppur.2022.122395.

[36] J.G. Tanquero, E.A. Abdel-Aal, R.S. Farinato, H. El-Shall, B.M. Moudgil, Inhibition of calcium sulphate hemihydrate crystallization under simulated conditions of phosphoric acid evaporation, Can J Chem Eng 100 (2022) 923–932. https://doi.org/10.1002/cjce.24210.

[37] A.A. El-Asmy, H.M. Serag, M.A. Mahdy, M.I. Amin, Purification of phosphoric acid by minimizing iron, copper, cadmium and fluoride, Separation and Purification Technology 61 (2008) 287–292. https://doi.org/10.1016/j.seppur.2007.11.004.

Chapter 4. Lanthanum-functionalized diatomite enabling highly efficient fluoride removal from acidic phosphate chemical wastewater

4.1. Introduction

In recent years, with the rapid advancement of the phosphorus chemical industry, lithium batteries, semiconductors, and other fields, the demand for fluoride-containing products had grown at an accelerating pace [1]. Along with this, a considerable volume of acidic chemical wastewater (pH of 1-3) containing fluoride was generated and discharged, which caused serious human diseases and environmental pollution. It has been reported that the excessive fluoride in water can lead to reproductive system problems, dental and skeletal fluorosis, Alzheimer's disease in humans [2–4]. The data show that more than 200 million people are suffering from the harm of water with high fluoride concentration [5]. Moreover, fluoride seeping into groundwater could also cause trees and crops to turn yellow and even die [6]. Considering the negative impacts outlined above, the legal limit for fluoride discharge in industrial wastewater promulgated by China is 10 mg/L [7]. Nevertheless, the data showed that the fluoride concentration in wastewater produced from the phosphorus chemical, phosphogypsum, mineral smelting, and other industrial sectors was usually at high levels (50 mg/L-200 mg/L) with strong acid, which was higher than the emission standard [8]. Hence, there is an urgent need to remove fluoride from acidic phosphate chemical wastewater for protecting the environment and ensuring human health.

Currently, precipitation [9], ion exchange [10], electrochemical treatment [11], membrane filtration [12], and adsorption [13] have been utilized by researchers to remove fluoride from chemical wastewater. Owing to the advantages of simple design, easy separation, good regeneration, and high efficiency, adsorption has been a promising and widely used technology. To this end, various adsorbents, including metal-organic frameworks (MOFs) [14], activated alumina, zeolite-based materials [15], porous nano-hydroxyapatite (HAP) [16], and others, have been developed. Nevertheless, some of these adsorbents exhibited poor removal performance under the acidic environment due to the collapse of structure and the dissolution of active sites, and this pH sensitivity significantly hindered the deep application of fluoride removal

from acidic wastewater. For example, Kikuchi and Konno synthesized a defective University of Oslo-66 (UiO-66) framework for fluoride removal from industrial wastewater. The results showed that the adsorption capacity was 32.80 mg/g at pH of 2.18 and increased to 53.00 mg/g when pH was raised to 6 [17]. The aluminum-based chitosan/zeolite molecular sieve (AC-Z) composite prepared by Gao et al. was also utilized to remove fluoride. The removal efficiency reached 93.50% at pH of 6 while that was approximately 12.50% at pH of 3 [18]. Therefore, the continued development of acid-resistant adsorbents with stable structures, robust active sites, and good adsorption performance is always the direction of efforts.

To achieve the above goals, natural silicate minerals and natural silicate mineral-based composites, such as attapulgite, montmorillonite (MMT), and diatomite, have becoming a new favorite for the removal of fluoride, phosphates, and other pollutants due to their acid resistance, rich pore structure, easily modified surface functional groups, low cost, and non-toxicity [19,20]. Diatomite, a natural silicate mineral composed primarily of silicon dioxide (SiO_2) with abundant reserves, is a siliceous sedimentary rocks formed from the fossilized remains of diatoms. Because of the high chemical inertness of amorphous SiO_2, strong covalent silicon-oxygen (Si-O) bonds, sturdy biogenic nanostructure, and the absence of soluble alkaline-earth metals [21], diatomite showed excellent acid resistance under the acidic environments, which provides a solid basis as a stable carrier for fluoride removal from acidic wastewater. Typically, Zhang et al. used polyethylenimine modified diatomite (PEI/DT) to remove fluoride from mine water, and the maximum adsorption capacity with 28.62 mg/g at pH of 2 was observed [22]. Klr et al. synthesized acid-activated diatomite for fluoride removal from aqueous solution, which showed the maximum adsorption capacity of 12.03 mmol/g at pH of 6 [23]. Unfortunately, natural diatomite and currently developed diatomite-based adsorbents have the disadvantage of low adsorption capacities for fluoride at acidic environments. This was mainly due to the permanent negative surface charge of diatomite, which had a repulsive force to the similarly negatively charged fluoride [23]. Based on the above mentioned excellent stability and negative surface charge of diatomite, it might be a good strategy to prepare the composite using diatomite as a carrier and load acid-resistant cationic metal compounds on its surface, which could modulate the surface charge of diatomite, increase the adsorption active sites, and thus enhance the fluoride adsorption capacity of diatomite.

In long-term experiments, researchers demonstrated that certain rare earth metal

oxides could remove anionic pollutants effectively owing to their special physicochemical properties [24]. Lanthanum (La), Cerium (Ce), Zirconium (Zr), and other rare earth elements have been introduced into the field of fluoride removal from wastewater [25]. Based on the Hard-Soft-Acid-Base (HSAB) theory, La (hard acid), abundant reserves in China, typically exhibits a strong affinity toward fluoride (hard base) [26]. Meanwhile, it is noticing that La also possessed excellent acid resistance at acidic environments due to the extremely small solubility product constant (K_{sp}, about 2.00×10^{-19}) of its hydroxide, which could provide a good theoretical basis for the application of La in the field of fluoride removal from acidic wastewater. As a result, several La-based adsorbents, including La-MOFs, La-metal, and La-modified waste residue composites, had been developed and applied for fluoride removal [27,28]. Unfortunately, many developed La-based adsorbents were primarily focused on the fluoride removal from drinking water, and the application in the field of acidic phosphate chemical wastewater and the acid-resistant property of La hydroxide ($La(OH)_3$) were ignored. Also, the binding and removal mechanisms by combining La with diatomite to prepare composites for fluoride removal from acidic phosphate chemical wastewater were rarely studied. Hence, it would be meaningful to synthesize La-diatomite composite, which could offer a broader framework for efficient fluoride removal from acidic phosphate chemical wastewater.

In this work, a $La(OH)_3$ modified diatomite (La/D) composite was synthesized via the loading engineering strategy based on the inherent acid resistance of both diatomite and $La(OH)_3$ to achieve efficient fluoride removal from acidic phosphate chemical wastewater. The characteristics of morphological structure and composition were investigated. Thereafter, the adsorption behavior and acid resistance of the La/D composite were evaluated through single-factor experiments, including pH, adsorption kinetics, adsorption isotherms, adsorption thermodynamics, coexisting anions, and recyclability. Then, the removal mechanism of fluoride on the La/D composite was revealed in depth by a series of analyses. Finally, the practical application performance of the La/D composite was verified through actual acidic phosphogypsum wastewater adsorption experiments.

4.2. Experimental

4.2.1. Material and reagents

The diatomite (composition shown in Table 4.1) used in this study was obtained

from Lingshou Minerals Co., Ltd, China. The main composition of diatomite was SiO_2 with content of 94.18 wt%. Lanthanum chloride heptahydrate ($LaCl_3 \cdot 7H_2O$, 99%) was purchased from Shanghai Aladdin Biochemical Technology Co., Ltd. (China). Sodium fluoride (NaF, 98%), hydrochloric acid (HCl, 36%-38%), sodium hydroxide (NaOH, 96%), trisodium citrate ($Na_3C_6H_5O_7 \cdot 7H_2O$, 99%), and glacial acetic acid (CH_3COOH, 99.5%), all purchased from Sinopharm Chemical Reagent Co., Ltd. (China), were used to adjust pH and measure fluoride concentration. The deionized water (18.25 MΩ), produced by the Milli-Q Direct 16 water purification system (Millipore Q, USA), was used for all experiments.

Table 4.1 The compositions of diatomite used in the experiments (wt%).

Compositions	SiO_2	Na_2O	Al_2O_3	Fe_2O_3	Others
Contents	94.18	1.97	2.15	1.06	0.64

4.2.2. Preparation of La/D composite

The La/D composite was synthesized via a simple one-step procedure (Fig. 4.1) [29]. Typically, 3 g of diatomite was added into 100 mL of deionized water to form a dispersed suspension under heating and vigorous stirring for 1 h. The stirring speed and heating temperature were 1500 rpm and 80°C, respectively. $LaCl_3 \cdot 7H_2O$ was added into the above suspension, and then 40 mL of concentrated ammonia water (25%) was also added dropwise to regulate pH. Afterwards, the mixture was continuously heated and stirred for 8 h. The mixture was allowed to age at room temperature for 2 h when the reaction was finished. Finally, the precipitate was collected by filtering, washing and drying at 90 °C for 12 h to obtain the La/D composite.

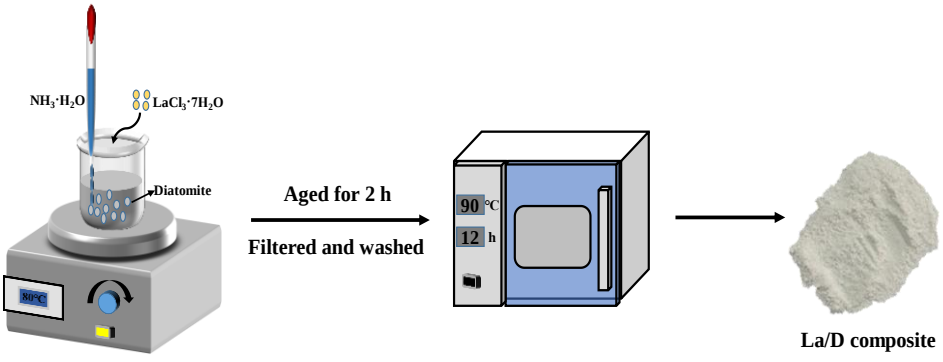


Fig. 4.1 The synthesis process of the La/D composite.

4.2.3. Adsorption experiments

The effect of initial pH was first investigated. 20 mg of the La/D composite was mixed with 40 mL of fluoride solution (100 mg/L) with initial pH values of 1-5. The effect of coexisting anions was then studied to assess the selectivity of the La/D

composite. Sodium chloride (NaCl), sodium sulfate (Na_2SO_4), and sodium phosphate (Na_3PO_4) were added into the fluoride solution (100 mg/L and pH= 3) to achieve final concentration of coexisting anions of 10mg/L, 25 mg/L and 50 mg/L, respectively. Also, four adsorption-desorption cycles were carried out to investigate the stability of the La/D composite. Typically, 50 mg of the La/D composite was mixed with 100 mL of fluoride solution (100 mg/L and pH= 3) for the adsorption experiment. After adsorption, the used adsorbents were immersed and stirred for 6 h in NaOH solution (0.5 mol/L) to desorb. Subsequently, the regenerated adsorbents were washed several times with deionized water and vacuum freeze-dried for the next adsorption cycle. During this process, the La leaching percentage (L_d) was calculated according to Eq. (4.1) [30]. As for adsorption kinetics, a certain volume of suspension was sampled at predetermined time intervals and filtered to measure the residual fluoride concentration. Similarly, for adsorption isotherms, the La/D composite was mixed with fluoride solution (0-200 mg/L, pH= 3) and stirred for 12 h at three temperatures (25℃, 35℃ and 45℃) to attain adsorption equilibrium.

The above experiments except for adsorption isotherms were all carried out in a thermostatic oscillator at 200 rpm and 25℃. The adsorbed suspension was filtered by 0.22 μm polyamide membrane, and the equilibrium adsorption capacity (q_e, mg/g) and removal efficiency (R, %) of fluoride were calculated through Eq. (4.2) and Eq. (4.3), respectively.

$$L_d = \frac{c_{La} V}{mw} \times 100\% \tag{4.1}$$

$$q_e = \frac{(c_0 - c_e) V}{m} \tag{4.2}$$

$$R = \frac{c_0 - c_e}{c_0} \times 100\% \tag{4.3}$$

where c_{La} is the La concentration in the solution after fluoride adsorption (g/L); c_0 and c_e represent the initial and equilibrium concentration of fluoride (mg/L), respectively; V is the volume of solution (L); m is the mass of the La/D composite (g); and w is the mass fraction of La in the La/D composite (%).

4.2.4. Characterizations

X-ray diffraction (XRD, Bruker D8 Advance, Japan) and Fourier transform infrared spectrometer (FTIR, Thermo Nicolet Nexus, America) were adopted to gain the phase identification and bonding of samples. Surface area analyzer (BET, ASAP2460, America) was used to analyze the nitrogen adsorption and desorption

isotherms. The features of morphology and elemental distribution of samples were studied using scanning electron microscope with energy dispersive spectrometer (SEM-EDS: Phenom G6, Thermo Fisher Scientific, America). X-ray photoelectron spectroscopy (XPS, Thermo Escalab 250Xi, America) was conducted to investigate the elemental valence states and bonding configurations. The binding energy scale was calibrated based on the C 1s peak at 284.80 eV. The potential changes of samples were measured using Malvern Zeta Sizer (England). The concentration of ions in real wastewater were measured by ion chromatograph (IC, Metrohm, ICS-1100) and inductively coupled plasma optical emission spectrometer (ICP-OES, Thermo Fisher Scientific, ICAP 7400, America). Fluoride Ion Selective Electrode (PF-2-01) was used in this work to measure the fluoride concentration (Standard line in Fig. 4.2), and the details of this method had been described elsewhere [29].

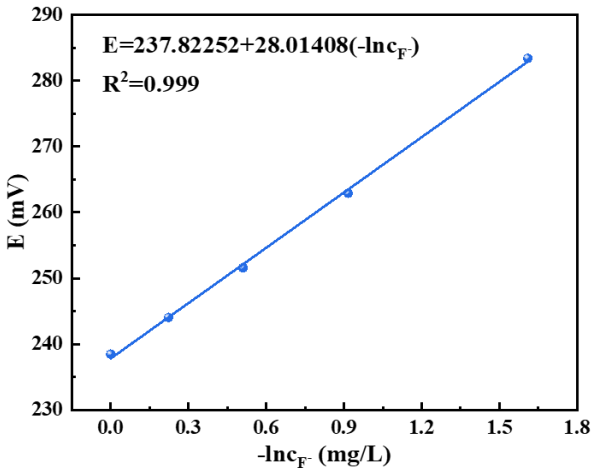


Fig. 4.2 Standard line of fluoride.

4.3. Results and discussion

4.3.1. Characterization of La/D composite

The crystal structures of diatomite and the La/D composite were first investigated. As shown in Fig. 4.3, the diatomite showed peaks at 21.947°, 28.400°, 31.374°, 36.055°, 42.610°, 46.922°, 48.529°, 57.014°, and 64.988°, which are assigned to the (1 0 1), (1 1 1), (1 0 2), (2 0 0), (2 1 1), (1 1 3), (2 1 2), (3 0 1), and (3 1 2) planes of JCPDS card 71-0785, respectively, indicating that the main physical phase was SiO_2. After modification, three new peaks appeared at 15.616°, 27.970°, and 39.425° that could be assigned to the (1 0 0), (1 0 1), and (2 0 1) planes, respectively; these values agreed well with the standard data from JCPDS card 83-2034, confirming that the substance loaded onto the surface of diatomite corresponded to $La(OH)_3$. In addition, the

characteristic peaks of diatomite remained well in the composite, which suggested that La was effectively immobilized onto the diatomite surface in the form of $La(OH)_3$ while the original structure of diatomite was retained. Beneficially, the extremely low K_{sp} value (about 2.00×10^{-19}) of $La(OH)_3$ could enhance the acid resistance of the La/D composite, which provided the capability to adapt to the complex acid environment of acidic chemical wastewater and was consistent with our design starting point.

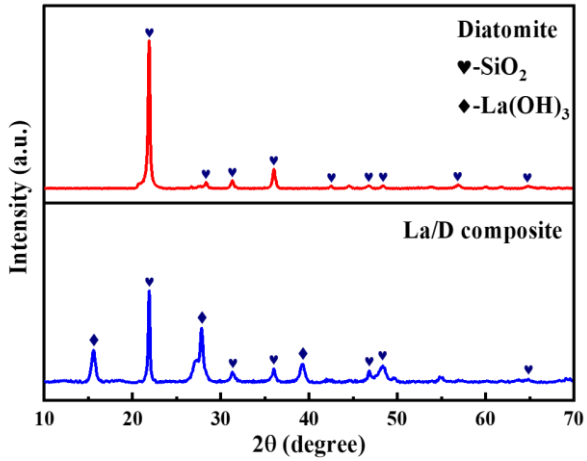


Fig. 4.3 XRD patterns of diatomite and the La/D composite.

The textural properties of the La/D composite were also studied by nitrogen (N_2) adsorption-desorption isotherms. It could be seen from Fig 4.4a that diatomite showed limited textural properties, with a specific surface area of merely 1.91 m^2/g and an average pore width of 8.33 nm, respectively (Fig. 4.4b and Table 4.2), which was consistent with the typical mesoporous structure and low surface area characteristics of natural diatomite. In contrast, the La/D composite displayed a type IV isotherm featuring distinct H4 hysteresis loops at high relative pressures. The specific surface area and average pore width were increased to 20.26 m^2/g and 24.44 nm, respectively (Fig. 4.4b and Table 4.2), indicating the presence of mesoporous structure in the La/D composite [31]. This change was due to the formation of wrinkled $La(OH)_3$ nanophases on diatomite surface, which was similar to the previous studies [32,33]. Therefore, it was believed that the larger specific surface area and average pore width of the La/D composite would provide more favorable conditions for fluoride adsorption.

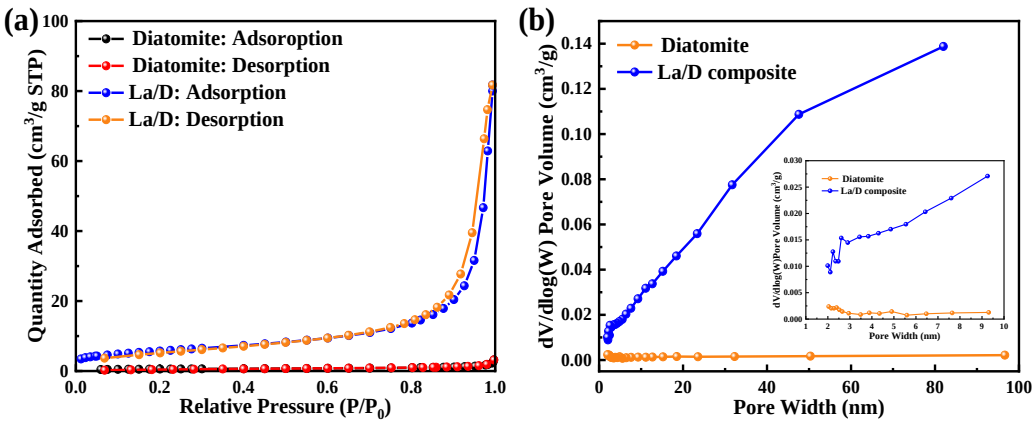


Fig. 4.4 (a) The N_2 adsorption-desorption isotherms and (b) related pore size distributions of diatomite and the La/D composite.

Table 4.2 Information about the pore distribution of diatomite and the La/D composite.

Samples	BET surface area (m^2/g)	Average pore width (nm)	Pore volume (cm^3/g)
Diatomite	1.91	8.33	0.0040
La/D composite	20.26	24.44	0.12

Furthermore, the FTIR spectra of diatomite and the La/D composite are shown in Fig 4.5a. For diatomite, the characteristic bands at 475 cm^{-1}, 793 cm^{-1}, and 1092 cm^{-1} are corresponded to antisymmetric bending vibration, symmetric stretching vibration, and antisymmetric stretching vibration of Si-O-Si, respectively [34,35]. The characteristic bands at 1629 cm^{-1} and 3439 cm^{-1} are attributed to the bending vibration and stretching vibration of hydroxyl (-OH) groups with crystalline water [36]. After modification with $La(OH)_3$, two new characteristic bands appeared at 1383 cm^{-1} and 1487 cm^{-1}, which was corresponded to the bending vibration and stretching vibration of La bonding hydroxyl (La-OH bonds) groups, respectively [37,38]. Meanwhile, another new characteristic band assigning to the stretching vibration of -OH was found at 3610 cm^{-1} [39], which was in full agreement with the results of XRD analysis, indicating the successful preparation of the La/D composite. The XPS survey spectrum of the La/D composite shown in Fig. 4.5b also demonstrated these results, and two new peaks corresponding to La $3d_{5/2}$ and La $3d_{3/2}$ appeared in the La/D composite.

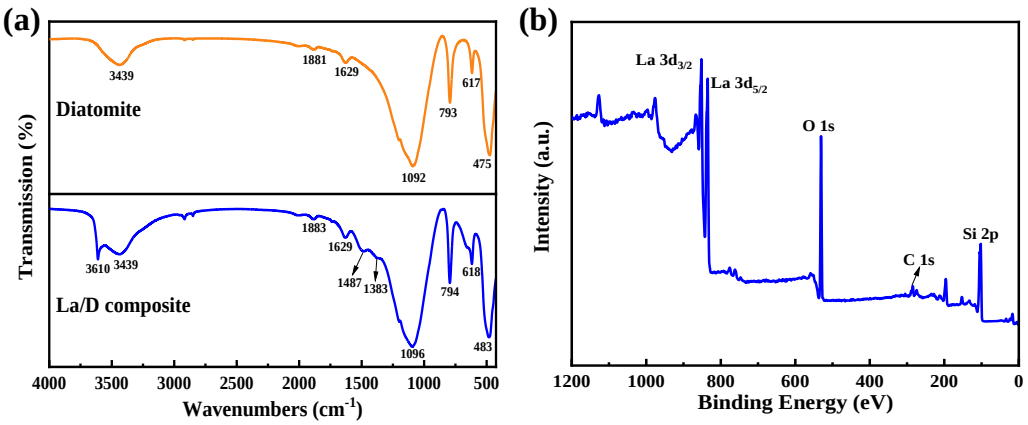


Fig. 4.5 (a) FTIR spectra of diatomite and the La/D composite and (b) XPS survey scan of the La/D composite.

SEM-EDS analysis (Fig. 4.6) was also used to investigate the morphological structure and composition of the La/D composite. It is well known that the morphology of diatomite appeared as a round cake. After modification, it was obvious that a layer of folded $La(OH)_3$ nanophases covered the surface of diatomite. Additionally, the EDS mapping showed that the elements of Si, O, and La were uniformly distributed onto the diatomite surface, further confirming that $La(OH)_3$ was successfully loaded and dispersed onto diatomite surface, which was in agreement with the above analyses.

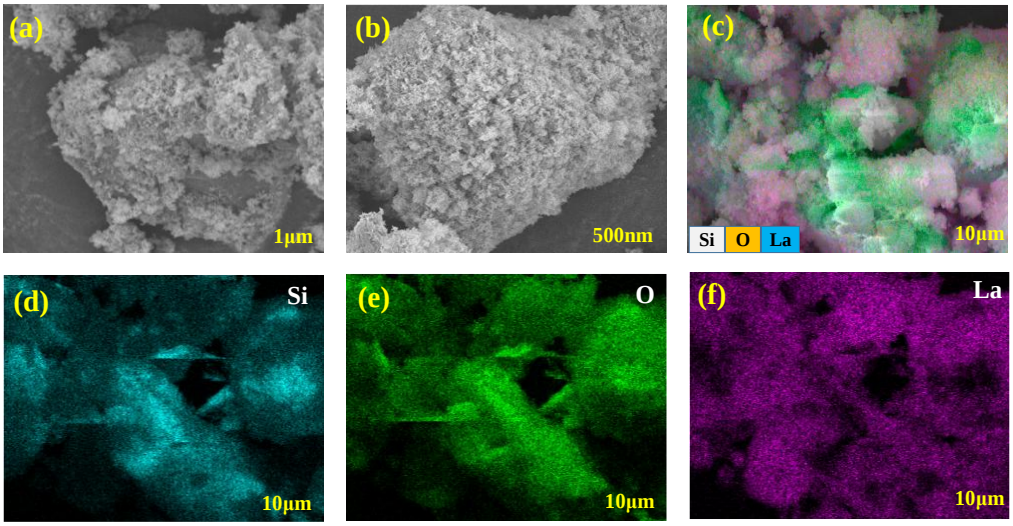


Fig. 4.6 (a-b) SEM images and (c-f) EDS mapping images of the La/D composite.

4.3.2. Adsorption experiments

4.3.2.1 Effect of initial pH on adsorption performance

The interaction mechanism between fluoride and adsorbents, and the removal performance of adsorbents are both related to the initial pH of solution [40]. Therefore, the effect of initial pH on fluoride adsorption performance of diatomite and the La/D composite was investigated. From Fig.4.7, the diatomite showed negligible fluoride

adsorption capacities at the test pH range of 1-5. This was attributed to the high negative charge on the surface of diatomite, which would generate electrostatic repulsion with fluoride [41]. The zeta potential of diatomite in Table 4.3 also confirmed this result. After loading $La(OH)_3$, the enhanced adsorption performance of the La/D composite were observed at the pH range of 1-3 with the adsorption capacities being stable at 121.71-129.28 mg/g, which was 70.35-79.81 times that of diatomite. The results indicated that the acidic environment was more conducive to the adsorption of the La/D composite, and the reason could be explained by the dual effects of protonation and electrostatic adsorption [28]. At the pH values of 1-3, the surface of La/D composite charged positively due to protonation (Table 4.3). In this case, fluoride tended to move closer to the surface of the La/D composite. As the pH increased, the surface of La/D composite became deprotonated, and the decrease of surface protonation would suppressed the ligand exchange process between surface hydroxyl groups of La/D composite and fluoride, which resulted the significant reduction of adsorption capacities [42]. In general, the La/D composite exhibited a specific and excellent adsorption property under the acidic environments, suggesting the considerable potential for removing fluoride from acidic phosphate chemical wastewater, which further validated the original design intention of composite.

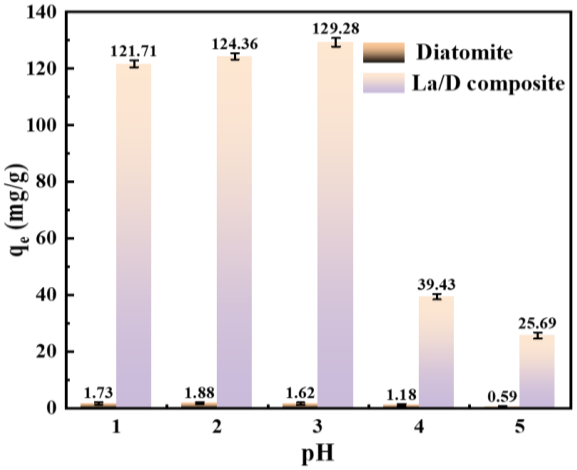


Fig. 4.7 Effect of initial pH on fluoride adsorption performance of the La/D composite (fluoride concentration: 100 mg/L, the La/D composite dosage: 0.5 g/L, T: 25°C, and t: 12 h).

Table 4.3 Zeta potential of diatomite, the La/D composite and after adsorption at pH of 3.

Samples	Zeta potential (mV)			Average (mV)
Diatomite	-35.30	-36.40	-36.60	-36.10
La/D composite	25.40	25.20	25.60	25.40
La/D-fluoride	-1.62	-1.39	-1.43	-1.48

4.3.2.2 Adsorption kinetics, isotherms, and thermodynamics

The adsorption kinetics were crucial for assessing the efficiency of adsorbents during the adsorption process. Hence, the adsorption kinetics of fluoride on the La/D composite were studied. As shown in Fig. 4.8a, the adsorption capacities of the La/D composite for fluoride increased quickly within the first 180 min and then gradually reached equilibrium. This is mainly attributed to the abundant active sites on the surface of the La/D composite, enabling a rapid initial adsorption rate [43]. As adsorption progressed, the number of active sites decreased, leading to a gradual stabilization of adsorption rate. The kinetics data were analyzed by pseudo-first-order (PFO), pseudo-second-order (PSO), and intra-particle diffusion kinetics models in this study, and the detailed information of Eqs. were shown in Table 4.4. The fitting results and corresponding parameters are illustrated and summarized in Fig. 4.8a and Table 4.5. Obviously, PSO kinetics model had a higher correlation coefficient (R^2) value (0.98) than PFO kinetics model (0.92), and the calculated q_e value (126.49 mg/g) from PSO kinetics model was closer to the experimental value (129.28 mg/g), indicating that PSO kinetics model provided a better description for fluoride adsorption kinetics of the La/D composite, which suggested that the adsorption process between the La/D composite and fluoride might involve chemical interaction [40].

The intra-particle diffusion model fitting results shown in Fig. 4.8b and Table 4.5 revealed the rate-limiting step of fluoride adsorption by the La/D composite. The fluoride diffusion process could be described in three stages, which included the boundary layer diffusion (first stage), intra-particle diffusion (second stage), and dynamic equilibrium processes of adsorption and desorption (third stage). Concomitantly, the non-zero intercepts (C_1=31.68, C_2=81.83, and C_3=117.27) indicated that the intra-particle diffusion was not the only rate-limiting step for fluoride adsorption of the La/D composite, which might also be affected by various kinetics mechanisms, such as surface chemical interaction [14].

Table 4.4 The detail information of adsorption kinetics, isotherm and thermodynamic equations.

	Adsorption models	Equations	Corresponding parameters
Adsorption kinetics	PFO	$q_t = q_e - \frac{q_e}{exp(K_1 t)}$	t: adsorption time (min); q_t: adsorption capacity at time t (mg/g); K_1: PFO model constant (1/min); K_2: PSO model constant (g/(mg·min)); K_i: Diffusion rate constant (mg·min$^{1/2}$/g); C: boundary layer constant.
	PSO	$q_t = \frac{K_2 q_e^2 t}{1 + K_2 q_e t}$	
	Intra-particle diffusion	$q_t = K_i t^{1/2} + C$	
Adsorption isotherm	Langmuir	$q_e = \frac{q_m K_L c_e}{1 + K_L c_e}$	c_e: equilibrium fluoride concentration (mg/L); q_m: maximum adsorption capacity (mg/g); K_L: Langmuir constants (L/mg); K_F and n: Freundlich constants.
	Freundlich	$q_e = K_F c_e^{\frac{1}{n}}$	
Adsorption thermodynamic		$K_d = \frac{q_e}{c_e}$	K_d: standard equilibrium constant of thermodynamic; R (8.314 J/(mol·K)): gas constant; T (K): the absolute temperature; ΔG (kJ/mol), ΔH (kJ/mol) and ΔS (J/(mol·K)): Gibbs free energy, the changes of enthalpy, and the changes of entropy, respectively.
		$lnK_d = \frac{\Delta S}{R} - \frac{\Delta H}{RT}$	
		$\Delta G = \Delta H - T\Delta S$	

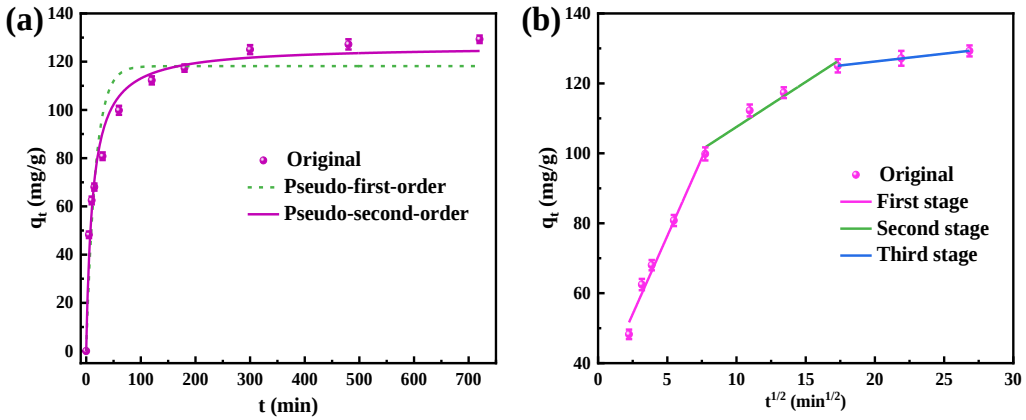


Fig. 4.8 (a) Adsorption kinetics, (b) intra-particle diffusion model of fluoride on the La/D composite (initial pH: 3, the La/D composite dosage: 0.5 g/L, and T: 25°C).

Table 4.5 Adsorption kinetics model parameters of fluoride on the La/D composite.

PFO model			Intra-particle diffusion (First stage)		
K_1 (1/min)	q_e (mg/g)	R^2	K_{i1} (mg·min$^{1/2}$/g)	C_1	R^2
5.89×10^{-2}	118.15	0.92	8.93	31.68	0.98
PSO model			Intra-particle diffusion model (Second stage)		
K_2 (g/(mg·min))	q_e (mg/g)	R^2	K_{i2} (mg·min$^{1/2}$/g)	C_2	R^2
6.65×10^{-4}	126.49	0.98	2.57	81.83	0.95
			Intra-particle diffusion model (Third stage)		
			K_{i3} (mg·min$^{1/2}$/g)	C_3	R^2
			0.45	117.27	0.998

The affinity between the La/D composite and fluoride could be described by adsorption isotherm, which provided insights for the adsorption mechanism and surface behavior of the La/D composite. From Fig. 4.9a, the adsorption capacities all showed a gradual increase until reaching equilibrium with increasing initial fluoride concentration at three temperatures. This might be because the high initial fluoride concentration reduced the mass transfer resistance between the La/D composite and fluoride, thereby enhancing the adsorption capacities of the La/D composite [44]. Further, higher temperatures resulted in lower adsorption capacities, which indicated that the increase of temperature was detrimental to fluoride adsorption by the La/D composite. The Langmuir and Freundlich isotherm models (Eqs in Table 4.4) were chosen in this work to reveal the interaction between fluoride and the La/D composite. Similarly, the fitting results and corresponding parameters are summarized in Fig. 4.9a-b and Table 4.6. The Langmuir isotherm model ($R^2 \geq 0.98$) provided a more accurate description for fluoride adsorption behavior on the La/D composite under three temperatures, suggesting that the fluoride adsorption on the La/D composite was a monolayer adsorption process [45]. Moreover, the feasibility of adsorption process was analyzed by the separation factor (R_L), and the results are shown in Fig. 4.9c. All R_L values were between 0 and 0.50 under the experimental concentrations of three temperatures, indicating that the adsorption of fluoride on the La/D composite was highly favorable.

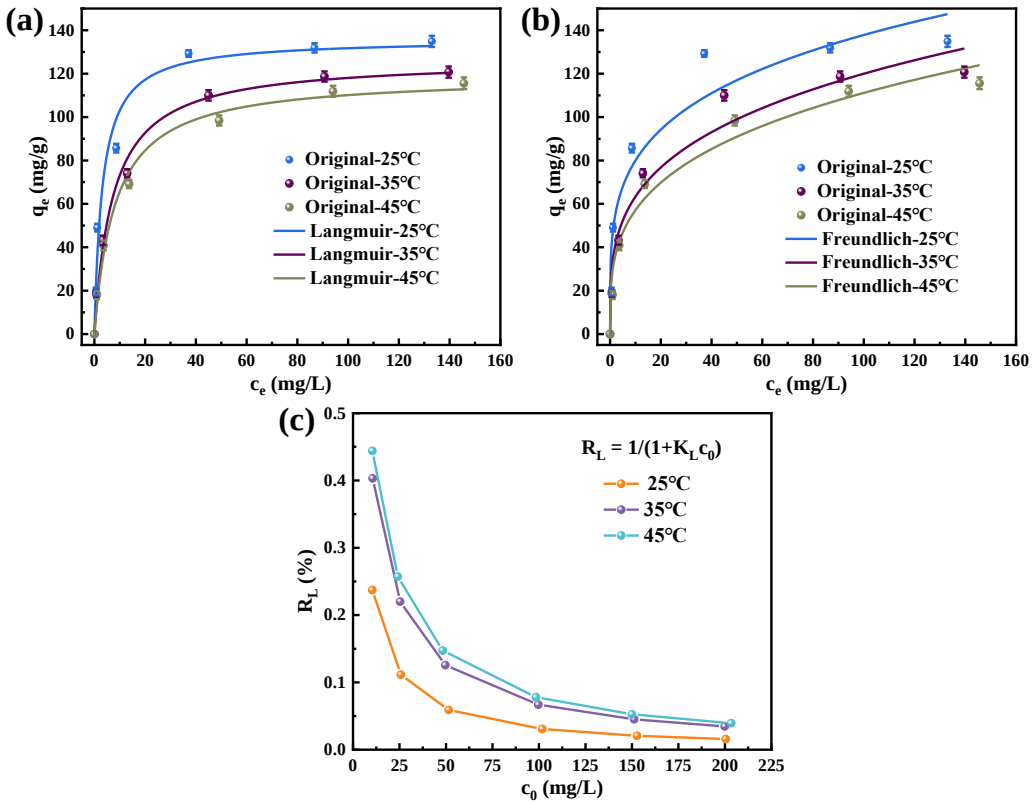


Fig. 4.9 (a-b) Adsorption isotherms and (c) the R_L values of fluoride on the La/D composite (initial pH: 3, the La/D composite dosage: 0.5 g/L, and T: 25°C).

Table 4.6 Adsorption isotherms models parameters of fluoride on the La/D composite.

T (K)	Langmuir			Freundlich		
	K_L (L/mg)	q_{max} (mg/g)	R^2	K_F	n	R^2
298	0.31	135.93	0.98	46.40	4.23	0.93
308	0.14	126.68	0.99	33.43	3.60	0.95
318	0.12	119.10	0.99	29.35	3.46	0.97

Adsorption thermodynamics of fluoride on the La/D composite was further discussed to reveal the characteristics of energy changes and spontaneity of adsorption process. The Eqs. for calculating the thermodynamic parameters are also provided in Table 4.4, and the results are summarized in Fig. 4.10 and Table 4.7. The negative Gibbs free energy changes (ΔG) at the tested temperatures indicated that the fluoride adsorption on the La/D composite was a spontaneous process. The negative entropy change (ΔS) implied that the fluoride adsorption process resulted in the decreased disorder within the system, likely due to the loss of translational freedom of immobilized fluoride. The negative enthalpy change (ΔH) demonstrated the exothermic adsorption process and a strong affinity between the La/D composite and fluoride, which was consistent with the results of adsorption isotherms [46].

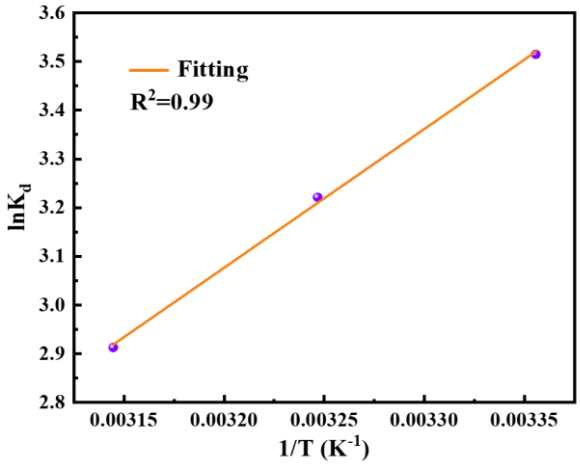


Fig. 4.10 Adsorption thermodynamic of fluoride on the La/D composite (initial pH: 3, the La/D composite dosage: 0.5 g/L, and T: 25°C).

Table 4.7 Adsorption thermodynamics parameters of fluoride on the La/D composite.

T (K)	ΔH (kJ/mol)	ΔS (kJ/(mol·K))	ΔG (kJ/mol)
298			-8.78
308	-23.68	-0.05	-8.28
318			-7.78

To further evaluate the adsorption performance of the La/D composite, a comparative analysis with previously reported clay-based adsorbents was conducted, and the summary is presented in Table 4.8. The maximum adsorption capacity of the La/D composite was 135.93 mg/g, which was considerably higher than that of some reported adsorbents. Meanwhile, the raw material used in this work was industrial diatomite, which is abundant in nature and readily available. Also, La is a rare earth mineral with abundant reserves in China. This means that the prepared composite in this work has high economic feasibility and significant potential for industrial application.

Table 4.8 Comparison of the adsorption capacities and corresponding parameters of various adsorbents.

Adsorbents	pH	Initial concentration range (mg/L)	Adsorption time (min)	Adsorbent dosage (g/L)	q_m (mg/g)	Reference
Cationic surfactant/H_2O_2 modified clay	2.00	20-120	60	2.0	53.66	[19]
Mesoporous silica modified by cerium (Ms-Ce)	3.00	2-80	180	2.0	17.96	[47]
Glauconite clay/chitosan	3.50	10-100	180	2.0	9.00	[48]

nanocomposites						
Calcium-deficient anorthite (de-Ca An)	3.00	0-130	120	1.0	82.50	[49]
Polyethylenimine modified diatomite (PEI/DT)	2.00	1-5	70	0.2	28.62	[22]
Diatomite modified with aluminum hydroxide (Al-DA)	6.00	0-140	120	4.0	45.81	[50]
Kaolin clay	5.00	0-15	60	12.0	3.58	[51]
Montmorillonite	5.00	50-500	60	1.0	40.00	[52]
Aluminum substituted hydroxyapatite (Al-HAp)	7.00	0-10000	1440	20.0	105.00	[42]
La/D composite	3.00	0-200	300	0.5	135.93	This work

4.3.2.3 Effect of coexisting anions on adsorption performance

In common acidic phosphate chemical wastewater, chloride (Cl^-), sulfate (SO_4^{2-}), and phosphate (PO_4^{3-}) were usually coexisting with fluoride, which might compete with fluoride for adsorption active sites. Hence, the effects of above coexisting anions on fluoride adsorption performance were investigated. As shown in Fig. 4.11, the presence of Cl^-, SO_4^{2-}, and PO_4^{3-} decreased the adsorption capacities of the La/D composite, and PO_4^{3-} exhibited the strongest negative effect, followed by SO_4^{2-} and Cl^-. This trend could be attributed to the higher charge/radius value of PO_4^{3-} (3/3.40) compared to SO_4^{2-} (2/2.40) and Cl^- (1/1.81). It has been reported that anions with large charge/radius value exhibited stronger adsorption affinities, which would intensify competition with the target anions during the adsorption process of adsorbents [53]. More importantly, although the coexisting anions exerted a certain negative effect on fluoride adsorption, it could not be ignored that the fluoride adsorption capacities on the La/D composite all remained above 110 mg/g under all experimental concentrations. This result confirmed that the La/D composite maintained a good affinity and selectivity for fluoride even in complex coexisting anions environments.

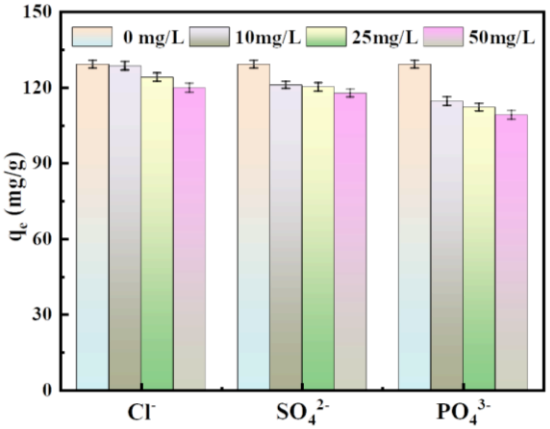


Fig. 4.11 Effect of co-exist anion types and concentration on the fluoride adsorption on the La/D composite (fluoride concentration: 100 mg/L, the La/D composite dosage: 0.5 g/L, T: 25℃, and t: 12 h).

4.3.2.4 Recyclability study

The reusability is an important economic indicator for assessing the adsorption performance of adsorbents. Hence, regeneration experiments were carried out through four adsorption-desorption cycles of the La/D composite. The fluoride adsorption capacity retention of the La/D composite reduced from the initial 100% to 77.46% after four cycles (Fig. 4.12a). Through the analysis of the experimental phenomenon, the reason for this might be that there was a strong bonding between the La/D composite and fluoride, resulting in a low desorption efficiency in NaOH solution [54]. Nevertheless, it was worth noting that the average leaching concentration and leaching percentage of La from the La/D composite were only about 0.16 mg/L and 0.075%, respectively, in acidic fluoride solution during the four regeneration cycles (Fig. 4.12b), suggesting that the La/D composite exhibited excellent acid resistance and stability. In other words, the application of the La/D composite would pose a low risk of secondary pollution to the water environment.

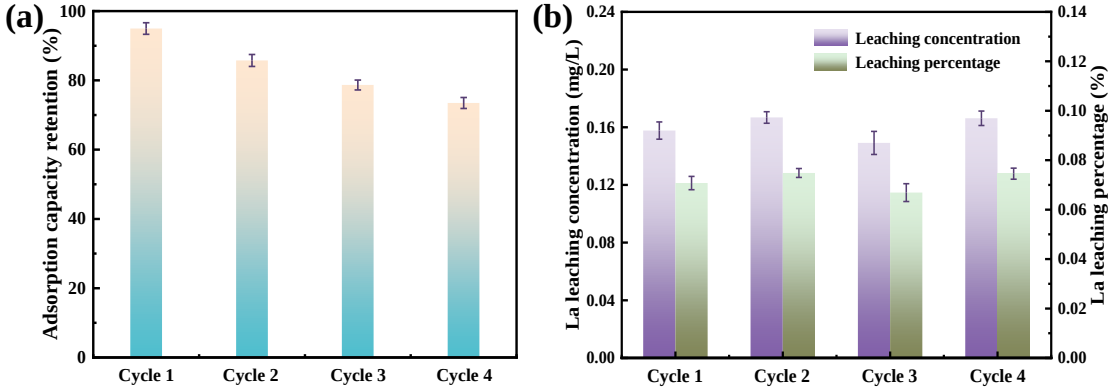


Fig. 4.12 (a) Regeneration performance of the La/D composite; (b) La leaching concentration and leaching percentage in fluoride solution during regeneration

process (initial pH: 3, fluoride concentration: 100 mg/L, the La/D composite dosage: 0.5 g/L, T: 25°C, and t: 12 h).

4.3.3. Removal mechanism of La/D composite

Fig. 4.13 shows the SEM-EDS images of the La/D composite after fluoride adsorption. The structure of the La/D composite did not collapse after adsorption (Fig. 4.13a), indicating that the La/D composite maintained good stability during the adsorption process, which was consistent with the results of the recyclability study. Also, the uniform distribution of F closely matched those of Si, O, and La on the surface of the La/D composite, confirming the successful adsorption of fluoride by the La/D composite. Elemental analysis (Table 4.9) revealed that the contents of La and Si showed no significant changes after fluoride adsorption. Nevertheless, the O content decreased from 36.95 to 20.34 wt%, whereas the F content increased to 19.92 wt%, suggesting that oxygen-containing groups in the La/D composite might participate in the adsorption of fluoride. In addition, the fibrous concave-convex rod-like generated on the La/D composite surface was noted (Fig. 4.13c). It has been proposed that this phenomenon is caused by electrostatic interactions [29]. The zeta potential (Table 4.3) further confirmed this result, where the potential values decreased from 25.40 mV to -1.48 mV after adsorption.

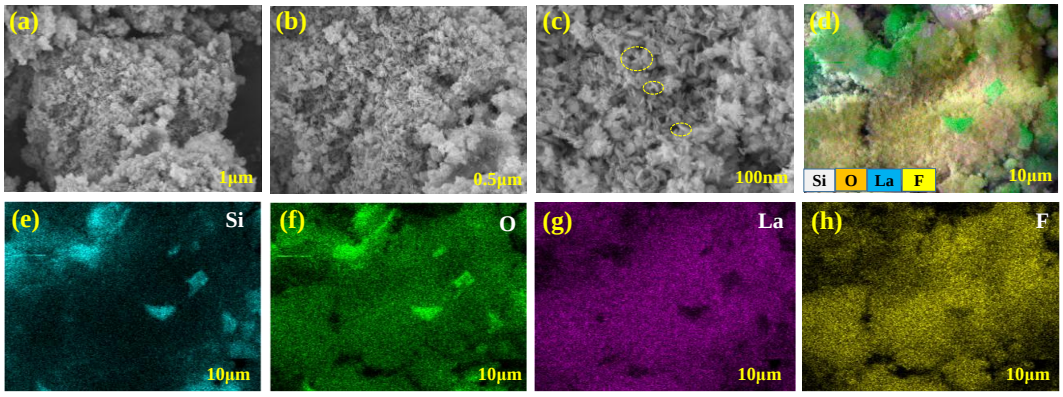


Fig. 4.13 SEM images (a-c) and EDS mapping images (d-h) of La/D composite after fluoride adsorption.

Table 4.9 Elements contents of the La/D composite before and after adsorption of fluoride (wt%).

La/D composite	Si	O	La	F
Before adsorption	18.47	36.95	44.58	-
After adsorption	12.92	20.34	46.82	19.92

The FTIR spectra of the La/D composite before and after fluoride adsorption were

analyzed. As indicated in Fig. 4.14, the characteristic peaks at 1383 cm^{-1} (La-OH) and 3610 cm^{-1} (-OH) both disappeared, while the characteristic peak at 1487 cm^{-1} shifted to 1467 cm^{-1} after adsorption, indicating the involvement of -OH groups on the La/D composite during the fluoride adsorption process. The strong coordination between La and fluoride led to the substitution of -OH groups in La-OH by fluoride [55,56].

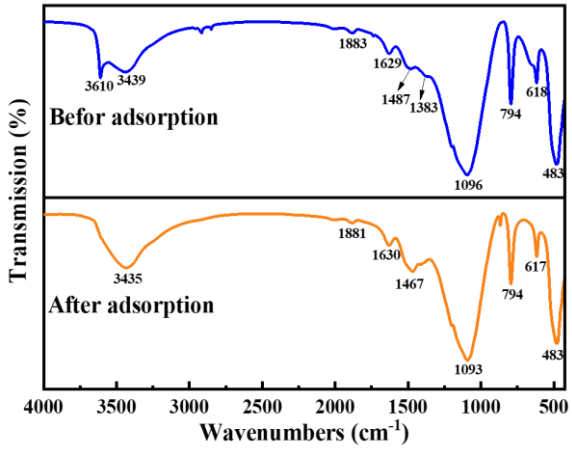


Fig. 4.14 FTIR spectra of the La/D composite before and after fluoride adsorption.

Furthermore, XPS spectra were conducted to reveal the adsorption mechanism between the La/D composite and fluoride in detail. From Fig. 4.15a, the peaks of Si 2p, C 1s, O 1s, La $3d_{3/2}$, and La $3d_{5/2}$ were observed in wide scan XPS spectrum of the La/D composite. After fluoride adsorption, a new peak attributed to F 1s appeared at 685.10 eV (Fig. 4.15b), suggesting the successful immobilization of fluoride on the La/D composite [57]. The atomic concentrations presented in Table 4.10 also supported these findings. Compared with the La/D composite, the concentrations of O 1s decreased from initial 31.41% to 16.94%, while the F 1s concentrations increased from 0% to 15.67% after adsorption, further indicating that the oxygen-containing groups in the La/D composite played crucial roles during the fluoride removal process, which was in consistent with the SEM-EDS and FTIR analyses.

As shown in Fig. 4.15c, the high-resolution O 1s spectrum of the La/D composite before adsorption could be deconvoluted into three peaks at 530.77 eV, 531.47 eV, and 532.68 eV, which referred to metal-oxide (M-O, 20.79%), La-OH (49.35%), and adsorbed water (H_2O, 29.86%), respectively [58,59]. After fluoride adsorption, the peak area ratio of La-OH decreased significantly from 49.35% to 26.99%, further indicating that ligand exchange had occurred between fluoride and -OH groups of the La/D composite [60]. The high-resolution La 3d spectrum are shown in Fig. 4.15d. For the La/D composite, two peaks at 835.61 eV and 839.12 eV were assigned to La $3d_{5/2}$,

whereas other two peaks at 852.31 eV and 855.99 eV were ascribed to La $3d_{3/2}$, which are all in agreement with the previous studies [61,62]. After fluoride adsorption, the binding energies of La $3d_{5/2}$ and La $3d_{3/2}$ shifted from 835.61 eV / 839.12 eV and 852.31 eV / 855.99 eV to 837.30 eV / 840.12 eV and 853.77 eV / 856.79 eV, respectively, which both shifted to higher values (0.80 eV-1.69 eV), demonstrating the change of the electron environment of La. Meanwhile, a new peak assigned to La-F species was observed at 830.37 eV [63]. These findings suggested that fluoride was also adsorbed onto the La/D composite through chemisorption with a probable electron migration or strong interactions, and a La-F complex had formed [64].

Table 4.10 Atomic concentrations of the La/D composite before and after adsorption of fluoride (%).

La/D composite	Si 2p	O 1s	La 3d	C 1s	F 1s
Before adsorption	52.01	31.41	8.43	8.16	-
After adsorption	49.75	16.94	9.46	8.18	15.67

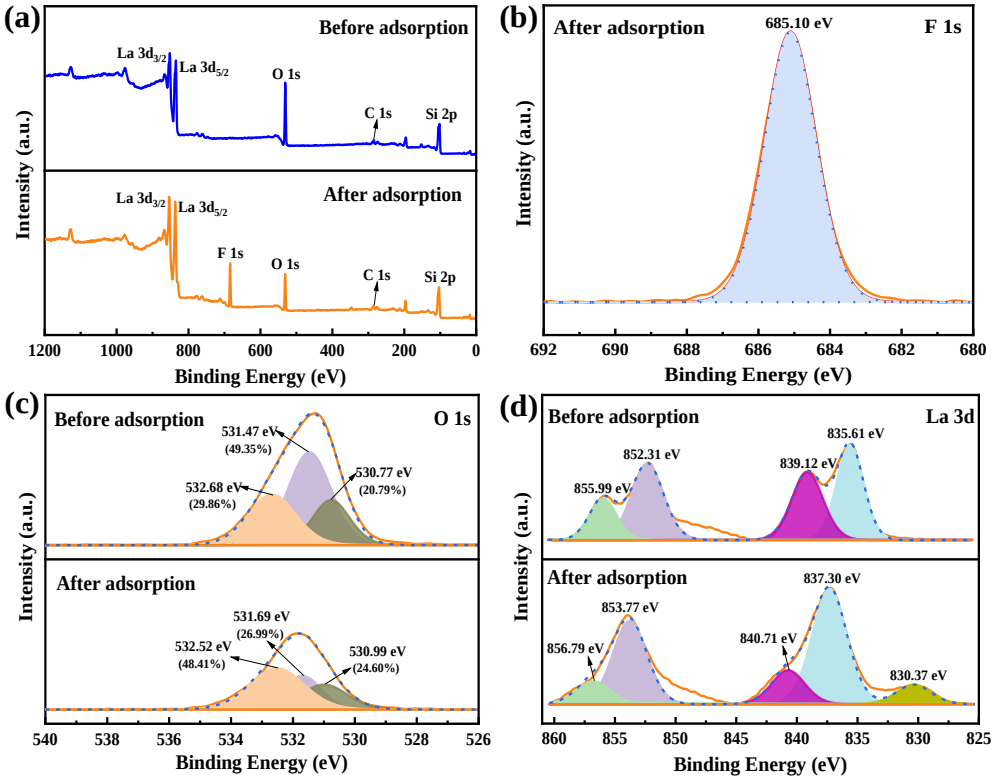


Fig. 4.15 (a) The wide scan XPS, (b) F 1s, (c) O 1s, and (d) La 3d spectra of the La/D composite before and after fluoride adsorption.

In summary, the removal mechanism of the La/D composite for fluoride is analyzed and proposed in Fig. 4.16. Diatomite provided a stable carrier for fluoride removal by the La/D composite. The introduction of $La(OH)_3$ nanophases could be stably loaded on the diatomite surface, thereby further enhancing the acid resistance of

the La/D composite, altering the surface charge of diatomite, and increasing the number of adsorption active sites, which played an important role during the fluoride removal process. Electrostatic interaction, ligand exchange, and coordination complexation dominated the strong combination between fluoride and the La/D composite.

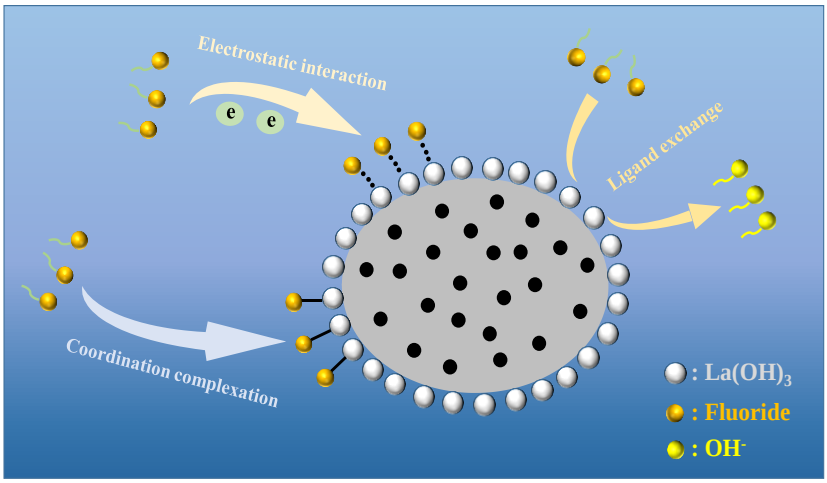


Fig. 4.16 Schematic diagram of fluoride adsorption on the La/D composite.

4.3.4. Fluoride removal from real acidic phosphate chemical wastewater

To investigate the industrial application potential of the La/D composite, the fluoride removal on real acidic phosphate chemical wastewater was further tested. The used wastewater sample was phosphogypsum wastewater that obtained from a chemical company of Hubei, China. The pH and ions concentration are shown in Table 4.11, and the effects of the La/D composite dosage on q_e and R of fluoride are shown in Fig. 4.17. The R values gradually increased with increasing the dosage of La/D composite. When the dosage of La/D composite was 3.0 g/L, the fluoride concentration was decreased from initial 70.49 mg/L to 3.83 mg/L with the removal efficiency of 94.56%, which meets the discharge standard of national industrial wastewater of China (GB39371-2020, less than 10 mg/L). This finding suggested that the La/D composite had the ability to achieve efficient fluoride removal under the complex environment of acidic phosphate chemical wastewater.

Table 4.11 The concentration of anions and cation in real phosphogypsum wastewater (mg/L).

Compositions	pH	F^-	Cl^-	SO_4^{2-}	PO_4^{3-}	Ca^{2+}	Mg^{2+}	Al^{3+}	Fe^{3+}	Na^+	K^+
Concentration	3.08	70.49	35.86	85.34	42.00	243.12	28.17	30.06	422.12	65.15	97.99

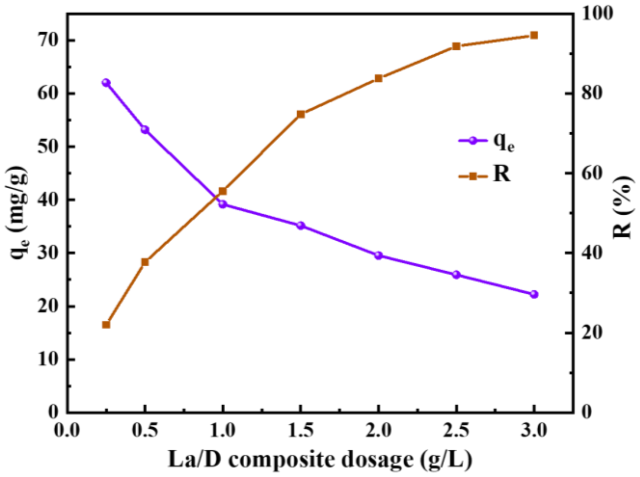


Fig. 4.17 Effect of the La/D composite dosage on fluoride q_e and R in real acidic phosphogypsum wastewater (T: 25 ℃ and t: 12 h).

4.4. Conclusions

In this work, diatomite was successfully engineered with $La(OH)_3$ through a loading strategy, yielding a novel La/D composite with outstanding acid resistance and defluorination capability. The La/D composite exhibited remarkable adsorption performance in acidic environments, with a maximum adsorption capacity of 135.93 mg/g, far exceeding that of pristine diatomite and many reported clay-based adsorbents. The adsorption kinetics, isotherms, and thermodynamics were best described by the PSO and Langmuir models, respectively, suggesting a spontaneous and exothermic chemisorption process on homogeneous active sites. The La/D composite also demonstrated good selectivity in the presence of coexisting anions (Cl^-, SO_4^{2-}, PO_4^{3-}) and retained 77.46% of its initial adsorption capacity with an average La leaching percentage of only about 0.075% after four regeneration cycles, underscoring its excellent stability and reusability. Mechanistic analyses revealed that fluoride removal proceeded predominantly via electrostatic attraction, ligand exchange, and coordination complexation. Importantly, the practical feasibility of the La/D composite was validated using real phosphogypsum wastewater, where the fluoride concentration was reduced from 70.49 mg/L to 3.83 mg/L (removal efficiency of 94.56%) at a dosage of 3.0 g/L, meeting the Chinese industrial wastewater discharge standard. Overall, this study establishes a scalable lanthanum-loading approach to re-engineer diatomite into a high-performance adsorbent, offering a promising solution for the treatment of acidic phosphate chemical wastewater, particularly phosphogypsum wastewater.

4.5. References

[1] Q. Wang, X. Bai, S. Sun, Y. Li, M. Tan, Y. Wang, N. Wang, T. Wang, L. Zhou, Z. Zhou, X. Huang, H. Hao, Deep eutectic system based C_3N_4-Zr composite material for highly efficient removal of fluoride in hydrochloric acid, Separation and Purification Technology 342 (2024) 126985. https://doi.org/10.1016/j.seppur.2024.126985.

[2] J.-H. Ou, C.-C. Wang, F. Verpoort, C.-C. Chien, H.-B. Zhong, C.-M. Kao, Development of innovative and green adsorbents for in situ cleanup of fluoride-polluted groundwater: Mechanisms and field-scale studies, Chemosphere 350 (2024) 141035. https://doi.org/10.1016/j.chemosphere.2023.141035.

[3] M. Zhang, Enhanced fluoride removal using montmorillonite clay modified with $CoFe_2O_4$ and metal-organic frameworks, Environmental Research 258 (2024) 119389. https://doi.org/10.1016/j.envres.2024.119389.

[4] L. Huang, L. Sheng, K. Wan, M. Wang, H. Zhang, J. Yan, Y. Liu, S.I. Alhassan, Y. Chen, S.R.B. Arulmani, The diversified mechanism of adsorption and electro-adsorption technologies by using Ti3AlC2 for removing fluoride, Desalination 578 (2024) 117449. https://doi.org/10.1016/j.desal.2024.117449.

[5] A. Sarwar, J. Wang, N. Riaz, M.S. Khan, B.S. Zeb, I.A. Khan, M. Akmal, A. Khalid, A. Khan, A. Al-Harrasi, Q. Mahmood, Optimizing the fluoride removal from drinking water through adsorption with mesoporous magnetic calcite nanocomposites, Results in Engineering 22 (2024) 102100. https://doi.org/10.1016/j.rineng.2024.102100.

[6] Y. Chen, J. Viridiana Garc á-Meza, B. Zhou, Z. Peng, Q. Chen, R.M. Kasomo, X. Weng, H. Li, S. Song, Efficient recovery of fluorine from wet-process phosphoric acid using silicon powder as a new and eco-friendly reagent, Separation and Purification Technology 337 (2024) 126435. https://doi.org/10.1016/j.seppur.2024.126435.

[7] L. Tong, X. Liu, Y. Liu, K. Zhou, S. Zhang, Q. Jia, W. Lu, Y. Huang, G. Ni, Accumulation of high concentration fluoride in the Ulungur Lake water through weathering of fluoride containing rocks in Xinjiang, China, Environmental Pollution 323 (2023) 121300. https://doi.org/10.1016/j.envpol.2023.121300.

[8] K. Wan, L. Huang, J. Yan, B. Ma, X. Huang, Z. Luo, H. Zhang, T. Xiao, Removal of fluoride from industrial wastewater by using different adsorbents: A review, Science of The Total Environment 773 (2021) 145535. https://doi.org/10.1016/j.scitotenv.2021.145535.

[9] X. Hu, F. Zhu, L. Kong, X. Peng, A novel precipitant for the selective removal of fluoride ion from strongly acidic wastewater: Synthesis, efficiency, and mechanism, Journal of Hazardous Materials 403 (2021) 124039. https://doi.org/10.1016/j.jhazmat.2020.124039.

[10] T. Yu, Y. Chen, Y. Zhang, X. Tan, T. Xie, B. Shao, X. Huang, Novel reusable sulfate-type zirconium alginate ion-exchanger for fluoride removal, Chinese

Chemical Letters 32 (2021) 3410–3415. https://doi.org/10.1016/j.cclet.2021.04.057.

[11] P. Thamarai, V.C. Deivayanai, S. Karishma, P.R. Yaashikaa, A. Saravanan, Effective removal of fluoride ions from contaminated water using electrochemical techniques: A critical review on recent developments and environmental perspective, Journal of Hazardous Materials Advances 16 (2024) 100483. https://doi.org/10.1016/j.hazadv.2024.100483.

[12] W. Xue, F. Zhang, W. Ding, K. Zhang, Q. Zhang, Enhanced removal of fluoride ions using lanthanum-doped coconut shell biochar in PVDF ultrafiltration membranes, Journal of Hazardous Materials 480 (2024) 136393. https://doi.org/10.1016/j.jhazmat.2024.136393.

[13] S. Zhou, X. Chen, Q. Li, L. Huang, X. Qiu, J. Yan, H. Zhang, Q. Zheng, Q. Liu, A comprehensive review of fluoride removal using low-cost adsorbents for environmental and industrial applications, Environmental Surfaces and Interfaces 3 (2025) 146–162. https://doi.org/10.1016/j.esi.2025.04.002.

[14] Y. Pan, L. Li, B. Yang, G. Ji, Z. Zhao, H. Zhang, F. Wang, M. Xia, Y. Tao, Adaptive structural modification of Zr-based MOF-808 via solvent and ligand engineering for enhanced fluoride ion adsorption efficiency, Separation and Purification Technology 348 (2024) 127731. https://doi.org/10.1016/j.seppur.2024.127731.

[15] M. Yu, Z. Gan, T. Liao, A. Tang, H. Yang, Interfacial hydration of Zeolite-Confined MgO for enhanced fluoride removal from water, Chemical Engineering Journal 513 (2025) 163053. https://doi.org/10.1016/j.cej.2025.163053.

[16] D.B. Adamu, L.T. Tufa, J. Lee, E. Zereffa, T.A. Segne, M.H. Razali, Facile synthesis of bismuth and iron co-doped hydroxyapatite nanomaterials for high-performance fluoride ions adsorption, Journal of Environmental Chemical Engineering 11 (2023) 111196. https://doi.org/10.1016/j.jece.2023.111196.

[17] H. Kikuchi, H. Konno, Defective UiO-66 framework for the adsorptive removal of fluoride ions in water, Inorganic Chemistry Communications 179 (2025) 114755. https://doi.org/10.1016/j.inoche.2025.114755.

[18] Y. Gao, S. Liu, Adsorption characterization and mechanism of aluminum based chitosan/zeolite molecular sieve composite for fluoride removal, Desalination and Water Treatment 247 (2022) 108–120. https://doi.org/10.5004/dwt.2022.28082.

[19] M. Mobarak, A.Q. Selim, E.A. Mohamed, M.K. Seliem, Modification of organic matter-rich clay by a solution of cationic surfactant/H_2O_2: A new product for fluoride adsorption from solutions, Journal of Cleaner Production 192 (2018) 712–721. https://doi.org/10.1016/j.jclepro.2018.05.044.

[20] S.I. Alhassan, H. Wang, Y. He, L. Yan, Y. Jiang, B. Wu, T. Wang, H. Gang, L. Huang, L. Jin, Y. Chen, Fluoride remediation from on-site wastewater using optimized bauxite nanocomposite (Bx-Ce-La@500): Synthesis maximization, and mechanism of F- removal, Journal of Hazardous Materials 430 (2022) 128401. https://doi.org/10.1016/j.jhazmat.2022.128401.

[21] J. Wang, G. Zhang, S. Qiao, J. Zhou, Magnetic Fe^0/iron oxide-coated diatomite as a highly efficient adsorbent for recovering phosphorus from water, Chemical Engineering Journal 412 (2021) 128696. https://doi.org/10.1016/j.cej.2021.128696.

[22] Y. Zhang, H. Zhang, J. Zhao, X. Zhang, Enhanced adsorption of fluoride ion by polyethylenimine modified diatomite in aqueous solution: adsorption optimization, models, and mechanism, Desalination and Water Treatment 283 (2023) 130–140. https://doi.org/10.5004/dwt.2023.29218.

[23] E. Kır, H. Oruc, I. Kır, T. Sardohan-Koseoglu, Removal of fluoride from aqueous solution by natural and acid-activated diatomite and ignimbrite materials, Desalination and Water Treatment 57 (2016) 21944–21956. https://doi.org/10.1080/19443994.2015.1124346.

[24] J. Wang, L. Wu, J. Li, D. Tang, G. Zhang, Simultaneous and efficient removal of fluoride and phosphate by Fe-La composite: Adsorption kinetics and mechanism, Journal of Alloys and Compounds 753 (2018) 422–432. https://doi.org/10.1016/j.jallcom.2018.04.177.

[25] Y. He, L. Zhang, X. An, G. Wan, W. Zhu, Y. Luo, Enhanced fluoride removal from water by rare earth (La and Ce) modified alumina: Adsorption isotherms, kinetics, thermodynamics and mechanism, Science of The Total Environment 688 (2019) 184–198. https://doi.org/10.1016/j.scitotenv.2019.06.175.

[26] Y. Zhang, X. Lin, Q. Zhou, X. Luo, Fluoride adsorption from aqueous solution by magnetic core-shell Fe_3O_4@alginate-La particles fabricated via electro-coextrusion, Applied Surface Science 389 (2016) 34–45. https://doi.org/10.1016/j.apsusc.2016.07.087.

[27] L. Ma, Y. Zhang, P. He, B. Zhao, X. Zhang, H. Xiao, M. Diwu, D. Liu, Q. Gu, C. Lu, Development of a rare earth modified residue of leaching aluminium from gangue for fluoride ion adsorption from mine water, Minerals Engineering 232 (2025) 109536. https://doi.org/10.1016/j.mineng.2025.109536.

[28] L. Kong, Y. Tian, Z. Pang, X. Huang, M. Li, N. Li, J. Zhang, W. Zuo, J. Li, Needle-like Mg-La bimetal oxide nanocomposites derived from periclase and lanthanum for cost-effective phosphate and fluoride removal: Characterization, performance and mechanism, Chemical Engineering Journal 382 (2020) 122963. https://doi.org/10.1016/j.cej.2019.122963.

[29] X. Sun, C. Ke, Q. Lu, L. Liang, G. Xie, Adsorption of fluoride ion on Al/La modified acidified attapulgite composite materials, Separation and Purification Technology 354 (2025) 128791. https://doi.org/10.1016/j.seppur.2024.128791.

[30] N. Wang, J. Li, F. Jia, H. Zhou, Y. Xie, P. Chen, S. Song, M. Quintana, Unraveling nitrogen-doped and vacancy-engineered synergistically modified molybdenum oxide promoting gallium selective adsorption, Separation and Purification Technology 358 (2025) 130158. https://doi.org/10.1016/j.seppur.2024.130158.

[31] L. Kong, Y. Tian, Z. Pang, X. Huang, M. Li, R. Yang, N. Li, J. Zhang, W. Zuo, Synchronous phosphate and fluoride removal from water by 3D rice-like

lanthanum-doped La@MgAl nanocomposites, Chemical Engineering Journal 371 (2019) 893–902. https://doi.org/10.1016/j.cej.2019.04.116.

[32] J. Wang, G. Zhang, S. Qiao, J. Zhou, Comparative assessment of formation pathways and adsorption behavior reveals the role of NaOH of MgO-modified diatomite on phosphate recovery, Science of The Total Environment 876 (2023) 162785. https://doi.org/10.1016/j.scitotenv.2023.162785.

[33] H. Xi, H. Jiang, D. Zhao, A.H. Zhang, B. Fan, Y. Yang, J. Zhang, Highly selective adsorption of phosphate from high-salinity water environment using MgO-loaded and sodium alginate-immobilized bentonite beads, Journal of Cleaner Production 313 (2021) 127773. https://doi.org/10.1016/j.jclepro.2021.127773.

[34] A.M. Abou-Elanwar, S.Y. Lee, J. Yu, J. Kim, C. Hwang, H. Park, Y. Noh, M. Xie, J. Lin, S.-J. Park, D.H. Seo, Y. Kim, Co-adsorption of methylene blue/Pb(II) from aqueous solutions using sulfonated mesoporous diatomite, Journal of Water Process Engineering 71 (2025) 107334. https://doi.org/10.1016/j.jwpe.2025.107334.

[35] G.S. Dos Reis, G.L. Dotto, J. Vieillard, M.L.S. Oliveira, S.F. Lütke, L.F.O. Silva, É.C. Lima, N.P.G. Salau, U. Lassi, Uptake the rare earth elements Nd, Ce, and La by a commercial diatomite: kinetics, equilibrium, thermodynamic and adsorption mechanism, Journal of Molecular Liquids 389 (2023) 122862. https://doi.org/10.1016/j.molliq.2023.122862.

[36] X. Cui, Z. Zhong, X. Xie, P. Jiang, Sorptive removal of cadmium using the attapulgite modified by the combination of calcination and iron, Environ Sci Pollut Res 30 (2023) 120820–120831. https://doi.org/10.1007/s11356-023-30323-z.

[37] Y. Shang, X. Xu, B. Gao, Q. Yue, Highly selective and efficient removal of fluoride from aqueous solution by Zr La dual-metal hydroxide anchored bio-sorbents, Journal of Cleaner Production 199 (2018) 36–46. https://doi.org/10.1016/j.jclepro.2018.07.162.

[38] T. Wang, K. Zhu, Z. Xu, T. Wang, Y. Zhang, H. Li, W. Jin, Enhanced phosphate adsorption via controlled synthesis of lanthanum hydroxide by surfactants with varied alkyl chain lengths, Separation and Purification Technology 338 (2024) 126506. https://doi.org/10.1016/j.seppur.2024.126506.

[39] Y. Wang, C. Guo, Y. Liu, X. Li, Y. Liu, R. Naidu, M.M. Rahman, High efficiency of phosphate adsorption by yolk-shell Mn–La binary nanocomposites from aqueous solution: Adsorption and mechanism studies, Journal of Water Process Engineering 71 (2025) 107347. https://doi.org/10.1016/j.jwpe.2025.107347.

[40] L. Sheng, K. Wan, L. Huang, J. Yan, Q. Huang, Y. Liu, Y. Guo, H. Zhang, Adsorption effect for removing fluoride with species of nitrogen by using La-BDC-NH_2/C_3N_4: Experiments and mechanism, Journal of Environmental Chemical Engineering 12 (2024) 114439. https://doi.org/10.1016/j.jece.2024.114439.

[41] L. Zhuang, G. Wang, K. Yu, C. Yao, Enhanced adsorption of anionic dyes from aqueous solution by gemini cationic surfactant-modified diatomite, Desalination

and Water Treatment 51 (2013) 6526–6535. https://doi.org/10.1080/19443994.2013.766903.

[42] B. Bera, S. Saha Chowdhury, V.R. Sonawane, S. De, High capacity aluminium substituted hydroxyapatite incorporated granular wood charcoal (Al-HApC) for fluoride removal from aqueous medium: Batch and column study, Chemical Engineering Journal 466 (2023) 143264. https://doi.org/10.1016/j.cej.2023.143264.

[43] D. Chen, W. Shen, S. Wu, C. Chen, X. Luo, L. Guo, Ion exchange induced removal of Pb(II) by MOF-derived magnetic inorganic sorbents, Nanoscale 8 (2016) 7172–7179. https://doi.org/10.1039/C6NR00695G.

[44] L. Zhang, S. Zheng, P. Li, Z. Zhu, Y. Zou, P. Zhang, Resource utilization of organic spent adsorbent to prepare three-dimensional sulfate-functionalized layered double oxide for superior removal of azo dye, Environ Sci Pollut Res 28 (2021) 53021–53033. https://doi.org/10.1007/s11356-021-14327-1.

[45] X. Weng, X. Zhang, P. Ai, Q. Chen, R.M. Kasomo, J. Viridiana Garcá-Meza, H. Li, Y. Chen, S. Song, Efficient adsorption of sodium oleate from wastewater with graphene oxide/polyethyleneimine composite hydrogel: Performance and mechanism, Chemical Physics Letters 856 (2024) 141625. https://doi.org/10.1016/j.cplett.2024.141625.

[46] S. Liu, J. Wang, J. Ren, M. Zhang, H. Mao, Environmentally benign tannin-modified chitosan aerogel decorated with Zr(IV) enabled high-performance adsorption of fluoride, Chemical Engineering Journal 519 (2025) 165351. https://doi.org/10.1016/j.cej.2025.165351.

[47] L. Zhang, W. Tan, R. Wang, Y. Yang, M. Yang, H. Wang, The characterization of mesoporous silica (Ms) supporting cerium carbonate (Ms-Ce) and its adsorption performance for defluorination in aqueous solutions, Desalination and Water Treatment 135 (2018) 362–371. https://doi.org/10.5004/dwt.2018.23276.

[48] M.M. Sobeih, M.F. El-Shahat, A. Osman, M.A. Zaid, M.Y. Nassar, Glauconite clay-functionalized chitosan nanocomposites for efficient adsorptive removal of fluoride ions from polluted aqueous solutions, RSC Adv. 10 (2020) 25567–25585. https://doi.org/10.1039/D0RA02340J.

[49] W. Liu, P. Liu, Y. Yang, J. Wu, J. Wang, M. Xu, W. Zhou, Y. Li, H. Li, Engineering oxygen vacancies on anorthite for efficient surface adsorption of fluoride, Surfaces and Interfaces 57 (2025) 105785. https://doi.org/10.1016/j.surfin.2025.105785.

[50] B. Xiang, J. Tang, X. Feng, Y. Zhu, Y. Li, T. Tan, Preparation of aluminium-hydroxide-modified diatomite and its fluoride adsorption mechanism, Sci Rep 13 (2023) 3871. https://doi.org/10.1038/s41598-023-30901-8.

[51] A.A. Ayalew, Comparative adsorptive performance of adsorbents developed from kaolin clay and limestone for de-fluoridation of groundwater, South African Journal of Chemical Engineering 44 (2023) 1–13. https://doi.org/10.1016/j.sajce.2022.11.002.

[52] S. Guiza, F. Brouers, M. Bagane, Fluoride removal from aqueous solution by montmorillonite clay: Kinetics and equilibrium modeling using new generalized fractal equation, Environmental Technology & Innovation 21 (2021) 101187. https://doi.org/10.1016/j.eti.2020.101187.

[53] Y. Chen, Q. Chen, R.M. Kasomo, Y. Jin, P. Yang, H. Zheng, X. Weng, H. Li, S. Song, Adsorption of fluoride from aqueous solutions using graphene oxide composite materials at a neutral pH, Journal of Molecular Liquids 377 (2023) 121467. https://doi.org/10.1016/j.molliq.2023.121467.

[54] A. Savari, S. Hashemi, H. Arfaeinia, S. Dobaradaran, R. Foroutan, A.H. Mahvi, M. Fouladvand, G.A. Sorial, S. Farjadfard, B. Ramavandi, Physicochemical characteristics and mechanism of fluoride removal using powdered zeolite-zirconium in modes of pulsed& continuous sonication and stirring, Advanced Powder Technology 31 (2020) 3521–3532. https://doi.org/10.1016/j.apt.2020.06.039.

[55] C. Jia, J. Wang, H. Wang, S. Zhu, X. Zhang, Y. Wang, Performance and mechanism of La-Fe metal-organic framework as a highly efficient adsorbent for fluoride removal from mine water, Journal of Environmental Sciences 139 (2024) 245–257. https://doi.org/10.1016/j.jes.2023.05.039.

[56] H. Ma, Y. Huang, J. Tang, W. Wang, B. Liu, H. Sun, S. Yang, G. Han, Enhanced fluoride removal via adsorption flotation based on La-MOF carrier morphology modulation strategy, Separation and Purification Technology 365 (2025) 132652. https://doi.org/10.1016/j.seppur.2025.132652.

[57] D. Liu, Y. Li, C. Liu, B. Li, Porous Lanthanum-Zirconium phosphate with superior adsorption capability of fluorine for water treatment, Journal of Colloid and Interface Science 636 (2023) 588–601. https://doi.org/10.1016/j.jcis.2023.01.062.

[58] Q. He, H. Zhao, Z. Teng, Y. Wang, W. Sun, Y. Guo, X. Ji, W. Hu, S. Shiung Lam, M. Li, Efficient recovery of phosphate by Fe_3O_4/La-MOF: An insight of adsorption performance and mechanism from electrochemical properties, Separation and Purification Technology 314 (2023) 123529. https://doi.org/10.1016/j.seppur.2023.123529.

[59] Q. Zhang, Z. Zhang, X. Sang, L. Wang, Q. Li, S. Li, X. Yang, Lanthanum chloride/eggshells modified diatomite for phosphorus recovery: Advanced performance and mechanisms study, Journal of Environmental Chemical Engineering 12 (2024) 114062. https://doi.org/10.1016/j.jece.2024.114062.

[60] L. He, G. Wang, X. Zhang, Y. Zhang, Y. Chen, Lanthanum-doped activated carbon derived from municipal sludge for enhanced defluoridation: characteristics and mechanism, Water Science and Technology 82 (2020) 1643–1652. https://doi.org/10.2166/wst.2020.435.

[61] Z. Zhu, L. Qin, Y. Liu, Q. Zhang, P. Cheng, W. Liang, Fabrication and mechanism of La/Al bimetallic organic frameworks for phosphate removal, Chemical Engineering Journal 479 (2024) 147081. https://doi.org/10.1016/j.cej.2023.147081.

[62] Y. Wang, Y. Liu, T. Guo, H. Liu, J. Li, S. Wang, X. Li, X. Wang, Y. Jia, Lanthanum hydroxide: a highly efficient and selective adsorbent for arsenate removal from aqueous solution, Environ Sci Pollut Res 27 (2020) 42868–42880. https://doi.org/10.1007/s11356-020-10240-1.

[63] B. Jia, Y. Li, J. Guo, F. Zhou, Y. Guo, Y. Yang, Nanometer lanthanum hydroxide modified anionic polymer for deep fluoride removal: Adsorption properties and mechanism study, Progress in Natural Science: Materials International 33 (2023) 833–842. https://doi.org/10.1016/j.pnsc.2023.12.016.

[64] R. Liu, J. Song, J. Zhao, Z. Wang, J. Xu, W. Yang, J. Hu, Novel MOF(Zr)–on-MOF(Ce/La) adsorbent for efficient fluoride and phosphate removal, Chemical Engineering Journal 497 (2024) 154780. https://doi.org/10.1016/j.cej.2024.154780.

Chapter 5. Synergistic and efficient fluoride removal from acidic phosphate chemical wastewater enabled by bimetallic hydroxides-loaded montmorillonite

5.1. Introduction

With the vigorous development of the phosphorus chemical industry in the last several years, the production of phosphogypsum (PG), a major solid-waste generated from the wet-process phosphoric acid process, has shown rapid growth [1]. The data showed that the current PG stockpile in China exceeded 500 million tons and increased at a rate of tens of million tons per year [2]. Regrettably, only about 15% of PG was utilized in building materials, roadbed filling and other fields, while the remaining 85% was still stored in open-air [3]. Due to the requirements of preparation process of wet-process phosphoric acid and the complexity of phosphate rock composition, PG had the characteristics of low pH and many kinds of impurities (organic matter, fluoride, phosphate and others) [4,5]. Based on these, flotation technology was considered to be the most effective way to pre-treat PG for its subsequent resource utilization. Nevertheless, the concomitantly produced PG wastewater containing strong acidity (about 1-4) and the above impurities would be discharged outside during flotation process, which caused serious pollution and harm to surrounding environment and people [6]. For these impurities, fluoride pollution (concentration range of 50-200 mg/L) was inevitable and the most serious. Studies showed that the excess fluoride in water could lead to withering of trees and cause cartilage disease, tooth damage, Alzheimer's disease, etc. in humans [7,8]. Unfortunately, the presence of acidic environment resulted in an excessively high hydrogen ion concentration, which severely hindered the fluoride removal. Therefore, developing targeted strategies to enhance efficient fluoride removal from acidic PG flotation wastewater is of great significance for the environmental clean development and human health.

Until now, precipitation [9], ion exchange [10], membrane separation [11], electrocoagulation [12], adsorption [13], and electroadsorption [14] technologies have been utilized for fluoride removal from PG flotation wastewater. Among these, adsorption or the derived electroadsorption, endowed with simple operation, high efficiency and low residual fluoride concentration, has become a widely used

technology [15]. The fluoride removal by adsorption was primarily through directly physical or chemical interactions between the adsorbent and fluoride, whereas electroadsorption applied an external electric field to drive the further directional migration of fluoride on the basis of adsorption. The adsorbents play crucial roles during this process. Consequently, many adsorbents, such as activated carbon, metal-organic frameworks (MOFs), molecular sieves, metal-based composites and so on, were developed by researchers [16-18]. For instance, Li et al. synthesized the cerium/iron oxides-loaded zeolite (Ce/Fe-ZL) for enhanced fluoride removal from PG leachate, which exhibited the maximum adsorption capacity of 45.68 mg/g. [19]. Nevertheless, the currently developed adsorbents exhibited weak fluoride removal performance in acidic environment, which was mainly attributed to the unsatisfactory acid resistance with the structural collapse and active sites dissolution under the attack of high hydrogen ion concentration. Hence, there is still an urgent need for targeted research on fluoride-removal composites with excellent acid resistance, high removal performance and stable structure to adapt to the complex acidic PG flotation wastewater environment.

As a cheap, easily available and abundant natural silicate mineral, montmorillonite (MMT) has been a new favorite in water treatment known for its large specific surface area, high porosity, strong cation exchange capacity and good mechanochemical stability, which provides an ideal carrier platform for the loading and dispersion of functional components, such as efficient fluoride removal active sites and others [20,21]. The studies reported that MMT was widely utilized in the removal of dyes, heavy metals, and other pollutants from wastewater, which all achieved ideal effects [22,23]. Unfortunately, MMT faced two key challenges in fluoride removal of acidic PG flotation wastewater: (1) isostructural substitution within the MMT lattice caused a permanent negative charge on its surface (about 0.2-0.6 e^- per unit cell), resulting in electrostatic repulsion towards anions [24]. (2) natural MMT showed very poor settleability in water environment after adsorption, which caused troubles to subsequent recycling [25]. These challenges obviously limited the further application of MMT in fluoride removal field of PG flotation wastewater.

Based on the excellent stability and negative charge of MMT, metal and functional groups loading, pillaring, intercalation, or surface grafting is considered to be an effective strategy to regulate surface charge of MMT, which could provide more active sites and enhance adsorption performance [20,26-28]. Among these modifications,

bimetallic hydroxides modified composites have received widespread attention in wastewater treatment in recent years [29]. Compared to single metal hydroxide, bimetallic system would combine the advantages of both metals, which further achieved the synergistic effect in adjusting adsorption performance, enhancing structural stability, and extending service life [30,31]. For example, Zhang prepared MMT/$CoFe_2O_4$/Al-Fe Fum to remove fluoride from aqueous solution. He found that the modified composite showed the maximum fluoride adsorption capacity of 27.20 mg/g, which was 1.89 times that of natural MMT (14.38 mg/g) [32]. In this case, under the guidance of Hard-Soft-Acid-Base (HSAB) theory, rare earth elements, such as lanthanum (La) and so on (hard acids), usually exhibited a strong affinity for fluoride (hard bases) [33]. Meanwhile, as an abundant rare earth element and the fact of extremely small solubility product constant (Ksp, about 2.00×10^{-19}) of its hydroxide, La possessed excellent acid resistance at acidic environment. This provided a solid theoretical basis for the application of La in fluoride removal from acidic PG flotation wastewater. In addition, polyaluminium chloride (PAC), a popular macromolecular coagulant, was also commonly used in fluoride removal and sedimentation enhancement due to its unique physicochemical properties and the strong affinity of aluminium (Al) element (hard acids) for fluoride [34,35]. With this consideration, the introduction of La and Al bimetallic hydroxides into MMT will be rational. This means that La hydroxide ($La(OH)_3$) can provide acid resistance and core adsorption active sites, while Al hydroxide ($Al(OH)_3$) can build a sedimentation framework and auxiliary adsorption active sites. Through this way, the above bimetallic hydroxides can achieve a synergistic effect in enhancing fluoride removal from acidic wastewater.

As such, the La and Al bimetallic hydroxides combined MMT (LAM) composites were synthesized in this study via loading engineering, and the optimal mass ratio of the two metals was found for the synergistic and efficient fluoride removal from acidic PG flotation wastewater. The composition and morphological features of the LAM-3 composite were characterized initially. Subsequently, the removal performance of composites was comprehensively evaluated through adsorption experiments. The removal mechanism was also elucidated in conjunction with various analyses. Finally, the practical applications feasibility of the LAM-3 composite was verified by real PG flotation wastewater fluoride removal experiments.

5.2. Experiments

5.2.1. Materials and reagents

All used materials and reagents in this work are provided in Table 5.1.

Table 5.1 The used materials and reagents of the experiments in this work.

Materials and reagents	Purity	Role	Manufacturer
Montmorillonite	Industrial grade	For the preparation of LAM composite	Maclean Biochemical Technology Co., Ltd. (Shanghai)
Lanthanum chloride heptahydrate ($LaCl_3 \cdot 7H_2O$)	Analytical grade	Foe the preparation of LAM composite	Aladdin Biochemical Technology Co., Ltd. (Shanghai)
Polyaluminium chloride (PAC)	$Al_2O_3 \geq 28\%$	For the preparation of LAM composite	Aladdin Biochemical Technology Co., Ltd. (Shanghai)
Sodium fluoride (NaF)	Analytical grade	For the preparation of fluoride solution	Sinopharm Chemical Reagent Corporation Ltd., China
Hydrochloric acid (HCl)	Analytical grade	For the adjustment of pH	Sinopharm Chemical Reagent Corporation Ltd., China
Sodium hydroxide (NaOH)	Analytical grade	For the adjustment of pH	Sinopharm Chemical Reagent Corporation Ltd., China
Trisodium citrate ($Na_3C_6H_5O_7 \cdot 7H_2O$)	Analytical grade	For the measurement of fluoride concentration	Sinopharm Chemical Reagent Corporation Ltd., China
Glacial acetic acid (CH_3COOH)	Analytical grade	For the measurement of fluoride concentration	Sinopharm Chemical Reagent Corporation Ltd., China

5.2.2 Syntheses of LAM composite

The LAM composites were synthesized by loading engineering, and the preparation schematic is similar to the La/D composite in Chapter 4. In detail, 3 g of MMT was added into 100 mL of deionized water and dispersed uniformly by stirring at 1800 r/min and 80 °C for 2 h. Then, lanthanum chloride heptahydrate ($LaCl_3 \cdot 7H_2O$) and PAC with different mass ratios (total mass of 2 g) were added into the suspension simultaneously under stirring status. Moreover, 40 mL of concentrated ammonia (25%)

was slowly dropped to the above suspension to adjust pH into alkaline. The mixture was heated and stirred constantly for 6 h to make the reagents react fully. Afterwards, the resulting suspension was aged for 1 h at room temperature, and the solid products were collected by filtration and washed three times. Finally, the products were dried in an oven at 90 ℃ for 12 h to obtain the LAM composites. With the predetermined mass ratios of La: Al = 0: 4, 1: 3, 2: 2, 3: 1, and 4: 0, the obtained LAM composites were named as Al-M-0, LAM-1, LAM-2, LAM-3, and La-M-4, respectively.

5.2.3. Adsorption experiments

To evaluate the adsorption performance of LAM composites, batch adsorption experiments were carried out with the adsorbent dosage of 0.5 g/L, 180 rpm, 12 h, and 25℃. The effects of initial fluoride solution pH (1-10) and co-exist anions (Cl^-, HCO_3^-, SO_4^{2-}, CO_3^{2-} and PO_4^{3-} with the concentration of 10 mg/L, 25 mg/L or 50 mg/L) were explored at an initial fluoride concentration of 100 mg/L. The pH of the fluoride solution was adjusted using hydrochloric acid (HCl, 0.1 mol/L) or sodium hydroxide (NaOH, 0.1 mol/L). About adsorption kinetics and isotherms, the specific conditions and parameters could be found in Table 5.2. In addition, based on the results of previous researches, the recyclability of the LAM composite was studied for four cycles by immersing and stirring them in NaOH solution (0.5 mol/L) for 6 h. The leaching percentages (L_d) of La and Al during each cycle were calculated through Eq. (5.1) [36]. After the experiments, the samples were filtered through 0.22 μm filter membranes, and the residual fluoride concentration was measured with the ion-selective electrode method (GB 7484-87 of China). The equilibrium adsorption capacity (q_e) and removal efficiency (R) were calculated using Eq. (5.2) and Eq. (5.3) [37]. The standard line of fluoride is shown in Fig. 5.1.

$$L_d = \frac{c_M V}{mw} \times 100\% \tag{5.1}$$

$$q_e = \frac{(c_0 - c_e)V}{m} \tag{5.2}$$

$$R = \frac{c_0 - c_e}{c_0} \times 100\% \tag{5.3}$$

where c_M (g/L) is the La or Al concentration in the solution after fluoride adsorption; w (%) is the mass fraction of La or Al in the LAM composites; m (g) is the mass of the LAM composites, V (L) represents the volume of fluoride solution, c_0 and c_e (mg/L) denote the initial and equilibrium concentrations, respectively.

Table 5.2 The specific conditions and parameters of adsorption kinetics and isotherms.

Experiments	Conditions
Adsorption kinetics	LAM-3 composite dosage: 0.5 g/L, fluoride concentration: 100 mg/L, initial pH: 3, temperature: 25℃, stirring speed: 180 rpm
Adsorption isotherms	LAM-3 composite dosage: 0.5 g/L, fluoride concentration: 0~300 mg/L, initial pH: 3, temperature: 25℃, stirring speed: 180 rpm, adsorption time: 12 h

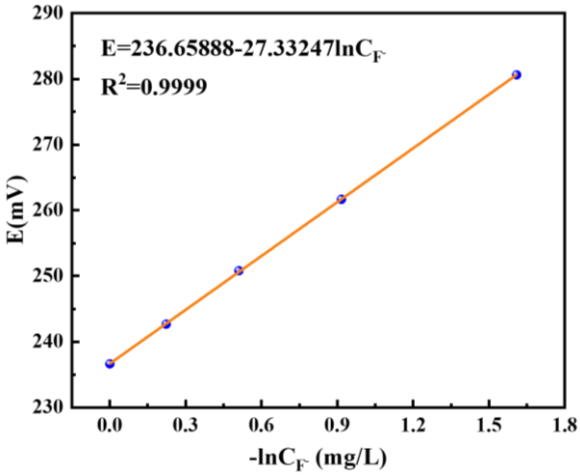


Fig. 5.1 The standard line of fluoride.

5.2.4. Characterizations

The physicochemical characterizations and removal mechanism of prepared adsorbents, such as morphology, composition, structure and others, were determined through several technologies, including X-ray diffraction (XRD), Fourier Transform Infrared Spectroscopy (FTIR), Brunauer-Emmett-Teller (BET), scanning electron microscope with energy dispersive spectrometer (SEM-EDS), Zeta potential, and X-ray photoelectron spectroscopy (XPS). The relevant details are available in Table 5.3.

Table 5.3 The relevant details of characterizations for prepared adsorbents.

Characterizations	Type	Country of production
XRD	Bruker D8 Advance	Japan
FTIR	Therno Nicolet Nexus	America
BET	ASAP2460	America
SEM-EDS	Thermo Fisher Scientific	America
XPS	Thermo Escalab 250Xi	America
Zeta potential	Malvern Zeta Sizer	England

5.3. Results and discussion

5.3.1. Effect of La/Al mass ratio on fluoride adsorption

To ensure the optimal La/Al mass ratio of the LAM composites, the effect of different La/Al mass ratio on fluoride adsorption capacities was evaluated (Fig. 5.2a). The adsorption capacities showed a gradually decreasing trend with the decrease of La/Al mass ratio. Specifically, the single La-modified MMT (La-M-4) composite had the highest adsorption capacity (131.57 mg/g), while the single Al-modified MMT (Al-M-0) composite showed the lowest one (only 32.28 mg/g), which indicated that the affinity of La for fluoride was stronger than that of Al. This was primarily attributed to the lower electronegativity and larger ionic radius of La compared with Al. Meanwhile, the empty orbitals of La was more likely to accept the lone pair of electrons of fluoride, resulting in a stronger affinity between La and fluoride [38]. Nevertheless, it was observed that the fluoride solution using the La-M-4 composite as adsorbent remained turbid after 12 h of quiescence (Fig. 5.2b). In other words, the La-M-4 composite still had the defect of difficult filtration and settleability after adsorption, which would cause a huge obstacle to adsorbent recovery. In contrast, the composites with PAC addition exhibited good sedimentation properties, and the solution after adsorption became clear within only 2 h. This indicated that the introduction of the secondary metal was beneficial for improving the sedimentation property of natural MMT. Overall, both La and Al could be loaded stably onto the MMT surface, and La exhibited a superior affinity than Al for fluoride. Although the appropriate introduction of PAC replaced some original La adsorption active sites, it significantly improved the recyclability of the LAM composite and also provided auxiliary active sites for fluoride adsorption. This synergistic effect compensated for the limitations of single metal modified composites, which was consistent with the design concept of this work. Therefore, the LAM-3 composite was selected as the optimal adsorbent for fluoride removal based on its excellent settleability and adsorption performance.

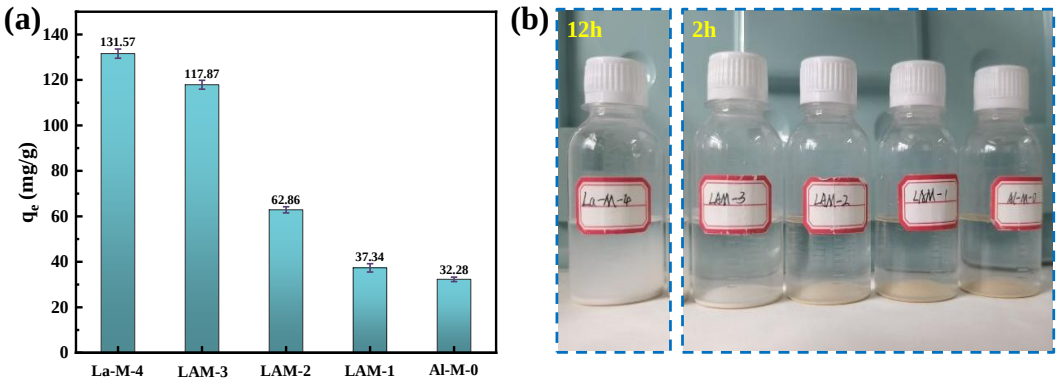


Fig. 5.2 (a) Effect of La/Al mass ratio on fluoride adsorption capacities, and (b) the pictures of different adsorbents after sedimentation of different time (fluoride concentration: 100 mg/L, the LAM composite dosage: 0.5 g/L, T: 25℃, and t: 12 h).

5.3.2. Characterization of the LAM-3 composite

The XRD patterns of natural MMT and the LAM-3 composite are shown in Fig. 5.3a and b. For natural MMT sample, the crystalline peaks at 5.89° (0 0 1), 19.71° (1 0 0), 21.95° (2 0 1) and 62.12° (3 0 0) were assigned to the typical diffraction peaks of MMT. The other crystalline peaks at 20.86° (1 0 0) and 26.64° (1 0 1) belonged to quartz [39]. After modification, three new crystalline peaks appeared at 15.67° (1 0 0), 27.95° (1 0 1), and 48.65° (2 1 1), which all corresponded to the formation of new $La(OH)_3$ phase, and another new crystalline peak at 39.66° (1 2 0) was assigned to $Al(OH)_3$ phase [40]. Meanwhile, the initial crystalline peaks of MMT and quartz were still observed in the LAM-3 composite. The coexistence of the original phases with the newly formed hydroxide phases indicated that MMT had been successfully modified by La and Al bimetallic hydroxides without destroying its crystal structure. More importantly, as alkaline hydroxide with an extremely low Ksp (about 2.00×10^{-19}), the dispersed loading of $La(OH)_3$ significantly enhanced the acid resistance of both MMT and surrounding $Al(OH)_3$, which provided a stable and effective foundation for fluoride removal from acid PG flotation wastewater by using the LAM-3 composite.

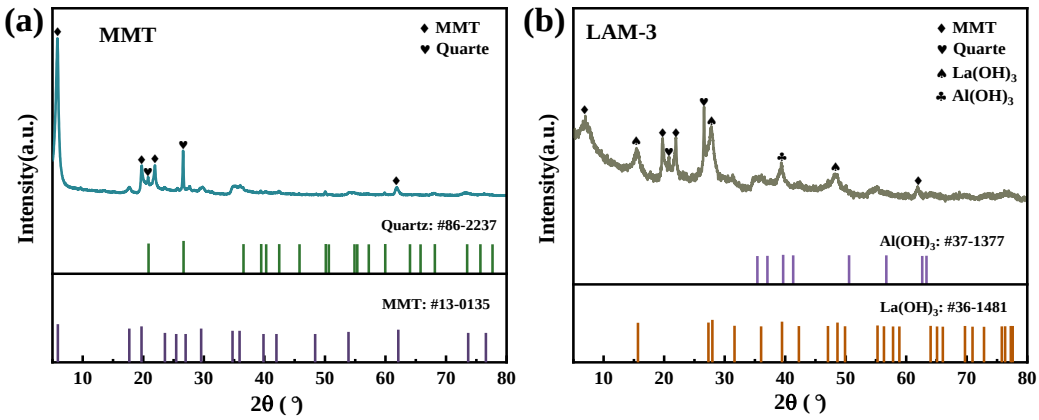


Fig. 5.3 XRD patterns of MMT and the LAM-3 composite.

Fig. 5.4 depicts the FTIR spectra of natural MMT and the LAM-3 composite. The adsorption peaks at 467 cm^{-1}, 624 cm^{-1}, and 1035 cm^{-1} of MMT were all assigned to the bending vibration of Si-O-Si [41]. The bending vibration of Si-O-Al was attributed to the characteristic peaks of 518 cm^{-1} and 915 cm^{-1} [42].Meanwhile, the peaks at 1637 cm^{-1} and 3432 cm^{-1} corresponded to the bending and stretching of adsorbed water, respectively, whereas the peak at 3625 cm^{-1} belonged to -OH groups [43,44]. After loading, two new characteristic peaks appeared at 1403 cm^{-1} and 1491 cm^{-1}, which were attributed to the bending vibration and stretching vibration of metal hydroxyls (M-OH, M=La and Al), respectively [45,46]. The results of FTIR analysis suggested that La and Al were mainly loaded onto MMT surface in the form of hydroxides, thus providing more adsorption active sites, which was consistent with the XRD analysis.

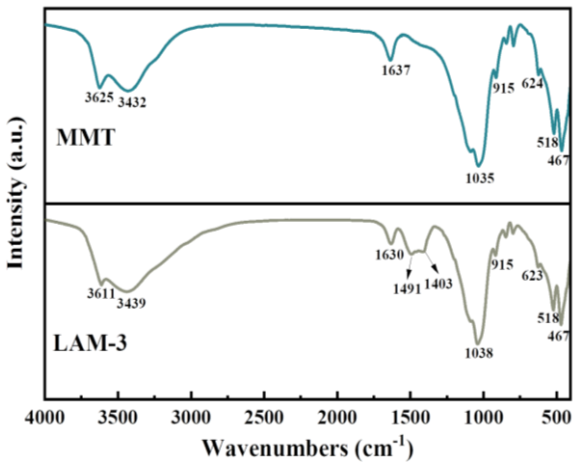


Fig. 5.4 FTIR spectra of MMT and the LAM-3 composite.

The specific surface area and pore volume of natural MMT and the LAM-3 composite were studied through N_2 adsorption-desorption isotherms. For MMT, the specific surface area, average pore diameter and pore volume were 53.89 m^2/g, 8.25 nm and 0.11 cm^3/g, respectively (Fig. 5.5b and Table 5.4). When $La(OH)_3$ and $Al(OH)_3$

were added, it could be seen from Fig. 5.5a that the LAM-3 composite confirmed to the typical IV type isotherms with H3 hysteresis rings at higher relative pressures (IUPAC classification), demonstrating the typical mesoporous structures in the LAM-3 composite [47]. Moreover, the specific surface area of LAM-3 composite decreased to 33.53 m^2/g. In contrast, the average pore diameter and pore volume increased to18.53 nm and 0.16 cm^3/g, respectively (Fig. 5.5b and Table 5.4), which might be primarily attributed to the deposition of generated La and Al hydroxides on the surface of MMT, leading to the blockage of micro pores (reduction of specific surface area) and the formation of agglomeration effects (increase of average pore diameter and pore volume). This also provided clearer evidence for the excellent sedimentation property and the presence of mesoporous structures of the LAM-3 composite. Thus, it is reasonable to speculate that the large pore diameter and high pore volume of LAM-3 composite would significantly promote the diffusion and enhance fluoride adsorption by reducing the mass transfer resistance [48].

Table 5.4 Information about the pore distribution of natural MMT and the LAM-3 composite.

Samples	BET surface area (m^2/g)	Average pore diameter (nm)	Pore volume (cm^3/g)
MMT	53.89	8.25	0.11
LAM-3 composite	33.53	18.53	0.16

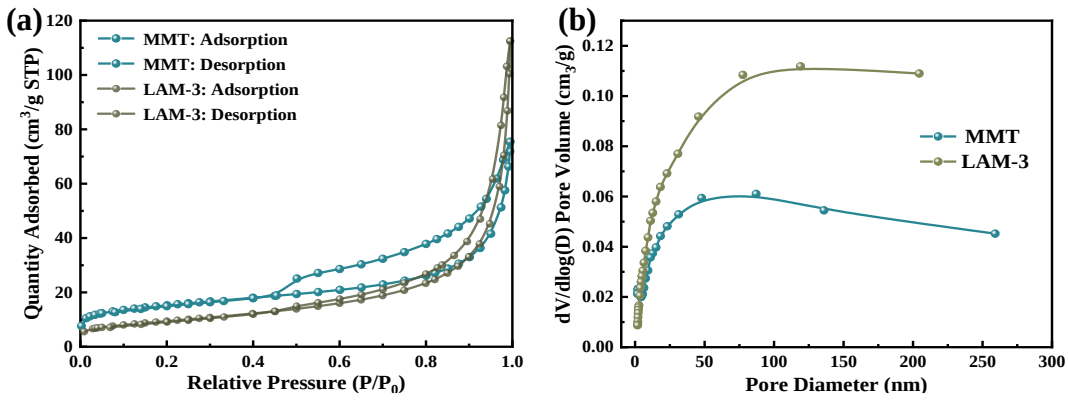


Fig. 5.5 (a) The N_2 adsorption-desorption isotherms and (b) related pore size distributions of MMT and the LAM-3 composite.

The successful preparation of the LAM-3 composite was also confirmed through SEM-EDS analysis. As shown in Fig. 5.6a, there were many pore structures on the surface of the LAM-3 composite, which was agreement with the BET results. Furthermore, the EDS results indicated that La and Al elements were successfully loaded and uniformly distributed onto MMT surface (Fig. 5.6b-f). This phenomenon

also provided a theoretical basis for excellent fluoride adsorption performance of the LAM-3 composite.

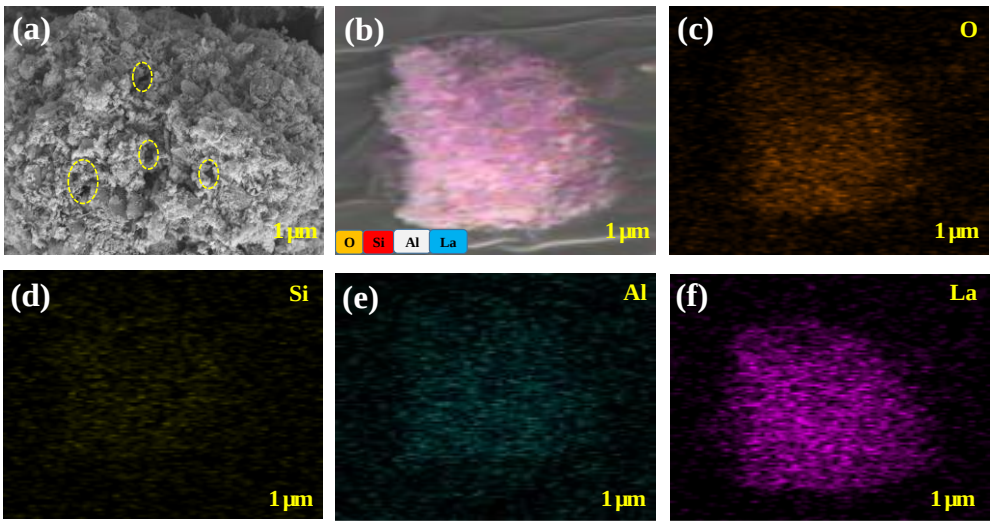


Fig. 5.6 (a) SEM and (b-f) EDS images of the LAM-3 composite.

5.3.3. Fluoride adsorption on the LAM-3 composite

5.3.3.1 Effect of pH and coexisting anions on fluoride adsorption

The initial solution pH can significantly affect the interaction between adsorbent and fluoride. As shown in Fig. 5.7a, natural MMT showed negligible adsorption capacities for fluoride at the entire tested pH range. This was because MMT was a natural silicate mineral with a natural negative charge on its surface, which would generate electrostatic repulsion with negatively charged fluoride during the adsorption process [49]. After modification with $La(OH)_3$ and $Al(OH)_3$, the LAM-3 composite exhibited excellent adsorption performance at acidic environment (adsorption capacities all exceeded 110 mg/g in the pH range of 1-3) and reached the maximum adsorption capacity at pH of 3 (117.87 mg/g), which was 32.56 times that of natural MMT. This enhancement was explained by the protonation of the LAM-3 composite surface, which would generate strong attraction for fluoride [50,51]. The zeta potential at pH of 3 (Table 5.5) further proved the above point with the values increasing from -13.97 mV of natural MMT to +2.03 mV of the LAM-3 composite. As the initial solution pH continued to increase, the adsorption capacities of LAM-3 composite reduced to about 40 mg/g within the pH ranges of 5-9. The reason was attributed to the deprotonation of LAM-3 composite and the increased abundance of -OH groups, both of which intensified the competition with fluoride for adsorption sites, thereby resulting in a significant decrease of adsorption capacities [52]. The results suggested that the LAM-3 composite exhibited excellent adsorption performance at acidic environment,

which would have a broad application prospects for solving fluoride pollution in PG flotation wastewater.

In real acidic PG flotation wastewater, the presence of other anions is inevitable, which might affect the adsorption performance of the LAM-3 composite. Hence, the effect of coexisting anions (including Cl^-, SO_4^{2-}, HCO_3^-, CO_3^{2-}, and PO_4^{3-}) on fluoride adsorption of the LAM-3 composite was systematically investigated and the results are illustrated in Fig. 5.7b. Cl^- and SO_4^{2-} had a minimal effect on fluoride adsorption. Conversely, the presence of HCO_3^-, CO_3^{2-}, and PO_4^{3-} reduced the fluoride adsorption capacity of the LAM-3 composite, and the reduction was more pronounced with the increase of their concentration. For the HCO_3^- and CO_3^{2-} system, the observed inhibition was attributed to their hydrolysis in solution, which caused an increase of OH^- concentration. The resulting OH^- raised the solution pH, thereby reducing the positive surface charge of the LAM-3 composite and weakening the interaction with fluoride. In addition, the generated OH^- would also compete with fluoride for active sites of the LAM-3 composite [53,54]. This dual negative impact significantly hindered the efficient fluoride removal by the LAM-3 composite. The inhibitory effect of PO_4^{3-} was mainly due to the direct competition with fluoride for La active sites on the surface of the LAM-3 composite. The previous reports had confirmed that, for some La-based composites, PO_4^{3-} exhibited a certain affinity for La, which would occupy the La active sites during the adsorption process and reduce the fluoride adsorption capacity [55]. Nevertheless, it was noteworthy that the adsorption capacities of fluoride on the LAM-3 composite still exceeded 100 mg/g in the presence of coexisting anions, demonstrating that the LAM-3 composite had an excellent selectivity toward fluoride.

Table 5.5 Zeta potential of natural MMT, the LAM-3 composite and after adsorption at pH of 3.

Samples	Zeta potential (mV)			Average (mV)
MMT	-13.50	-14.20	-14.20	-13.97
LAM-3 composite	2.02	2.01	2.05	2.03
After adsorption	-13.80	-15.00	-15.60	-14.80

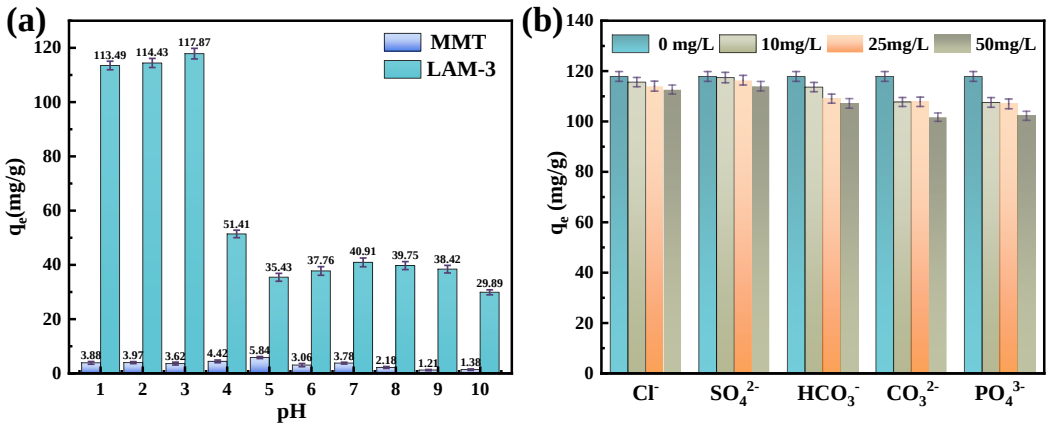


Fig. 5.7 Effect of (a) initial pH and (b) coexisting ions on the adsorption performance of the LAM-3 composite (fluoride concentration: 100 mg/L, the LAM-3 composite dosage: 0.5 g/L, T: 25℃, and t: 12 h).

5.3.3.2 Adsorption kinetics, isotherms and thermodynamics

To reveal the adsorption and transfer behaviors of fluoride on the LAM-3 composite, adsorption kinetics, adsorption isotherms (25℃, 35℃, and 45℃) and adsorption thermodynamics were carried out, respectively.

From Fig. 5.8a, the adsorption process of fluoride by the LAM-3 composite was rapid during first 30 min, with adsorption capacities increasing from 0 mg/g to 94.03 mg/g. Subsequently, the adsorption rate gradually decelerated and reached equilibrium due to the depletion of adsorption active sites on LAM-3 composite surface [56]. To further study the adsorption process, pseudo-first-order (PFO), pseudo-second-order (PSO), and intra-particle diffusion kinetics models were selected to fit the adsorption kinetics data (Eqs same as in Table 4.4 of Chapter 4). The PFO and PSO kinetics fitting results are displayed in Fig. 5.8a and Table 5.6. Obviously, the PSO model provided a good fit to the adsorption kinetics data, and the correlation coefficients (R^2) reached 0.99. Meanwhile, the q_e value obtained from the experiments (117.87 mg/g) was also in close agreement with the calculated q_e value (110.98 mg/g) from the PSO model. Therefore, the PSO model was more suitable for describing the adsorption kinetics of fluoride on the LAM-3 composite, suggesting that the adsorption process mainly involved the chemical interaction between fluoride and the active sites on the LAM-3 composite surface [57,58].

The intra-particle diffusion model fitting results shown in Fig. 5.8b and Table 5.6 revealed the rate-limiting step of fluoride adsorption by the LAM-3 composite. The intra-particle diffusion model could be described in three stages. The first stage constituted the boundary layer diffusion, which meant that fluoride rapidly transferred

to the surface of the LAM-3 composite. The second stage represented intra-particle diffusion, which suggested the gradual penetration of fluoride from the surface into the internal pores. The final stage reflected the dynamic equilibrium processes of adsorption and desorption. More important, the non-zero intercepts indicated that the intra-particle diffusion was not the sole rate-limiting step for fluoride adsorption of the LAM-3 composite, which might also include the control of chemical interaction as confirmed by the PSO kinetic model [59].

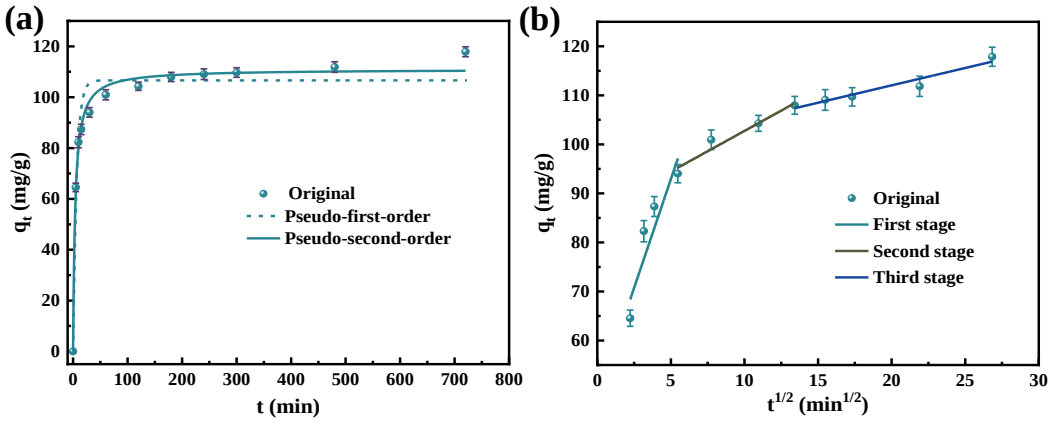


Fig. 5.8 (a) Adsorption kinetics and (b) intra-particle diffusion of fluoride on the LAM-3 composite (initial pH: 3 and the LAM-3 composite dosage: 0.5 g/L).

Table 5.6 Adsorption kinetics parameters of fluoride on the LAM-3 composite.

PFO model			Intra-particle diffusion model (stage I)		
K_1 (1/min)	q_e (mg/g)	R^2	K_{i1} (mg·min$^{1/2}$/g)	C_1	R^2
0.15	106.63	0.95	8.87	48.55	0.81
PSO model			Intra-particle diffusion model (stage II)		
K_2 (g/(mg·min))	q_e (mg/g)	R^2	K_{i2} (mg·min$^{1/2}$/g)	C_2	R^2
2.35×10^{-3}	110.98	0.99	1.66	86.16	0.93
			Intra-particle diffusion model (stage III)		
			K_{i3} (mg·min$^{1/2}$/g)	C_3	R^2
			0.71	97.87	0.92

The adsorption isotherms of fluoride on the LAM-3 composite under different temperatures are shown in Fig. 5.9a. With the increase of temperature from 25°C to 45°C, the maximum equilibrium adsorption capacities decreased from 130.87 mg/g to 113.64 mg/g, indicating that high temperatures were detrimental to fluoride adsorption. Furthermore, to explain the adsorption behavior, the obtained data were fitted with the Langmuir and Freundlich isotherms models (details also in Table 4.4 of Chapter 4). As summarized in Fig. 5.9a-b and Table 5.7, the Langmuir isotherm model exhibited higher R^2 values than the Freundlich isotherm model, suggesting that the adsorption of fluoride

on the LAM-3 composite was a single-layer adsorption process, and the adsorption layer was homogeneous on the LAM-3 composite surface [60].

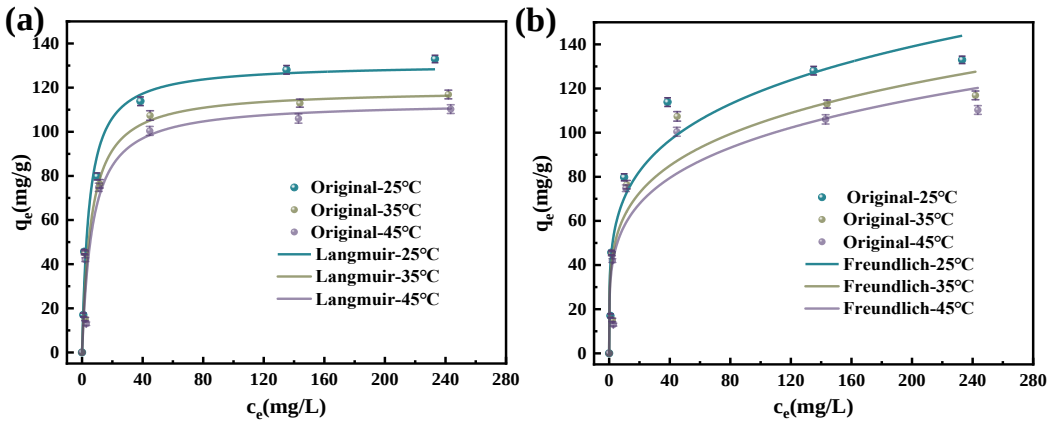


Fig. 5.9 Adsorption isotherms of fluoride on the LAM-3 composite (initial pH: 3 and the LAM-3 composite dosage: 0.5 g/L).

Table 5.7 Adsorption isotherm parameters of fluoride on the LAM-3 composite.

T(K)	Langmuir			Freundlich		
	K_L (L/mg)	q_{max} (mg/g)	R^2	K_F	n	R^2
298	0.22	130.87	0.98	41.82	4.41	0.93
308	0.17	119.21	0.95	36.96	4.43	0.87
318	0.15	113.64	0.94	34.03	4.35	0.85

In addition, adsorption thermodynamics were also analyzed. The results are summarized Table 5.8. The negative Gibbs free energy change (ΔG) values at three temperatures implied that the fluoride adsorption on the LAM-3 composite was a spontaneous process. The negative enthalpy change (ΔH) and positive entropy change (ΔS) values suggested the exothermic process and the increased disorder for the adsorption system [61], which was in agreement with the results of adsorption isotherms.

Table 5.8 Adsorption thermodynamic parameters of fluoride on the LAM-3 composite.

T (K)	ΔH (kJ/mol)	ΔS (kJ/(mol·K))	ΔG (kJ/mol)
298			-20.48
308	-15.12	0.018	-20.66
318			-20.84

In order to further evaluate the fluoride removal performance of the LAM-3 composite, a comparison with similar modified clay composites or bimetallic modified adsorbents are listed in Table 5.9. The LAM-3 composite exhibited a superior adsorption capacity compared to some other reported adsorbents, including Zr-

La/pomelo peel composite, Co_2Al-LDHs, CAPC composite, Ce/Zr-MOFs, and so on. Besides, the base material used in this work was natural MMT, which was a Natural silicate mineral with abundant reserves and low cost. Meanwhile, the reserves of La was also highly abundant in China. These advantages made up for the defects of expensive preparation cost for some adsorbents. Therefore, it was believed that the LAM-3 composite showed great potential to achieve efficient fluoride removal from acidic wastewater, especially from PG flotation wastewater.

Table 5.9 Fluoride removal efficiency of the LAM-3 composite compared with other adsorbents reported in previous literature.

Adsorbents	pH	Concentration range (mg/L)	Adsorption time (min)	q_m (mg/g)	Reference
Zr-La/pomelo peel (Zr-La/PP) composite	3.00	2-50	500	32.50	[62]
Cationic surfactant/H_2O_2 modified clay	2.00	20-120	60	53.66	[63]
Co_2Al-LDHs	2.00	10-300	360	122.54	[64]
BC/Ce-SA-La hybrid hydrogel	2.00	80-380	180	123.00	[65]
Ce-Al bimetal hydroxides modified activated carbon (CAPC)	4.00	10-80	120	36.34	[66]
Carbon-doped aluminum-bentonite (CCDAB)	6.00	10-200	300	85.51	[67]
Ce/Zr-MOFs	6.00	10-60	360	113.8	[68]
Lanthanum hydroxide-modified zeolite (LMZ)	6.00	50-600	2880	117.48	[6]
LAM-3 composite	3.00	10-300	180	130.87	This work

5.3.4. Removal mechanism

To illustrate the fluoride removal mechanism, the characteristic changes in surface structure and chemical bond states of the LAM-3 composite before and after adsorption were analyzed by SEM-EDS, FTIR, and XPS. As presented in Fig. 5.10a, the morphology of the LAM-3 composite after adsorption did not exhibit significant changes compared with original adsorbent, which suggested that the LAM-3 composite maintained good structural stability during fluoride adsorption process. This meant that the acidic environment did not destroy the structure of LAM-3 composite, and the obtained LAM-3 composite had excellent acid resistance. EDS mapping (Fig. 5.10b) revealed that O, Al, Si, La and F elements were observed and distributed uniformly on

the LAM-3 composite surface, indicating the successful immobilization of fluoride. In addition, elemental analysis (Table 5.10) showed that the content of O element decreased from 39.75 wt% to 20.78 wt% and the F element content increased to 14.28 wt%, while the contents of other elements did not change significantly after adsorption, which suggested that oxygen-containing functional groups in the LAM-3 composite might participate in the fluoride removal.

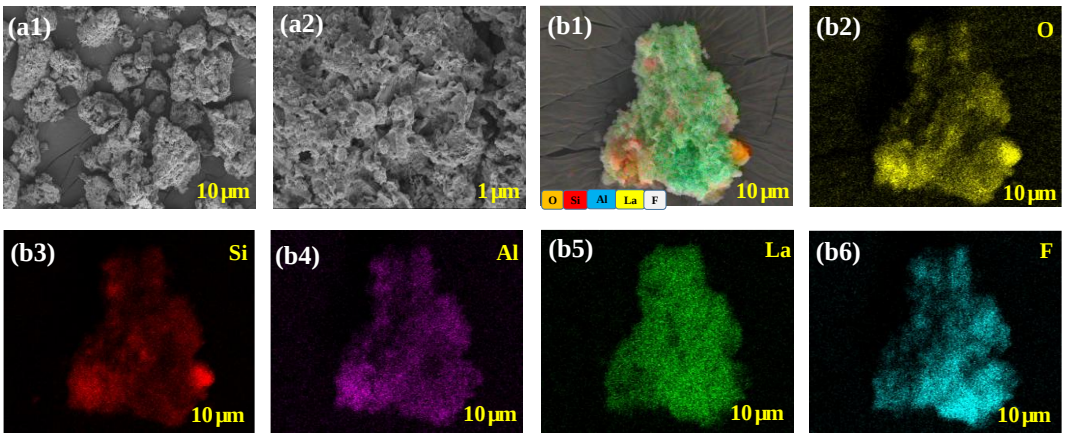


Fig. 5.10 (a1-a2) SEM and (b1-b6) EDS mapping images of the LAM-3 composite after fluoride adsorption.

Table 5.10 Elements contents of the LAM-3 composite before and after fluoride adsorption (wt%).

La-D composite	O	Si	La	Al	F
Before adsorption	39.75	18.36	32.01	9.88	-
After adsorption	20.78	17.48	42.60	4.86	14.28

The FTIR spectra of the LAM-3 composite before and after fluoride adsorption are indicated in Fig. 5.11. Obviously, the characteristic peaks at 1403 cm^{-1} and 1491 cm^{-1}, corresponded to M-OH, disappeared after adsorption, which confirmed that the adsorption of fluoride onto the LAM-3 composite involved ligand exchange. The strong coordination between La or Al and fluoride allowed the -OH groups in M-OH to be replaced by fluoride [69,70]. Moreover, the characteristic peak at 845 cm^{-1}, assigned to metal-oxygen (La-O) band [71], decreased after adsorption. This could be explained by the electrostatic interaction between La and fluoride during the removal process of fluoride [72]. The Zeta potential (Table 5.5) further demonstrated this mechanism with the potential values decreasing from +2.03 mV to -14.80 mV after adsorption. On the other hand, the characteristic peaks at 1630 cm^{-1}, 3439 cm^{-1}, and 3611 cm^{-1} (belong to adsorbed water and -OH groups) shifted to 1637 cm^{-1}, 3432 cm^{-1}, and 3624 cm^{-1} after adsorption, respectively, implying that the hydrogen bonding environmental of surface

adsorbed water and -OH groups in the LAM-3 composite was altered [73]. At pH of 3, it was well documented that some fluoride species existed in the form of HF in solution. Hence, these observations suggested that hydrogen bonding interactions were also involved during fluoride removal process and HF was removed through the formation of hydrogen bonds with surface -OH groups and adsorbed water molecules.

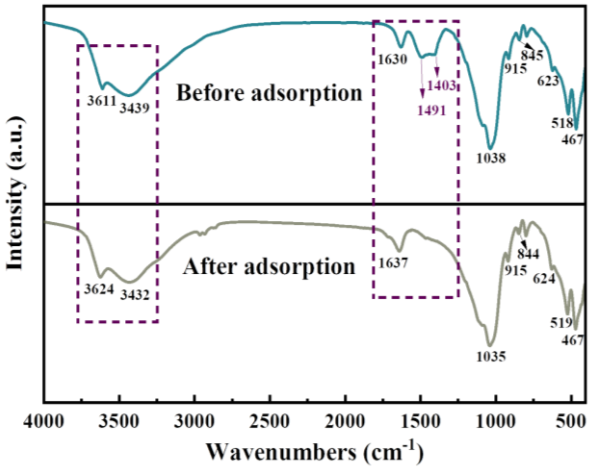


Fig. 5.11 FTIR spectra of the LAM-3 composite before and after fluoride adsorption.

Fig. 5.12a-e show the wide scan spectra, O 1s, La 3d, Al 2p and F 1s narrow spectra of the LAM-3 composite before and after fluoride adsorption. After adsorption, a new peak of F 1s emerged at 684.87 eV in wide scan XPS spectra (Fig. 5.12a), further confirming the successful adsorption of fluoride onto the LAM-3 composite. In the O 1s narrow spectra (Fig. 5.12b), the peaks observed at 531.32 eV, 532.17 eV, and 533.14 eV were attributed to M-O (35.35%), M-OH (52.50%), and adsorption water (12.15%), respectively [48,74]. After adsorption, the peak area of M-OH considerably decreased from 52.50% to 31.56%, demonstrating that fluoride participated in ligand exchange with -OH of the LAM-3 composite, which was consistent with the discovery of FTIR analysis [69]. Besides, for the La 3d narrow spectra shown in Fig. 5.12c, two typical peaks at 835.38 eV and 838.96 eV were assigned to La $3d_{5/2}$ and the other two peaks at 852.12 eV and 855.69 eV were assigned to La $3d_{3/2}$ [56,75]. After fluoride adsorption, the binding energies of La $3d_{5/2}$ and La $3d_{3/2}$ shifted to 837.60 eV/841.54 eV and 854.37 eV/858.48 eV, respectively, which both increased to higher values (+2.22 eV-+2.58 eV). Meanwhile, a new peak corresponding to La-F bond emerged at 830.90 eV [76]. These changes suggested the strong interactions or coordination complexation between fluoride and La in the LAM-3 composite, thus achieving the formation of La-F complex [52,72]. As seen from Fig. 5.12d, the peak of Al 2p at 74.76 eV belonged to Al-O bond in the LAM-3 composite [77]. After the adsorption of fluoride, the binding energy

shifted to 75.13 eV (+0.37 eV) and another new peak attributed to Al-F bond occurred at 75.52 eV [78]. The results implied that the electron cloud environment of Al 2p was changed, and the chemical coordination complexation between fluoride and -Al groups was also present during adsorption process [79]. The F 1s narrow spectra presented in Fig. 5.12e further confirmed the above findings that the peaks corresponding to La-F bond and Al-F bond were observed at 685.51 eV and 686.38 eV, respectively [80,81]. Concomitantly, the peak area proportion of La-F bond reached 79.55%, which suggested that $La(OH)_3$ in the LAM-3 composite was dominant during the removal process.

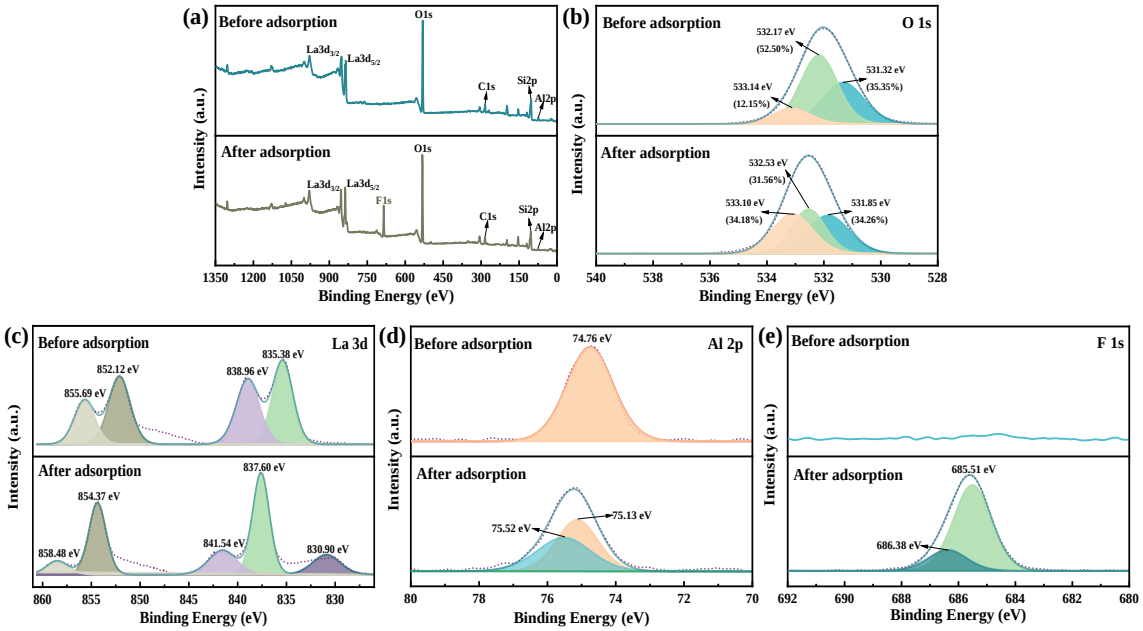


Fig. 5.12 (a) wide scan XPS spectra, (b) O 1s, (c) La 3d, (d) Al 2p, and (e) F 1s narrow spectra of the LAM-3 composite before and after fluoride adsorption.

To sum up, the fluoride removal mechanism of the LAM-3 composite is proposed in Fig. 5.13. MMT provided an excellent and stable supporting platform for fluoride removal in the LAM-3 composite. The loaded $La(OH)_3$ enhanced acid resistance and functioned as the primary active component during the removal process, thereby playing a dominant role in fluoride removal; while the introduction of $Al(OH)_3$ significantly improved the sedimentation performance of the LAM-3 composite and provided auxiliary active sites for fluoride removal. The fluoride removal by the LAM-3 composite involved multiple mechanisms, including ligand exchange, electrostatic interactions, hydrogen bonding, and coordination complexation. Based on the above synergistic loading effects and mechanisms, the LAM-3 composite exhibited an impressive affinity for fluoride, which enabled efficient fluoride removal under the

acidic environment.

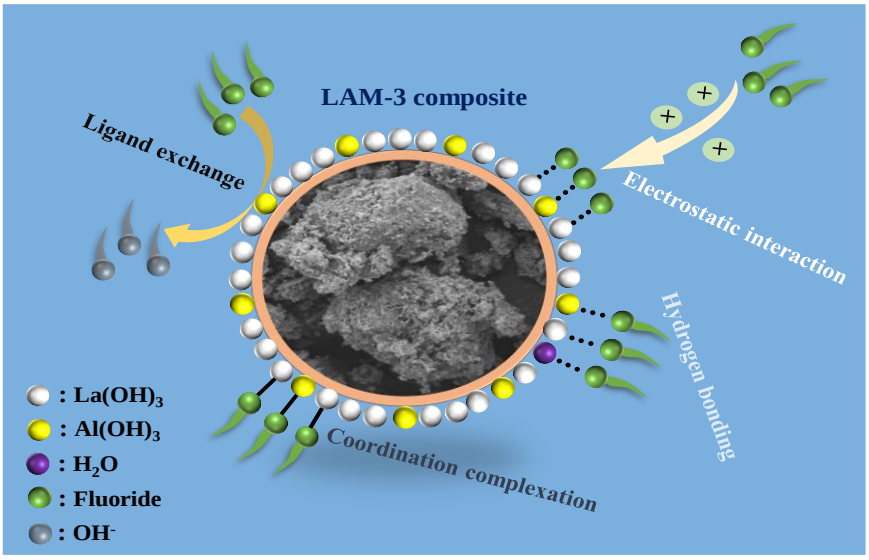


Fig. 5.13 Schematic diagram of fluoride removal mechanism by the LAM-3 composite.

5.3.5 Reusability and practical application performance

The regeneration performance of an adsorbent is crucial to evaluate its practical application potential. As illustrated in Fig. 5.14a, the adsorption capacity retention decreased from the initial 100 to 78.61% after four adsorption-desorption cycles. The reason for this decrease might be the incomplete desorption of the LAM-3 composite, resulting in the occupation of the functional groups and active sites on the surface of the LAM-3 composite [82]. The results of desorption efficiency further confirmed the above explanations that the efficiency values decreased from 94.66% to 82.33% after four adsorption-desorption cycles. Nevertheless, it was noted that the average La and Al leaching percentages were only about 0.043% and 6.27%, respectively, during the adsorption process (Fig. 5.14b), demonstrating that the LAM-3 composite could still maintain stable and sufficient adsorption active sites after repeated applications. These results meant that the LAM-3 composite exhibited excellent stability and fluoride removal performance under complex acidic environment, which further verified the design hypothesis of this work. Overall, the LAM-3 composite showed promising reusability and stability without the additional need for La and Al, suggesting that it had the potential for the efficient treatment of real acidic PG flotation wastewater.

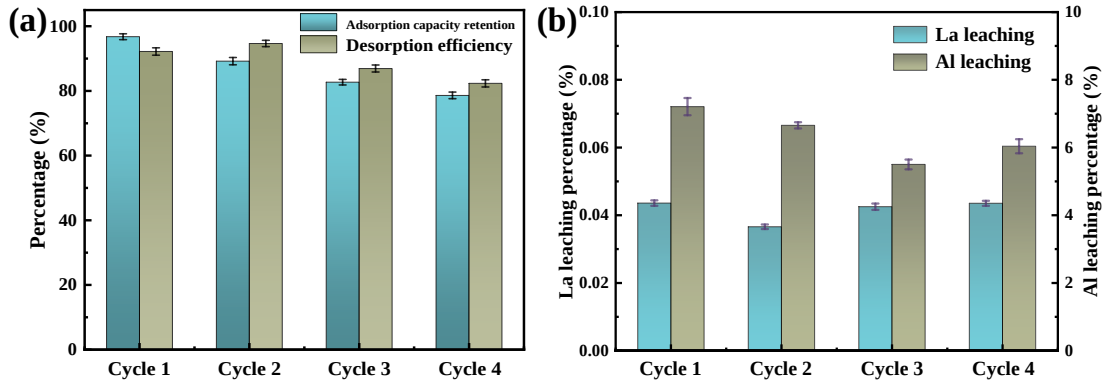


Fig. 5.14 (a) Regeneration performance and (b) La and Al leaching percentages during the adsorption–desorption cycles (initial pH: 3, fluoride concentration: 100 mg/L, the LAM-3 composite dosage: 0.5 g/L, T: 25 ℃, and t: 12 h).

Furthermore, the practical application effectiveness of LAM-3 composite was evaluated using real acidic PG flotation wastewater. The sample was collected from the phosphorus chemical company in Hubei, China, and the characteristics of pH and ions are listed in Table 5.11. From the results in Fig. 5.15, the fluoride removal efficiency increased from 0% to 95.07% with the increase of the LAM-3 composite dosage from 0 g/L to 3.00 g/L. Correspondingly, the fluoride concentration was reduced from initial 100.62 mg/L to 4.96 mg/L, which was far below national industrial wastewater discharge standard (10 mg/L, GB39371-2020). The above results confirmed the outstanding application performance of the LAM-3 composite for fluoride removal from acidic PG flotation wastewater.

Table 5.11 The characteristic information of pH, anions and cation concentration in the real wastewater (mg/L).

Compositions	pH	F^-	Cl^-	SO_4^{2-}	PO_4^{3-}	Ca^{2+}	Mg^{2+}	Al^{3+}	Fe^{3+}	Na^+	K^+
Concentration	2.97	100.62	17.49	80.65	21.77	27.54	3.39	2.83	11.74	125.75	9.57

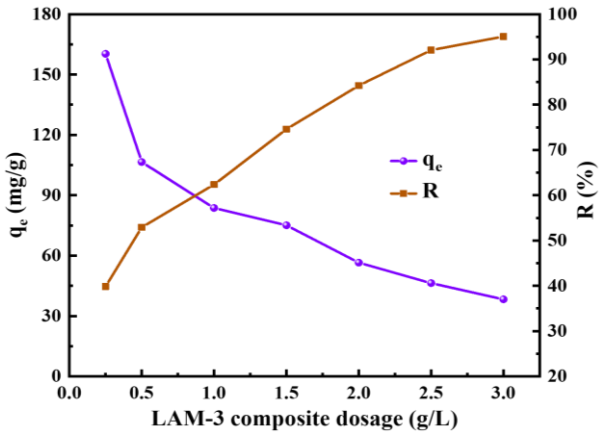


Fig. 5.15 Actual acidic wastewater treatment performance of the LAM-3 composite.

5.4. Conclusions

In this work, the LAM-3 composite was synthesized through bimetallic hydroxides ($La(OH)_3$ and $Al(OH)_3$) loading engineering with MMT as a basic material to synergistically achieve fluoride removal from acidic PG flotation wastewater. The introduction of bimetallic hydroxides remarkably enhanced the acid resistance and sedimentation properties of composite and provided abundant adsorption active sites. The obtained LAM-3 composite showed remarkable acid resistance, adsorption capacities (130.87 mg/g) and selectivity for fluoride at acidic environment and 25℃, which was higher than natural MMT and some previously reported adsorbents. The PSO kinetic model and Langmuir isotherm model could depict the adsorption behavior better, suggesting the monolayer chemical adsorption of fluoride onto the LAM-3 composite. Also, the adsorption of LAM composite toward fluoride was a spontaneous and exothermic process. After four regeneration cycles, the adsorption capacity retention still remained at 78.61% with only about average 0.043% and 6.27% of La and Al leaching percentages, underscoring good stability and reusability of the LAM-3 composite. The mechanism investigation revealed that fluoride removal by the LAM-3 composite involved ligand exchange, electrostatic interaction, hydrogen bonding, and coordination complexation. In addition, for real acidic PG flotation wastewater, the fluoride concentration reduced from initial 100.62 mg/L to 4.96 mg/L with the removal efficiency of 95.07% after the LAM-3 composite treatment, which was far below industrial wastewater discharge standard of China. Overall, the designed LAM-3 composite in this work exhibits superior acid resistance, fluoride removal performance, reusability, and practical application potential. The conduct of this study provides a valuable reference for the utilization of natural silicate minerals in the field fluoride removal of acidic phosphate chemical wastewater.

5.5. References

[1] H. Li, N. Wei, D. He, Y. Chen, R.M. Kasomo, Q. Chen, X. Weng, S. Song, Utilization of cetylpyridine bromide as an efficient collector for flotation separation of quartz from gypsum, Applied Surface Science 702 (2025) 163354. https://doi.org/10.1016/j.apsusc.2025.163354.

[2] J. Zhang, K. Cui, J. Chang, L. Wang, Phosphogypsum-based building materials: Resource utilization, development, and limitation, Journal of Building Engineering 91 (2024) 109734. https://doi.org/10.1016/j.jobe.2024.109734.

[3] K. Li, C. Shi, Y. Zeng, L. Huang, B. Chen, C. Liu, S. Bao, S. Yang, A high-efficiency purification method of waste phosphogypsum via hydrodynamic cavitation pretreatment and froth flotation, Journal of Cleaner Production 512 (2025) 145685. https://doi.org/10.1016/j.jclepro.2025.145685.

[4] J. Fang, Y. Ge, Z. Chen, B. Xing, S. Bao, Q. Yong, R. Chi, S. Yang, B.-J. Ni, Flotation purification of waste high-silica phosphogypsum, Journal of Environmental Management 320 (2022) 115824. https://doi.org/10.1016/j.jenvman.2022.115824.

[5] L. Chen, X. Luan, F. Han, Y. Zhao, H. Yang, L. Zhang, Y. Yin, W. Liu, Z. Cui, Life cycle environmental and economic assessment of Phosphogypsum utilization in China, Resources, Conservation and Recycling 212 (2025) 107938. https://doi.org/10.1016/j.resconrec.2024.107938.

[6] M. Zhao, X. Zhou, J. Li, F. Li, X. Li, J. Yu, L. Guo, G. Song, C. Xiao, F. Zhou, R. Chi, G. Feng, Efficient removal of phosphate and fluoride from phosphogypsum leachate by lanthanum-modified zeolite: Synchronous adsorption behavior and mechanism, Journal of Environmental Chemical Engineering 12 (2024) 113294. https://doi.org/10.1016/j.jece.2024.113294.

[7] Y. Chen, J. Viridiana Garc á-Meza, B. Zhou, Z. Peng, Q. Chen, R.M. Kasomo, X. Weng, H. Li, S. Song, Efficient recovery of fluorine from wet-process phosphoric acid using silicon powder as a new and eco-friendly reagent, Separation and Purification Technology 337 (2024) 126435. https://doi.org/10.1016/j.seppur.2024.126435.

[8] D. Shen, Y. Song, X. Chen, Y. Zhou, H. Li, J. Pan, Fabricating ultrafine zirconium oxide based composite sorbents in “soft confined space” for efficiently removing fluoride from environmental water, Chemical Engineering Journal 444 (2022) 136199. https://doi.org/10.1016/j.cej.2022.136199.

[9] Z. Zhou, Y. Lu, W. Zhan, L. Guo, Y. Du, T.C. Zhang, D. Du, Four stage precipitation for efficient recovery of N, P, and F elements from leachate of waste phosphogypsum, Minerals Engineering 178 (2022) 107420. https://doi.org/10.1016/j.mineng.2022.107420.

[10] Y. Qiu, L.-F. Ren, J. Shao, L. Xia, Y. Zhao, An integrated separation technology for high fluoride-containing wastewater treatment: Fluoride removal, membrane fouling behavior and control, Journal of Cleaner Production 349 (2022) 131225. https://doi.org/10.1016/j.jclepro.2022.131225.

[11] M.M. Damtie, R.H. Hailemariam, Y.C. Woo, K.-D. Park, J.-S. Choi, Membrane-based technologies for zero liquid discharge and fluoride removal from industrial wastewater, Chemosphere 236 (2019) 124288. https://doi.org/10.1016/j.chemosphere.2019.07.019.

[12] M.A. Sandoval, R. Fuentes, A. Thiam, R. Salazar, Arsenic and fluoride removal by electrocoagulation process: A general review, Science of The Total Environment 753 (2021) 142108. https://doi.org/10.1016/j.scitotenv.2020.142108.

[13] M. Yi, K. Wang, H. Wei, D. Wei, X. Wei, B. Wei, L. Shao, T. Fujita, X. Cui, Efficient preparation of red mud-based geopolymer microspheres (RM@GMs) and adsorption of fluoride ions in wastewater, Journal of Hazardous Materials 442 (2023) 130027. https://doi.org/10.1016/j.jhazmat.2022.130027.

[14] Q. Huang, L. Sheng, T. Wu, L. Huang, J. Yan, M. Li, Z. Chen, H. Zhang, Research progress on the application of carbon-based composites in capacitive deionization technology, Desalination 593 (2025) 118197. https://doi.org/10.1016/j.desal.2024.118197.

[15] J. He, Y. Yang, Z. Wu, C. Xie, K. Zhang, L. Kong, J. Liu, Review of fluoride removal from water environment by adsorption, Journal of Environmental Chemical Engineering 8 (2020) 104516. https://doi.org/10.1016/j.jece.2020.104516.

[16] C. Pongener, P.C. Bhomick, A. Supong, M. Baruah, U.B. Sinha, D. Sinha, Adsorption of fluoride onto activated carbon synthesized from Manihot esculenta biomass-Equilibrium, kinetic and thermodynamic studies, Journal of Environmental Chemical Engineering 6 (2018) 2382-2389. https://doi.org/10.1016/j.jece.2018.02.045.

[17] S. Jian, F. Shi, Y. Zhu, W. Jiang, Y. Liu, W. Yang, J. Hu, S. Jiang, Ce-MOFs and Ce/Mn bimetallic MOFs for efficient fluoride removal and their defluoridation mechanism, Colloids and Surfaces A: Physicochemical and Engineering Aspects 701 (2024) 134938. https://doi.org/10.1016/j.colsurfa.2024.134938.

[18] Y. Guo, X. Xing, Y. Shang, B. Gao, L. Zhang, Q. Yue, L. Qian, Z. Wang, Multiple bimetallic (Al-La or Fe-La) hydroxides embedded in cellulose/graphene hybrids for uptake of fluoride with phosphate surroundings, Journal of Hazardous Materials 379 (2019) 120634. https://doi.org/10.1016/j.jhazmat.2019.05.027.

[19] F. Li, X. Li, J. Yu, S. Li, L. Guo, C. Xiao, J. Li, Y. Zhang, R. Chi, Enhanced removal of phosphate and fluoride from phosphogypsum leachate by cerium/iron-based zeolite: Adsorption behaviors and competition mechanisms, Separation and Purification Technology 376 (2025) 134185. https://doi.org/10.1016/j.seppur.2025.134185.

[20] Z. Wang, H. Deng, Y. Gao, S. Zhou, F. Zhou, G. Ye, C. Yan, Microwave acid treatment induces endogenous active adsorption sites in montmorillonite for cadmium immobilization in soil, Applied Clay Science 276 (2025) 107939. https://doi.org/10.1016/j.clay.2025.107939.

[21] X. Jiang, L. Zhang, Y. Miao, L. Chen, J. Liu, T. Zhang, S. Cheng, Y. Song, Y. Zhao, Intrinsic roles of nanosheet characteristics in two-dimensional montmorillonite membranes for efficient Li^{+}/Mg^{2+} separation, Water Research 276 (2025) 123291. https://doi.org/10.1016/j.watres.2025.123291.

[22] C. Hu, F. Teng, X. Yin, P. Wang, B. He, L. Zhu, Adsorption of heavy metals using cysteine-modified pillared montmorillonite: Mechanisms and characteristics, Applied Clay Science 276 (2025) 107923. https://doi.org/10.1016/j.clay.2025.107923.

[23] S. Arabmofrad, G. Lazzara, R. Miller, S.M. Jafari, Surface modification of bentonite and montmorillonite as novel nano-adsorbents for the removal of phenols, heavy metals and drug residues, Advances in Colloid and Interface Science 334 (2024) 103334. https://doi.org/10.1016/j.cis.2024.103334.

[24] W. Wang, Y. Zhao, H. Bai, T. Zhang, V. Ibarra-Galvan, S. Song, Methylene blue removal from water using the hydrogel beads of poly(vinyl alcohol)-sodium alginate-chitosan-montmorillonite, Carbohydrate Polymers 198 (2018) 518–528. https://doi.org/10.1016/j.carbpol.2018.06.124.

[25] G. Wang, M. Yin, G. Zhu, G. Liang, D. Wang, J. Yang, S. Ma, Preparation of a granular montmorillonite and fly ash composite adsorbent and application for Pb^{2+} and butyl xanthate adsorption, Minerals Engineering 228 (2025) 109345. https://doi.org/10.1016/j.mineng.2025.109345.

[26] G. Guo, X. Wang, F. Zou, W. Tian, W. Cao, Y. Zhong, C. Ma, One stone two birds: Chitosan intercalated montmorillonite microcapsules with cationic pollutant adsorption and self-healing for synergistic corrosion resistance, Chemical Engineering Journal 518 (2025) 164641. https://doi.org/10.1016/j.cej.2025.164641.

[27] C.-Y. Cao, M. Wang, Z.-G. Song, S. Zhao, X. Wan, Adsorption of methylene blue onto Al-pillared montmorillonite, Desalination and Water Treatment 227 (2021) 384-390. https://doi.org/10.5004/dwt.2021.27304.

[28] Z. Zeng, C. Yu, R. Liao, X. Cai, Z. Chen, Z. Yu, Z. Wu, Preparation and characterization of sodium polyacrylate grafted montmorillonite nanocomposite for the adsorption of cadmium ions form aqueous solution, Colloids and Surfaces A: Physicochemical and Engineering Aspects 656 (2023) 130389. https://doi.org/10.1016/j.colsurfa.2022.130389.

[29] J.-W. Yu, H.-T. Ren, T.-T. Li, C.-W. Lou, J.-H. Lin, X. Han, Efficient and selective removal of phosphate by La-Mg bimetallic oxide modified diatomite composites, Separation and Purification Technology 376 (2025) 133983. https://doi.org/10.1016/j.seppur.2025.133983.

[30] Y. Gu, D. Xie, Y. Wang, W. Qin, H. Zhang, G. Wang, Y. Zhang, H. Zhao, Facile fabrication of composition-tunable Fe/Mg bimetal-organic frameworks for exceptional arsenate removal, Chemical Engineering Journal 357 (2019) 579-588. https://doi.org/10.1016/j.cej.2018.09.174.

[31] H. Kong, W. Wang, J. Wang, G. Zhang, F. Shen, H. Jiang, Q. Li, Z. Huang, New insights into Lanthanum-Calcium bimetal for phosphate removal: Performance, molecular dynamics and life cycle assessment, Separation and Purification Technology 351 (2024) 128038. https://doi.org/10.1016/j.seppur.2024.128038.

[32] M. Zhang, Enhanced fluoride removal using montmorillonite clay modified with $CoFe_2O_4$ and metal-organic frameworks, Environmental Research 258 (2024) 119389. https://doi.org/10.1016/j.envres.2024.119389.

[33] S.A. Ratthika, K. Ramkumar, S.Sd. Elanchezhiyan, R. Kumar, S. Meenakshi, Synthesis and characterization of lanthanum-assisted aluminium metal-organic frameworks for the removal of fluoride ions from an aqueous environment, Journal

of Environmental Chemical Engineering 13 (2025) 118181. https://doi.org/10.1016/j.jece.2025.118181.

[34] Z. He, H. Lan, W. Gong, R. Liu, Y. Gao, H. Liu, J. Qu, Coagulation behaviors of aluminum salts towards fluoride: Significance of aluminum speciation and transformation, Separation and Purification Technology 165 (2016) 137-144. https://doi.org/10.1016/j.seppur.2016.01.017.

[35] N. Zhang, Y. Yang, L. Fan, X. Zheng, J. Wang, C. Jiang, S. Xu, H. Xu, D. Wang, Coagulation effect of polyaluminum-titanium chloride coagulant and the effect of floc aging in fluoride removal: A mechanism analysis, Separation and Purification Technology 325 (2023) 124674. https://doi.org/10.1016/j.seppur.2023.124674.

[36] N. Wang, J. Li, F. Jia, H. Zhou, Y. Xie, P. Chen, S. Song, M. Quintana, Unraveling nitrogen-doped and vacancy-engineered synergistically modified molybdenum oxide promoting gallium selective adsorption, Separation and Purification Technology 358 (2025) 130158. https://doi.org/10.1016/j.seppur.2024.130158.

[37] J. Hu, J. Song, X. Han, Q. Wen, W. Yang, W. Pan, S. Jian, S. Jiang, Fabrication of Ce-La-MOFs for defluoridation in aquatic systems: A kinetics, thermodynamics and mechanisms study, Separation and Purification Technology 314 (2023) 123562. https://doi.org/10.1016/j.seppur.2023.123562.

[38] H. Basu, M. Amarnath, B. Modak, H. Parab, R. Basu, S. Goyal, S. Saha, S. Singh, C.N. Patra, Development of magnetic La doped Al_2O_3 core-shell nanoparticle loaded hydrogel for selective recovery of fluoride from aquatic medium, Chemosphere 353 (2024) 141504. https://doi.org/10.1016/j.chemosphere.2024.141504.

[39] W. Wang, T. Wen, H. Bai, Y. Zhao, J. Ni, L. Yang, L. Xia, S. Song, Adsorption toward Cu(II) and inhibitory effect on bacterial growth occurring on molybdenum disulfide-montmorillonite hydrogel surface, Chemosphere 248 (2020) 126025. https://doi.org/10.1016/j.chemosphere.2020.126025.

[40] Y. Lyu, X. Su, S. Zhang, Y. Zhang, Preparation and characterization of La(III)-Al(III) co-loaded hydrothermal palygorskite adsorbent for fluoride removal from groundwater, Water Air Soil Pollut 227 (2016) 454. https://doi.org/10.1007/s11270-016-3084-8.

[41] T. Zhang, M. Li, L. Chen, H. Bai, W. Wang, Y. Zhao, Novel montmorillonite nanosheets-based hydrogel beads with high adsorption performance and structural strength for removal of dyes and heavy metals, Chemical Physics Letters 813 (2023) 140322. https://doi.org/10.1016/j.cplett.2023.140322.

[42] Z. Lv, P. Xue, T. Xie, J. Zhao, S. Tian, H. Liu, Y. Qi, S. Sun, X. Lv, High-performing PVDF membranes modified by Na^+ MMT/ionic liquids (ILs) with different chain lengths: dye adsorption and separation from O/W emulsion, Separation and Purification Technology 305 (2023) 122516. https://doi.org/10.1016/j.seppur.2022.122516.

[43] M.S. Fernando, A.K.D.V.K. Wimalasiri, S.P. Ratnayake, J.M.A.R.B. Jayasinghe, G.R. William, D.P. Dissanayake, K.M.N. De Silva, R.M. De Silva, Improved

nanocomposite of montmorillonite and hydroxyapatite for defluoridation of water, RSC Adv. 9 (2019) 35588-35598. https://doi.org/10.1039/C9RA03981C.

[44] D.F. Montaño, H. Casanova, W.I. Cardona, L.F. Giraldo, Functionalization of montmorillonite with ionic liquids based on 1-alkyl-3-methylimidazolium: Effect of anion and length chain, Materials Chemistry and Physics 198 (2017) 386-392. https://doi.org/10.1016/j.matchemphys.2017.06.027.

[45] T. Wang, K. Zhu, Z. Xu, T. Wang, Y. Zhang, H. Li, W. Jin, Enhanced phosphate adsorption via controlled synthesis of lanthanum hydroxide by surfactants with varied alkyl chain lengths, Separation and Purification Technology 338 (2024) 126506. https://doi.org/10.1016/j.seppur.2024.126506.

[46] G. Zhang, H. He, S. Liu, Z. Du, L. Lv, L. Sun, J. Zhang, J. Liang, La-Al modified Fe_3O_4 adsorbent for adsorption performance and mechanism of low P concentration in water, Journal of Water Process Engineering 68 (2024) 106344. https://doi.org/10.1016/j.jwpe.2024.106344.

[47] M. Du, Y. Zhang, Z. Wang, M. Lv, Q. Xu, Z. Chen, Q. Wen, A. Li, La-doped activated carbon as high-efficiency phosphorus adsorbent: DFT exploration of the adsorption mechanism, Separation and Purification Technology 298 (2022) 121585. https://doi.org/10.1016/j.seppur.2022.121585.

[48] Q. He, H. Zhao, Z. Teng, Y. Wang, W. Sun, Y. Guo, X. Ji, W. Hu, S. Shiung Lam, M. Li, Efficient recovery of phosphate by Fe_3O_4/La-MOF: An insight of adsorption performance and mechanism from electrochemical properties, Separation and Purification Technology 314 (2023) 123529. https://doi.org/10.1016/j.seppur.2023.123529.

[49] W. Li, E. Tao, X. Hao, N. Li, Y. Li, S. Yang, MMT and ZrO_2 jointly regulate the pore size of graphene oxide-based composite aerogel materials to improve the selective removal ability of Cu(II), Separation and Purification Technology 331 (2024) 125506. https://doi.org/10.1016/j.seppur.2023.125506.

[50] L. Kong, Y. Tian, Z. Pang, X. Huang, M. Li, N. Li, J. Zhang, W. Zuo, J. Li, Needle-like Mg-La bimetal oxide nanocomposites derived from periclase and lanthanum for cost-effective phosphate and fluoride removal: Characterization, performance and mechanism, Chemical Engineering Journal 382 (2020) 122963. https://doi.org/10.1016/j.cej.2019.122963.

[51] B. Bera, S. Saha Chowdhury, V.R. Sonawane, S. De, High capacity aluminium substituted hydroxyapatite incorporated granular wood charcoal (Al-HApC) for fluoride removal from aqueous medium: Batch and column study, Chemical Engineering Journal 466 (2023) 143264. https://doi.org/10.1016/j.cej.2023.143264.

[52] R. Liu, J. Song, J. Zhao, Z. Wang, J. Xu, W. Yang, J. Hu, Novel MOF(Zr)–on-MOF(Ce/La) adsorbent for efficient fluoride and phosphate removal, Chemical Engineering Journal 497 (2024) 154780. https://doi.org/10.1016/j.cej.2024.154780.

[53] L. Ma, Y. Zhang, P. He, B. Zhao, X. Zhang, H. Xiao, M. Diwu, D. Liu, Q. Gu, C. Lu, Development of a rare earth modified residue of leaching aluminium from

gangue for fluoride ion adsorption from mine water, Minerals Engineering 232 (2025) 109536. https://doi.org/10.1016/j.mineng.2025.109536.

[54] Q. Zhou, H. Xiang, Y. Dai, J. Xiong, F. Jiang, Z. Lin, S. Wang, X. Yang, Rational design of MOF-COF composites for synergistic low-concentration fluoride adsorption: Mechanistic insights and DFT validation, Separation and Purification Technology 384 (2026) 136374. https://doi.org/10.1016/j.seppur.2025.136374.

[55] Y. Zhu, K. Wang, J. Yuan, J. Wang, T. Zhang, F. Qiu, Assembling of waste biomass with Mg–La layered double hydroxide (LDH) nanoflowers for efficient phosphate removal performance: Multi-mechanism synergistic adsorption, Chemical Engineering Science 322 (2026) 123106. https://doi.org/10.1016/j.ces.2025.123106.

[56] Z. Zhu, L. Qin, Y. Liu, Q. Zhang, P. Cheng, W. Liang, Fabrication and mechanism of La/Al bimetallic organic frameworks for phosphate removal, Chemical Engineering Journal 479 (2024) 147081. https://doi.org/10.1016/j.cej.2023.147081.

[57] A. Massrour, S.J. Peighambardoust, M. Foroughi, R. Foroutan, B. Ramavandi, Crystal violet removal by sodium alginate-g-polyacrylamide/ hydroxyapatite/ Cu-Fe LDH nanocomposite, Environmental Technology & Innovation 38 (2025) 104149. https://doi.org/10.1016/j.eti.2025.104149.

[58] L. Zhang, J. Yan, S. Kang, Z. Wang, Y. Miao, R. Gao, T. Zhang, H.J. Ojeda-Galván, M. Quintana, H. Bai, S. Song, Y. Zhao, Tailoring multiple functional domains of lithium-ion sieves for sustainable lithium extraction from low-quality brines, ACS Nano 19 (2025) 33620-33631. https://doi.org/10.1021/acsnano.5c11936.

[59] S. Tong, L. Zhang, X. Yu, G. Liu, H. Xu, W. Liu, J. Shen, Y. Wang, Synergistic Co-pyrolysis of Fenton sludge biochar for fluoride removal: Strategy optimization and cooperative adsorption mechanisms, Journal of Water Process Engineering 78 (2025) 108717. https://doi.org/10.1016/j.jwpe.2025.108717.

[60] R. Foroutan, R. Mohammadi, J. Razeghi, M. Ahmadi, B. Ramavandi, Amendment of Sargassum oligocystum bio-char with $MnFe_2O_4$ and lanthanum MOF obtained from PET waste for fluoride removal: A comparative study, Environmental Research 251 (2024) 118641. https://doi.org/10.1016/j.envres.2024.118641.

[61] R. Foroutan, A. Tutunchi, A. Foroughi, B. Ramavandi, Defluorination of water solutions and glass industry wastewater using a magnetic pineapple hydrochar nanocomposite modified with a covalent organic framework, Journal of Environmental Management 377 (2025) 124651. https://doi.org/10.1016/j.jenvman.2025.124651.

[62] Y. Shang, X. Xu, B. Gao, Q. Yue, Highly selective and efficient removal of fluoride from aqueous solution by Zr La dual-metal hydroxide anchored bio-sorbents, Journal of Cleaner Production 199 (2018) 36-46. https://doi.org/10.1016/j.jclepro.2018.07.162.

[63] M. Mobarak, A.Q. Selim, E.A. Mohamed, M.K. Seliem, Modification of organic matter-rich clay by a solution of cationic surfactant/H_2O_2: A new product for

fluoride adsorption from solutions, Journal of Cleaner Production 192 (2018) 712-721. https://doi.org/10.1016/j.jclepro.2018.05.044.

[64] F. Liu, L. Wan, H. Wang, C. Zhong, X. Min, L. Zhang, Unexpected F^- removal by Co2Al-LDHs: Performance and new insight, Chemical Engineering Journal 452 (2023) 139400. https://doi.org/10.1016/j.cej.2022.139400.

[65] X. Zhou, B. Li, Q. Zhao, Effective removal and adsorption mechanism of fluoride from water by biochar-based Ce(III)-La(III)-crosslinked sodium alginate hybrid hydrogel, International Journal of Biological Macromolecules 272 (2024) 132925. https://doi.org/10.1016/j.ijbiomac.2024.132925.

[66] F. Zheng, S. Guo, J. Xu, J. Jiang, C. Wu, Q. Sun, Y. Zheng, Y. Lin, Polyvinylpyrrolidone-modified Ce Al bimetallic oxide loaded on recyclable activated carbon for selective fluoride ion removal from aqueous solutions, Journal of Water Process Engineering 75 (2025) 107984. https://doi.org/10.1016/j.jwpe.2025.107984.

[67] Y. Miao, J. Gu, D. Zhu, C. Ye, Y. Yang, Q. Zhou, Characterization and performance of novel carbon-doped aluminum-modified bentonite for cost-effective fluoride removal, Materials Today Communications 42 (2025) 111156. https://doi.org/10.1016/j.mtcomm.2024.111156.

[68] J. Song, L. Ji, L. Rao, Z. Zhang, X. Chen, Y. Wang, J. Hu, X.-G. Li, J. Ma, Enhanced fluoride adsorption onto bimetallic Ce/Zr-MOFs with a high selectivity: Characterization and mechanism, Journal of Colloid and Interface Science 704 (2026) 139370. https://doi.org/10.1016/j.jcis.2025.139370.

[69] H. Ma, Y. Huang, J. Tang, W. Wang, B. Liu, H. Sun, S. Yang, G. Han, Enhanced fluoride removal via adsorption flotation based on La-MOF carrier morphology modulation strategy, Separation and Purification Technology 365 (2025) 132652. https://doi.org/10.1016/j.seppur.2025.132652.

[70] C. Jia, J. Wang, H. Wang, S. Zhu, X. Zhang, Y. Wang, Performance and mechanism of La-Fe metal-organic framework as a highly efficient adsorbent for fluoride removal from mine water, Journal of Environmental Sciences 139 (2024) 245-257. https://doi.org/10.1016/j.jes.2023.05.039.

[71] X. Lin, Y. Xie, H. Lu, Y. Xin, R. Altaf, S. Zhu, D. Liu, Facile preparation of dual La-Zr modified magnetite adsorbents for efficient and selective phosphorus recovery, Chemical Engineering Journal 413 (2021) 127530. https://doi.org/10.1016/j.cej.2020.127530.

[72] S. Jian, J. Liu, J. Wu, W. Yang, L. Ran, J. Hu, G. Duan, H. Yang, J. Ma, S. Jiang, Glutaraldehyde-crosslinked chitosan microspheres encapsulating $La(OH)_3$ by electrospraying for efficient remediation of fluoride ions, Chemical Engineering Journal 512 (2025) 162470. https://doi.org/10.1016/j.cej.2025.162470.

[73] J.A. Asare, S.I. Alhassan, R. Anaman, C. Amanze, H. Gang, D. Wei, H. Wang, L. Huang, Synergistic influence of lanthanum and cellulose on fly ash synthesized zeolite for enhanced fluoride removal from wastewater: performance and

mechanism, Separation and Purification Technology 379 (2025) 134810. https://doi.org/10.1016/j.seppur.2025.134810.

[74] W.-J. Xia, L.-X. Guo, L.-Q. Yu, Q. Zhang, J.-R. Xiong, X.-Y. Zhu, X.-C. Wang, B.-C. Huang, R.-C. Jin, Phosphorus removal from diluted wastewaters using a La/C nanocomposite-doped membrane with adsorption-filtration dual functions, Chemical Engineering Journal 405 (2021) 126924. https://doi.org/10.1016/j.cej.2020.126924.

[75] X. Yin, X. Li, E. Petropoulos, Y. Feng, B. Yang, L. Xue, L. Yang, S. He, Phosphate removal from actual wastewater via $La(OH)_3$-C_3N_4 adsorption: Performance, mechanisms and applicability, Science of The Total Environment 814 (2022) 152791. https://doi.org/10.1016/j.scitotenv.2021.152791.

[76] B. Jia, Y. Li, J. Guo, F. Zhou, Y. Guo, Y. Yang, Nanometer lanthanum hydroxide modified anionic polymer for deep fluoride removal: Adsorption properties and mechanism study, Progress in Natural Science: Materials International 33 (2023) 833-842. https://doi.org/10.1016/j.pnsc.2023.12.016.

[77] Y. Chen, Q. Chen, R.M. Kasomo, Y. Jin, P. Yang, H. Zheng, X. Weng, H. Li, S. Song, Adsorption of fluoride from aqueous solutions using graphene oxide composite materials at a neutral pH, Journal of Molecular Liquids 377 (2023) 121467. https://doi.org/10.1016/j.molliq.2023.121467.

[78] J. Feng, X. Li, Y. Yang, Z. Zhou, Preparation of low-cost aluminum-loaded longan shell adsorbent for fluoride removal: Experimental and modeling studies, Journal of Environmental Chemical Engineering 10 (2022) 108917. https://doi.org/10.1016/j.jece.2022.108917.

[79] X. Sun, C. Ke, Q. Lu, L. Liang, G. Xie, Adsorption of fluoride ion on Al/La modified acidified attapulgite composite materials, Separation and Purification Technology 354 (2025) 128791. https://doi.org/10.1016/j.seppur.2024.128791.

[80] J. Liu, Y. Wang, H. Li, X. Zhang, M. Zeng, B. Cao, Y. Liu, L. Qiu, T. Zhang, J. Lu, Carbonization-derived Al@Carbon composite for efficient fluoride elimination: Structural modification, selective adsorption, and dual ligand exchange mechanism, Journal of Colloid and Interface Science 698 (2025) 138060. https://doi.org/10.1016/j.jcis.2025.138060.

[81] L. Sheng, K. Wan, L. Huang, J. Yan, Q. Huang, Y. Liu, Y. Guo, H. Zhang, Adsorption effect for removing fluoride with species of nitrogen by using La-BDC-NH_2/C_3N_4: Experiments and mechanism, Journal of Environmental Chemical Engineering 12 (2024) 114439. https://doi.org/10.1016/j.jece.2024.114439.

[82] S. Liu, J. Wang, J. Ren, M. Zhang, H. Mao, Environmentally benign tannin-modified chitosan aerogel decorated with Zr(IV) enabled high-performance adsorption of fluoride, Chemical Engineering Journal 519 (2025) 165351. https://doi.org/10.1016/j.cej.2025.165351.

Chapter 6. Conclusions

This thesis focused on the efficient recovery of fluorine from WPA and the deep removal of fluoride from the associated acidic phosphate chemical wastewater. To achieve these objectives, a novel fluorine-spillover reagent (SP) and three natural silicate mineral-based adsorbents (the La/D composite, the LAM-3 composite, and the DSL composite) were successfully developed. The main conclusions are summarized as follows.

(1) Compared with the conventional industrial reagents, SP exhibited superior performance in promoting fluorine recovery during the concentration process of WPA by increasing the generation of SiF_4 gas and decreasing the formation of Na_2SiF_6 and K_2SiF_6 precipitates. The optimal concentration conditions were an SP dosage of 0.5 g per 100 g of WPA, a stirring speed of 1800 r/min, a concentration temperature of 150 ℃ and an initial mass of absorptive water of 200 g. Under these conditions, the fluorine contents in WPA and DS decreased to 0.29 wt% and 3.21 wt%, respectively, while the fluorine recovery increased from 50.05% in the blank concentration to 81.13%, representing an improvement of 31.08%.

(2) The La/D composite prepared through the loading engineering strategy demonstrated excellent fluoride removal performance under the acidic environment, with a maximum adsorption capacity of 135.93 mg/g and good selectivity, stability, and reusability. The fluoride removal was mainly attributed to electrostatic attraction, ligand exchange, and coordination complexation. Furthermore, the practical applicability of the La/D composite was validated through the treatment of real acidic phosphate chemical wastewater, in which the fluoride concentration was reduced from 70.49 to 3.83 mg/L at a dosage of 3.0 g/L, meeting the industrial wastewater discharge standard.

(3) The LAM-3 composite synthesized through bimetallic hydroxides loading engineering exhibited enhanced acid resistance and sedimentation properties while simultaneously achieving efficient fluoride removal under acidic conditions. Driven by ligand exchange, electrostatic interaction, hydrogen bonding, and coordination complexation, the LAM-3 composite had a maximum adsorption capacity of 130.87 mg/g, which was higher than those of natural MMT and some previously reported adsorbents. More importantly, the use of the LAM-3 composite reduced the fluoride concentration in real acidic phosphogypsum flotation wastewater from 100.62 to 4.96 mg/L, achieving its deep removal.

Overall, the fluorine-spillover reagent and natural silicate mineral-based composites developed in this thesis exhibited excellent performance in the efficient recovery of fluorine from WPA and the deep removal of fluoride from associated acidic phosphate chemical wastewater. These findings provided valuable insights into the efficient separation of fluoride from WPA and the associated acidic phosphoric chemical wastewater. This work provides effective support for the sustainable and green development of the phosphoric and fluorochemical industries, while also contributing to environmental protection.

Appendix I. Articles published during the Ph. D study

(Note: *indicates corresponding author)

1) **Yingxin Chen**, J. Viridiana García-Meza, Dongsheng He, Bo Zhan, Shixuan Lai, Qian Chen, Xiaoqing Weng, Hongqiang Li, Shaoxian Song, Lanthanum-functionalized diatomite enabling highly efficient fluoride removal from acidic chemical wastewater. ***Chemical Engineering Science***, 2026, 328, 123777.
2) **Yingxin Chen**, J. Viridiana García-Meza, Dongsheng He, Qian Chen, Xiaoqing Weng, Umarbek Alimov, Hongqiang Li, Shaoxian Song, Synergistic and efficient fluoride removal from acidic Phosphogypsum wastewater enabled by bimetallic hydroxides-loaded montmorillonite. ***Separation and Purification Technology***, 2026, 390, 136914.
3) **Yingxin Chen**, J. Viridiana García-Meza, Bowen Zhou, Zhaokai Peng, Qian Chen, Richard M. Kasomo, Xiaoqing Weng, Hongqiang Li, Shaoxian Song, Efficient recovery of fluorine from wet-process phosphoric acid using silicon powder as a new and eco-friendly reagent. ***Separation and Purification Technology***, 2024, 337, 126435.
4) Xiaoqing Weng, Xudong Zhang, Pengpeng Ai, Qian Chen, Richard M. Kasomo, J. Viridiana García-Meza, Hongqiang Li, **Yingxin Chen***, Shaoxian Song, Efficient adsorption of sodium oleate from wastewater with graphene oxide/polyethyleneimine composite hydrogel: Performance and mechanism. ***Chemical Physics Letters***, 2024, 856, 141625.
5) Hongqiang Li, Na Wei, Dongsheng He, **Yingxin Chen***, Richard M. Kasomo, Qian Chen, Xiaoqing Weng, Shaoxian Song, Utilization of cetylpyridine bromide as an efficient collector for flotation separation of quartz from gypsum. ***Applied Surface Science***, 2025, 702, 163354.
6) Xiaoqing Weng, Daozhong Li, **Yingxin Chen***, Hongqiang Li, Dongsheng He, Richard M. Kasomo, Qian Chen, Shaoxian Song, Flotation separation of apatite and potassium feldspar enabled by (tri-n-butyl)-n-tetradecylphosphonium chloride: Performance, mechanism, and application in simultaneous reverse flotation. ***Minerals Engineering***, 2026, 247, 110489.
7) Xuyang Qin, Fangyu Shi, Qinghan Wang, Wenrong Dong, **Yingxin Chen***, Peng Chen*, Hongqiang Li, Shaoxian Song, One-step whitening and deleterious elements (P, F) removal from phosphogypsum by heat-activated persulfate

oxidation. ***Colloids and Surfaces A: Physicochemical and Engineering Aspects***, 2026, 737, 139851.

Appendix II. Experimental data

Table II.1 Effect of SP dosage on the fluorine contents of AS, WPA, and DS and fluorine recovery.

SP dosage (g/100 g WPA)	Fluorine contents of AS (wt%)	Fluorine contents of WPA (wt%)	Fluorine contents of DS (wt%)	Fluorine recovery (%)
0.00	0.15	0.39	7.62	50.05
0.25	0.22	0.37	4.53	72.26
0.50	0.25	0.29	3.21	81.13
0.75	0.18	0.32	6.62	59.32
1.00	0.17	0.34	7.08	56.42

Table II.2 Effect of stirring speed on the fluorine contents of AS, WPA, and DS and fluorine recovery.

Stirring speed (r/min)	Fluorine contents of AS (wt%)	Fluorine contents of WPA (wt%)	Fluorine contents of DS (wt%)	Fluorine recovery (%)
1200	0.16	0.35	10.30	50.91
1500	0.18	0.33	8.44	57.29
1800	0.25	0.29	3.21	81.13
2100	0.246	0.295	3.14	80.50
2400	0.249	0.289	2.85	81.60

Table II.3 Effect of concentration temperature on the fluorine contents of AS, WPA, and DS and fluorine recovery.

Concentration temperature (°C)	Fluorine contents of AS (wt%)	Fluorine contents of WPA (wt%)	Fluorine contents of DS (wt%)	Fluorine recovery (%)
90	0.19	0.38	7.30	58.01
105	0.21	0.36	6.51	65.81
120	0.22	0.33	6.10	68.78
135	0.24	0.30	4.56	73.07
150	0.25	0.29	3.21	81.13

Table II.4 Effect of initial mass of absorptive water on the fluorine contents of AS, WPA, and DS and fluorine recovery.

initial mass of absorptive water (g)	Fluorine contents of AS (wt%)	Fluorine contents of WPA (wt%)	Fluorine contents of DS (wt%)	Fluorine recovery (%)
50	0.48	0.284	3.47	60.08
100	0.36	0.277	3.85	68.21
150	0.29	0.286	3.62	76.62
200	0.25	0.293	3.21	81.13
300	0.18	0.287	3.52	81.29

Table II.5 Effect of initial pH on fluoride adsorption performance of the La/D composite, and the LAM-3 composite.

pH	Adsorption capacity (mg/g)		
	La/D composite	LAM-3 composite	-
1	121.71	113.49	-
2	124.36	114.43	-
3	129.28	117.87	-
4	39.43	51.41	-
5	25.96	35.43	-
6	-	37.76	-
7	-	40.91	-
8	-	39.75	-
9	-	38.42	-
10	-	29.89	-

Table II.6 Effect of coexisting ions on fluoride adsorption performance of the La/D composite.

Coexisting ions	Adsorption capacity (mg/g)			
	0 mg/L	10 mg/L	25 mg/L	50 mg/L
Cl^-	129.28	128.67	124.15	119.92
SO_4^{2-}	129.28	121.10	120.29	117.83
PO_4^{3-}	129.28	114.62	112.24	109.17

Table II.7 Effect of coexisting ions on fluoride adsorption performance of the LAM-3 composite.

Coexisting ions	Adsorption capacity (mg/g)			
	0 mg/L	10 mg/L	25 mg/L	50 mg/L
Cl^-	117.87	115.62	114.02	112.68
SO_4^{2-}	117.87	117.44	116.37	114.02
HCO_3^-	117.87	113.65	109.95	107.18
CO_3^{2-}	117.87	107.73	107.80	101.71
PO_4^{3-}	117.87	107.54	106.97	102.24

Table II.8 Adsorption kinetics of fluoride on the La/D composite, and the LAM-3 composite.

Time (min)	Adsorption capacity (mg/g)		
	La/D composite	LAM-3 composite	-
0	0	0	-
5	48.24	64.54	-
10	62.47	82.30	-
15	68.02	87.33	-
30	80.79	94.03	-
60	99.83	100.95	-
120	112.26	104.30	-
180	117.34	107.97	-
300	125.01	109.70	-
480	127.19	111.84	-
720	129.28	117.87	-

Table II.9 Adsorption isotherms of fluoride on the La/D composite and the LAM-3 composite.

Initial concentration (mg/L)	Adsorption capacity (mg/g)					
	La/D composite			LAM-3 composite		
	25°C	35°C	45°C	25°C	35°C	45°C
10	19.58	18.52	18.08	17.02	15.12	12.99
25	49.05	43.28	40.90	45.68	45.06	42.01

50	85.70	74.10	69.13	79.76	76.40	74.82
100	129.28	110.00	98.43	117.87	107.36	100.37
150	131.89	118.67	111.87	-	-	-
200	134.87	120.72	115.57	128.07	112.95	106.00
300	-	-	-	132.99	116.87	110.25

Table II.10 Regeneration performance of the La/D composite and the LAM-3 composite.

Cycle numbers	Regeneration efficiency (%)		
	La/D composite	LAM-3 composite	-
1	94.97	96.77	-
2	85.74	89.20	-
3	78.66	82.70	-
4	73.46	78.61	-

Table II.11 Effect of the La/D composite and the LAM-3 composite dosage on fluoride q_e and R in real acidic phosphogypsum wastewater.

Dosage (g/L)	La/D composite		LAM-3 composite		-	
	q_e (mg/g)	R (%)	q_e (mg/g)	R (%)	-	-
0.25	62.03	22.00	160.30	39.83	-	-
0.50	53.17	37.72	106.53	52.94	-	-
1.00	39.16	55.56	83.67	62.37	-	-
1.50	35.15	74.81	75.08	74.62	-	-
2.00	29.53	83.78	56.51	84.24	-	-
2.50	25.90	91.87	46.33	92.09	-	-
3.00	22.22	94.56	38.26	95.07	-	-